



Norwegian University of
Science and Technology

Use of Turbulence Stimulation on Ship Models

Jens Berg Ildstad

Marine Technology

Submission date: June 2018

Supervisor: Sverre Steen, IMT

Co-supervisor: Kjetil Berget, SINTEF Ocean

Norwegian University of Science and Technology
Department of Marine Technology



NTNU Trondheim
Norwegian University of Science and Technology
Department of Marine Technology

MASTER THESIS IN MARINE TECHNOLOGY

SPRING 2018

FOR

Jens Berg Ildstad

Use of turbulence stimulation on ship models

When ships, propellers and hydrofoils are tested in model scale, the Reynolds number will usually be so low that the flow over the model will be partly laminar, while in full scale the flow will be almost entirely turbulent. For the flow to be similar and to enable reliable scaling to full scale, the flow should be turbulent also in model scale. SINTEF Ocean is operating the large towing tank and cavitation tunnel at the Marine Technology Centre. Turbulence stimulation is applied on a routine basis, but they see a need to renew their knowledge and apply turbulence stimulation on a more firm scientific basis. Therefore, the objectives of this master thesis are to:

Explain briefly the process of transition from laminar to turbulent flow, and the role of turbulence stimulation in this context.

Give an overview of the different methods of turbulence stimulation in use for ship models at SINTEF Ocean and other similar establishments.

Discuss benefits and drawbacks of the different methods.

Perform model experiments of a few different ship models with different, relevant turbulence stimulation methods, as well as testing without stimulation. The results shall be analysed, including expressing the uncertainty of the results.

On the basis of the model test results, as well as other considerations, give recommendations for types of turbulence stimulation to be used in practical model testing of ship models.

In the thesis the candidate shall present his personal contribution to the resolution of problem within the scope of the thesis work.

Theories and conclusions shall be based on mathematical derivations and/or logic reasoning identifying the various steps in the deduction.

The thesis work shall be based on the current state of knowledge in the field of study. The current state of knowledge shall be established through a thorough literature study, the results of this study shall be written into the thesis. The candidate should utilize the existing possibilities for obtaining relevant literature.

The thesis shall be organized in a rational manner to give a clear exposition of results, assessments, and conclusions. The text should be brief and to the point, with a clear language. Telegraphic language should be avoided.



NTNU Trondheim
Norwegian University of Science and Technology
Department of Marine Technology

The thesis shall contain the following elements: A text defining the scope, preface, list of contents, summary, main body of thesis, conclusions with recommendations for further work, list of symbols and acronyms, reference and (optional) appendices. All figures, tables and equations shall be numerated.

The supervisor may require that the candidate, in an early stage of the work, present a written plan for the completion of the work. The plan shall include a budget for the use of laboratory or other resources that will be charged to the department. Overruns shall be reported to the supervisor.

The original contribution of the candidate and material taken from other sources shall be clearly defined. Work from other sources shall be properly referenced using an acknowledged referencing system.

The thesis shall be submitted electronically (pdf) in DAIM:

- Signed by the candidate
- The text defining the scope (this text) (signed by the supervisor) included
- Computer code, input files, videos and other electronic appendages can be uploaded in a zip-file in DAIM. Any electronic appendages shall be listed in the main thesis.

The candidate will receive a printed copy of the thesis.

Supervisor : Professor Sverre Steen
Advisor : Kjetil Berget (SINTEF Ocean)
Start : 12.01.2018
Deadline : 11.06.2018

Trondheim, 26.01.2018

Sverre Steen
Supervisor

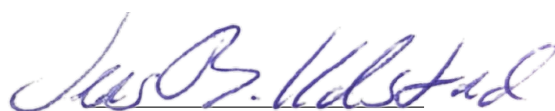
Preface

This thesis concludes my Master of Science degree within Marine Hydrodynamics in Naval Architecture at the Department of Marine Technology, NTNU. The work was carried out during the spring of 2018 at the Marine Technology Centre in Trondheim. Hopefully the work presented herein could be helpful when applying turbulence stimulation in future ship model experiments.

For valuable, frequent and highly appreciated guidance a large gratitude is due to Professor Sverre Steen. His knowledge and experience within hydrodynamics and ship model testing were crucial contributions to the final outcome of this report. For providing this task and ensuring the possibility of ship model testing, SINTEF Ocean and especially co-supervisor Kjetil Berget are deeply acknowledged.

Several people across two institutions gave up on valuable time to be included in this work, especially connected to the practical work in the towing tank. Among these were Kay Arne Skarpnes, Terje Rosten and Trond Innset of NTNU and Robert Opland of SINTEF Ocean. The results presented in this report would not be possible if not for their contributions. For this, I am truly grateful. At last, but not least a special thanks to my partner, Rebekka, although at times far away your support and motivation have been invaluable throughout this project.

Trondheim, 9th of June 2018



Jens Berg Ildstad

Abstract

In ship model testing the length based Reynolds number will be in the order of 100 times smaller than in full scale. As a consequence ship models often operate in the transition zone between laminar and turbulent flow. Thus, the boundary layer flow in model tests may well be partly or completely laminar if no turbulence stimulation device is applied, as opposed to a fully turbulent flow which is the case in full scale conditions. Hence, to provide a reliable extrapolation of model scale results to full scale, the need for turbulence stimulation in ship model testing is evident.

Various turbulence stimulation techniques are in use today. The most frequently used methods in ship model testing are tripwires, studs, sand strips and, to a limited extent, the Hama strip. Turbulence stimulation is today applied on a routine basis, largely based on assumptions and research conducted decades ago. The scope of this report is to both theoretically and experimentally provide a modern and scientific study on the field of turbulence stimulation in ship model testing.

To provide such a study a theoretical description of the laminar-turbulent transition and the role of turbulence stimulation in this context was carried out. In addition ship model experiments with the purpose of investigating any discrepancies in measured total resistance by the use of various turbulence stimulation techniques were performed.

The main parameters affecting laminar-turbulent transition are pressure gradient, wall roughness and background turbulence. Among these, only the wall roughness may be manipulated to cause an earlier transition in ship model testing. Test results indicate that all tested stimulation techniques are effective in generating turbulence at speeds relevant for ship models, when an appropriate roughness height is applied. Certain discrepancies in measured resistance between the stimulation techniques are evident over the entire speed range. Due to a good correlation with theoretical calculations, this discrepancy is believed to originate from differences in induced drag by each stimulation method.

Regarding placement of turbulence stimulation, some deviation from the recommended procedures seems to be suitable, depending on the model size. For a large ship model (5 m < L < 8 m) 2.5 % of L_{PP} aft of FP is a good location. For smaller models (2 m < L < 5 m) 5 % of L_{PP} , as according to ITTC-guidelines, seems like a suitable approach. Due to an easy mounting procedure, effective turbulence generation and an appropriate amount of induced drag, the tripwire is recommended as the preferred stimulation technique in conventional ship model testing.

Sammendrag

I skipmodellforsøk vil Reynolds tallet være i størrelsesorden 100 ganger mindre enn i full skala. På grunn av dette opererer skipsmodeller ofte i overgangssonen mellom laminær og turbulent strømning. Følgelig vil strømmingen rundt modellskroget ofte være delvis eller helt laminær dersom ingen turbulensstimulering påføres. Dette er i motsetning til fullskalaforhold der en turbulent strømning opptrer nesten umiddelbart etter forre perpendikulær. For å gi en pålitelig ekstrapolering av motstand fra modellskala til full skala, er derfor turbulensstimulering en nødvendighet i skipmodellforsøk.

Ulike turbulensstimuleringsteknikker er i bruk i dag. De mest brukte metodene i skipmodellforsøk er i dag bomullstråd, sandstriper, pinner satt inn i skroget og, i en begrenset grad Hamastriper. Turbulensstimulering blir i dag anvendt på en rutinemessig basis, og er i stor grad basert på antakelser og forskning utført for flere tiår siden. Hensikten med denne rapporten er å virke som en moderne og vitenskapelig studie angående turbulensstimulering i skipmodellforsøk på både et teoretisk og eksperimentelt grunnlag. I dette arbeidet ble det utført en teoretisk beskrivelse av den laminar-turbulente overgangen og rollen som turbulensstimulering har i denne sammenheng. I tillegg ble skipmodellforsøk med ulike turbulensstimuleringsteknikker gjennomført.

Hovedparameterne som påvirker laminær-turbulent overgang er trykkgradient, overflateruhet og bakgrunnsturbulens. I skipmodellforsøk er det bare mulig å endre ruheten for å forårsake en tidligere turbulent overgang. Testresultatene indikerer at alle stimuleringsteknikker er effektive i å generere turbulens ved de hastigheter som er relevante for skipsmodeller. En forutsetning er likevell at en passelig ruhetshøyde blir brukt. Forskjeller i målt motstand mellom de ulike stimuleringsteknikkene er tydelige og konsistente over hele hastighetsområdet. På grunn av en god korrelasjon med teoretiske beregninger antas denne forskjellen å stamme fra forskjeller i induisert egenmotstand ved hver stimuleringsmetode.

Når det gjelder plassering av stimuleringen, synes noen avvik fra de anbefalte prosedyrene å være passende avhengig av modellstørrelsen. For en stor skipmodell ($5 \text{ m} < L < 8 \text{ m}$) er 2,5 % av L_{PP} akter av forre perpendikulær en god plassering. For mindre modeller ($2 \text{ m} < L < 5 \text{ m}$) virker 5 % av L_{PP} , som i henhold til ITTC-retningslinjene, å være en egnet tilnærming. På grunn av en enkel monteringsprosedyre, effektiv turbulensgenerering og en passende mengde induisert sløyfe, anbefales bomullstråden som den foretrukne stimuleringsmetoden ved konvensjonell skipmodellforsøk.

Contents

- Preface iii
- Abstract v
- Sammendrag vii
- Nomenclature xii

- 1 Introduction 1**
- 1.1 Background and motivation 2
- 1.2 Scope of work 4
- 1.3 Thesis outline 5

- 2 Theoretical Background 7**
- 2.1 Ship resistance and model testing 7
- 2.2 Viscous flow and transition to turbulence 9
 - 2.2.1 Laminar and turbulent flow 11
 - 2.2.2 Transition from laminar to turbulent flow 14

- 3 Turbulence Stimulation 21**
- 3.1 ITTC-guidelines 21
- 3.2 Studs 22
- 3.3 Tripwire 25
- 3.4 Sand strips 27
- 3.5 Hama strip 28

- 4 Experimental Setup and Procedure 31**
- 4.1 Ship models 31
- 4.2 Placing of turbulence stimulation 33
- 4.3 Calculation of roughness height 34
- 4.4 Test conditions 35
 - 4.4.1 Stimulation devices 35
 - 4.4.2 Model velocities 37
 - 4.4.3 Waiting times 38
- 4.5 Experimental setup 39
- 4.6 Determination of uncertainty 40

5	Experimental Results	43
5.1	Model A	43
5.1.1	Uncertainty analysis	43
5.1.2	Measured resistance	44
5.1.3	Variation in waiting time	46
5.2	Model B	46
5.2.1	Uncertainty analysis	46
5.2.2	Measured resistance	47
5.2.3	Variation in location of stimulation	49
6	Theoretical Resistance Predictions	51
6.1	Drag induced by turbulence stimulation	51
6.2	Frictional resistance	56
6.2.1	Determination of form factor	57
6.2.2	Resistance predictions	61
6.3	Total ship model resistance	62
6.3.1	Theoretical	62
6.3.2	Semi theoretical	64
7	Comparison of Theoretical and Experimental Results	65
7.1	Resistance	65
7.1.1	Model A	65
7.1.2	Model B	67
7.2	Naturally extent of laminar region	70
8	Discussion	77
8.1	Turbulence stimulation techniques	77
8.2	Location of turbulence stimulation	82
8.3	Waiting time and other uncertainties	84
8.4	Necessity of flow observation techniques	86
9	Conclusion and Further Work	89
9.1	Conclusion	89
9.2	Recommendations for further work	90
	References	91
A	Complete Results for Each Run	I
A.1	Model A	I
A.2	Model B	X

B Complete Comparison of Experimental Results **XV**
B.1 Model A XV
B.2 Model B XVII

Nomenclature

Acronyms

AP	Aft perpendicular
BL	Boundary layer
CFD	Computational fluid dynamics
FP	Fore perpendicular
ITTC	International Towing Tank Committee
TS	Turbulence stimulation

Greek

α	Angle between ship centerline and a vector tangential to the surface
β	Complex frequency
δ	Boundary layer displacement thickness
δ_s	BL displacement thickness at location of TS
λ	Scale factor
μ	Dynamic viscosity
ν	Kinematic viscosity
τ_w	Viscous shear stress at a surface
θ	Inflow angle
Δ	Ship displacement
γ	Confidence interval
Φ	Dimensionless disturbance
ρ	Density

σ	Standard deviation
τ	Viscous shear stress
ρ	Turbulence intensity

Roman

C_b	Block coefficient
\bar{u}	Mean value of velocity component
\bar{X}	Mean value of experimental values
ΔR_T	Loss in viscous resistance due to a laminar flow region
A_T	Wet surface of transom stern
B_{WL}	Breadth of waterline
C_p	Pressure coefficient
C_w	Wave making resistance coefficient
$C_{\Delta R_T}$	Dimensionless loss in viscous resistance due to a laminar flow region
C_{Fc}	Partly laminar - partly turbulent friction coefficient
C_{Rtrip}	Dimensionless parasitic drag
C_{Tf}	Total viscous resistance coefficient
D_f	Frictional drag
k_f	Form factor
k_{exp}	Roughness height utilized in experiments
k_{req}	Calculated required roughness height
l_s	Length along surface from FP to location of TS
L_{WL}	Length of waterline
P_0	Hydrodynamic pressure far away
P_d	Local hydrodynamic pressure
P_s	Hydrostatic pressure at ship surface
P_X	Precision limit

P_{∞}	Hydrostatic pressure far away
p_{lam}	Part of hull subjected to laminar flow
p_{turb}	Part of hull subjected to turbulent flow
R_{Tf}	Total viscous resistance
R_{trip}	Parasitic drag of TS
S_X	Standard deviation
S_{trip}	Projected surface of TS
t_{wait}	Waiting between runs in towing tank
u'	Fluctuating velocity component
u_L	Local flow velocity along a shi hull
ΔC_F	Roughness allowance
C_A	Correlation allowance
C_F	Frictional resistance coefficient for a flat pate
C_R	Residuary resistance coefficient
C_T	Total resistance coefficient
C_{Flam}	Laminar friction coefficient flat plate
C_{Fturb}	Turbulent friction coefficient flat plate
C_{trip}	Drag coefficient of TS
F_x	Force component in x-direction
L_{PP}	Length between perpendiculars
P_a	Atmospheric pressure
R_T	Total ship resistance
Rn_k	Reynolds number based on roughness height
Rn_x	Reynolds number based on length, x
Rn_{δ}	Reynolds number based on BL thickness
Rn_{crit}	Reynolds number where transition to turbulence occurs

x_{crit}	Flow length in which transition to turbulence occurs
c	Phase velocity
Fn	Froude number
i	Imaginary unit
k	Roughness height
L	Length
l	Characteristic length
N	Number of repetitions of a measurement
p	Pressure
Rn	Reynolds number
S	Wetted surface
T	A given time interval
T	Draught
t	Time
U	Velocity
u	Velocity in x-direction
u(y)	Local flow velocity at a distance, y, from the surface
v	Velocity in y-direction
w	Velocity in z-direction
X	General experimental value

List of Figures

1.1	Flow field around a ship.	3
2.1	Resistance components of a ship	8
2.2	Laminar and turbulent friction lines.	10
2.3	Boundary layer velocity profiles.	11
2.4	Realization of velocity in a turbulent flow.	13
2.5	The process of laminar-turbulent transition	16
2.6	Tripwire in a flow.	18
3.1	Studs on a ship model.	22
3.2	Mounting and flow around studs.	23
3.3	Recommended placing of studs.	24
3.4	Tripwire on a ship model hull.	25
3.5	Disturbances generated by a tripwire.	26
3.6	Sand strips mounted on ship model hulls.	27
3.7	Hama strip, specifications and picture.	28
4.1	Ship model utilized in experiments.	32
4.2	Sketch indicating important aspects regarding geometry.	34
4.3	Hama strip at different locations, model B.	34
4.4	Turbulence stimulation applied on model A.	36
4.5	Sketch of towing tank.	40
4.6	Picture of experimental setup.	40
4.7	Weighting factor, t	42
5.1	Precision limit model A.	44
5.2	C_T -curve model A with different TS.	45
5.3	Precision limit model B.	47
5.4	C_T -curve for model B with different TS.	48
6.1	Pressure distribution around the hull of KVLCC2	53
6.2	Parameters affecting $u(k)$	54
6.3	Parasitic drag for different turbulence stimulators, Model A.	55
6.4	Parasitic drag for different turbulence stimulators, Model B.	56

6.5	Dimensionless parasitic drag for trip wire.	56
6.6	Prohaska plot, model A.	60
6.7	Prohaska plot, model B.	60
6.8	Predicted frictional resistance, model A.	61
6.9	Predicted frictional resistance, model B.	62
6.10	Loss in frictional resistance due to a partly laminar flow, model A	63
6.11	Loss in frictional resistance due to a partly laminar flow, model A	63
7.1	Theoretical and experimental results, model A, all TS	66
7.2	Theoretical and experimental results, model A, trip wires	67
7.3	Semi-theoretical and experimental results, model A, trip wires	68
7.4	Theoretical and experimental results, model B.	69
7.5	Theoretical and experimental results with TS at different locations, model B . . .	70
7.6	Semi theoretical and experimental results, model B.	71
7.7	C_T -curve for model B with Hama at 10 % of L_{pp}	72
7.8	Theoretical and experimental results regarding naturally extent of laminar flow.	73
7.9	Visual observations, extent of laminar region	74
7.10	Experimentally determined Rn_{crit}	75
8.1	Comparison between parasitic drag and loss in resistance due to laminar flow.	84
8.2	Timeseries of measured resistance at low speed.	86

List of Tables

- 1.1 Extent of laminar region if no TS is applied 4
- 4.1 Ship model data. 33
- 4.2 Length from FP to stimulator along the model surface. 33
- 4.3 Required roughness Reynolds number for each TS tested. 35
- 4.4 Calculated required roughness height and actually applied roughness height. . 37
- 4.5 Tested ship model speeds. 38
- 4.6 Speeds used in different waiting time testing, model A. 39
- 5.1 Precision limit, model A. 44
- 5.2 Mean values of measured resistance for model A. 45
- 5.3 Results from waiting time variation. 46
- 5.4 Precision limit, model B 47
- 5.5 Mean values of measured resistance for model B. 48
- 5.6 Mean values of measured resistance for different locations of the Hama strip. . 49
- 6.1 Describing values for Hama strips at different locations. 54
- 6.2 Calculated form factors. 58
- 6.3 Low speed towing test results. 59
- 6.4 Form factors, Prohaska’s method. 61
- 6.5 Wetted surface upstream of stimulators. 64
- 7.1 Differences between theoretical and experimental C_T 68

Chapter 1

Introduction

Every since the days of William Froude and the beginning of modern ship model testing in the 1870s, efforts have been made to make ship model test conditions resemble reality. This is essential in order to provide accurate results when extrapolating results from model tests to full scale. In the 1920s scientists within fluid dynamics became aware of the difference in measured resistance depending on the flow characteristics, as a persistent laminar flow over the model gave rise to smaller frictional resistance than a fully turbulent flow. The flow in a full scale ship situation will most certainly be turbulent due to a large ratio between inertia and viscous forces. In model scale however, inertia forces are obviously drastically decreased while viscous forces remains unaffected. A following consequence is a higher likelihood for the occurrence of laminar flow. Thus, the need for a turbulence enhancement method when performing tests in model scale is required. According to Van Manen and Van Oossanen (1988) the first recorded use of a turbulence stimulation device happened in 1922 in connection with tests in a wind tunnel. Three years later in Berlin, a similar device was utilized in ship model testing for the first time recorded.

By performing a brief familiarizing on the field of turbulence enhancement, one would quickly learn that several methods or mechanisms are utilized in order to achieve a turbulent boundary layer in model experiments. Such methods will often vary from an experiment to another, or from test facility to test facility even though similar experiments are carried out. Today, turbulence stimulators are mainly applied on a routine basis according to somewhat vague recommendations, or local standard procedures within each test facility often developed decades ago. Thus, a large development in ship model resistance measurements has occurred since these procedures were established, causing the effects of a partly laminar boundary layer to possibly be more accurately assessed.

By comprehensively study these effects, the usage of turbulence stimulators may be performed on a more scientific basis, making ship model experiments even more accurate. This may be highly favorable if the *competition* between hydrodynamic ship experiments and computational fluid dynamics (CFD) as a validation tool is to be considered. As CFD seems

to be rapidly increasing in both accuracy and ease of use, a larger amount of engineering analyses may be performed with this basis in the future. This trend implies that model basins might see a need for increased accuracy and a deeper knowledge of the uncertainties connected to scaling effects in order to still provide the preferred hydrodynamic validation technique. Amongst these scale effects are definitely the laminar-turbulent transition problem thoroughly described in this report.

1.1 Background and motivation

Today, most new ship designs are tested in a ship model towing tank or ocean basin often located at a research facility or university. When ship designs are tested in model scale Froude scaling is utilized. Meaning that the ratio between inertia and gravitational forces are correctly scaled. The Froude number is defined as

$$Fn = \frac{U}{\sqrt{gL}} \quad (1.1)$$

Where g is the acceleration of gravity, U and L is model velocity and length respectively, thus the Froude number is equal both in model and full scale. The viscous forces relative to inertia forces however may be represented by the Reynolds number, defined as

$$Rn = \frac{\rho Ul}{\mu} \quad (1.2)$$

Here l represents the characteristic length of the object, ρ is the density of the current fluid and μ is the dynamic viscosity. This expression is further simplified by using the definition of the kinematic viscosity as $\nu = \mu/\rho$. Thus the Reynolds number is expressed as $Rn = \frac{Ul}{\nu}$. By introducing the scale parameter $\lambda = L_F/L_M$ the model velocity may be found as $U_M = U_F/\sqrt{\lambda}$ using Froude scaling. Inserting the now Froude scaled velocity and length in equation 1.2 and demanding equality in full scale and model scale yields

$$Rn = \frac{L_F \cdot U_F}{\mu_F} = \frac{\frac{L_F}{\lambda} \cdot \frac{U_F}{\sqrt{\lambda}}}{\mu_M} \quad (1.3)$$

Solving equation 1.3 with respect to the kinematic viscosity gives the expression $\mu_M = \lambda^{-3/2} \mu_F$. As ship model tests obviously are performed in water, it is under no circumstances feasible to alter the viscosity to obtain an equality in Rn between model and full scale. Thus, it is clear that a proper scaling of both gravitational and viscous forces in model experiments is impossible. If only a proper Reynolds scaling was to be performed for ship models, it is evident by examining equation 1.2 that model velocities would rapidly arise to highly impractical and infeasible values. As a consequence, the Froude scaled ship models will experience a much

lower Reynolds number than the full scale ship.

A most important consequence of the high inertia forces compared to viscous forces is the development of turbulence. For a full scale ship, where the length based Reynolds number is typically in the order of 100 times larger than in model scale, the flow rapidly evolves from laminar to turbulent following the ship leading edge. In model scale however, the low Reynolds number will lead to a risk of experiencing a partly laminar flow over large parts of the ship model surface. This inaccurate representation of the flow in model scale will then result in a false depiction of reality, as the frictional forces are highly dependent of the flow characteristics to be laminar or turbulent. As a result of this physical phenomenon turbulence must be enhanced in model experiments in order to obtain a turbulent flow field resembling that of a full scale ship. Figure 1.1 gives a good impression of the flow in terms of laminar or turbulent in the flow field around a ship.

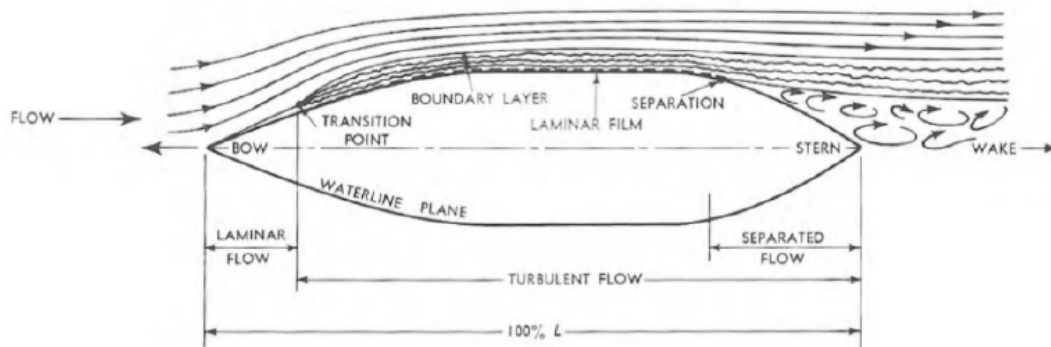


Figure 1.1: Flow field around a ship, from Gillmer and Johnson (1982).

By performing simple calculations it is evident that turbulence stimulation devices are a necessity in ship model testing. According to Munson et al. (2013) transition from laminar to turbulent flow in a free stream occurs in the range $2 \cdot 10^5 < Rn_x < 3 \cdot 10^6$. Where Rn_x is the length based Reynolds number. Then, the critical length before transition occurs, x_{crit} , may be given by

$$x_{crit} = \frac{Rn_x \nu}{U} \quad (1.4)$$

This length is now determined in the following example. By assuming $Rn_{xcrit} = 3 \cdot 10^5$ (a rather conservative approach in this context) and inserting a variety of typical ship model velocities x_{crit} is obtained. See table 1.1 for the results. Here x_{crit} is assumed to be approximately equal to the length of the laminar region over the ship model. The results are compared to a ship model length of 6 meter. Thus, it is clear that a substantial amount of the ship model surface will experience laminar flow for a large range of velocities if no turbulence stimulation is applied.

Today a variety of turbulence stimulation methods is in use in day to day ship model testing, and the International Towing Tank Committee (ITTC) provides recommended standard

U [m/s]	0.3	0.5	0.7	0.9	1.1
Fn [-]	0.039	0.065	0.091	0.117	0.143
x_{crit} [m]	1.08	0.65	0.46	0.36	0.29
<i>Part laminar</i>	18 %	10.8 %	7.71 %	6.0 %	4.9 %

Table 1.1: Example results showing the extent of laminar region if no turbulence stimulation is applied.

procedures for applying turbulence stimulation on ship models (ITTC, 2011). Herein is the recommended location of such stimulation devices well identified. However, little specification of the preferable stimulation method is given. Further, much of the available research on different turbulence stimulation techniques were performed over half a century ago. Notable contributions are here Hughes and Allan (1951) and Hama (1957). Up to this day, much of the practice dealing with turbulence stimulation is heavily based on such studies. It is fair to say that a certain development in ship model testing has taken place since the 1950's. Mainly connected to the ship model surface material itself and improved accuracy in measurement techniques. Hence a new and modern study on the field of turbulence stimulation was sought after.

The main objectives of this thesis may be summarized as follows:

- To provide insight in the process of laminar-turbulent transition and the role of turbulence stimulation devices in this context.
- Present an overview of the most used stimulation methods today, and determine each method's characteristics both theoretically and experimentally.
- Provide a quantitative comparison of the methods and following estimate the most preferable method in ship model testing.

1.2 Scope of work

In the present report, stimulation devices mainly relevant for ship models related to ship models has been studied. Thus disregarding the questions related to transition problems for and appendices and propeller model testing. However, the reader should note that key concepts discussed in this thesis are still valid for both ship models and propellers, as well as any other object subjected to a fluid flow.

In addition to give a brief overview of the theoretical aspects considering turbulence stimulation, ship model experiments was conducted as part of the work with this thesis. Two relatively similar ship models, but with largely different scaling factors were fitted with different turbulence enhancement devices and tested in a towing tank. Due to limitations in

both time and available budget no efforts to determine the flow characteristics, but visual observations, were made. Thus any discussion and conclusion made in this thesis are solely based on total resistance measurements in combination with relevant theoretical aspects.

1.3 Thesis outline

This present report follows a classical scientific structure. Firstly, the background and motivation behind the performed work is presented. Further, a brief overview of the essential theoretical aspects for this topic of study is given. An introduction to the most utilized turbulence stimulation techniques today is then provided before the experimental procedures are discussed. Experimental results are then presented in chapter 5, while the theoretical resistance predictions are given in chapter 6. A comparison of the experimental and theoretical results then follows, before a thorough discussion is presented in chapter 8. At last concluding remarks are drawn and recommendations for further work are given.

Chapter 2

Theoretical Background

2.1 Ship resistance and model testing

In order to determine the required power of a ship design newly developed or in development, a designer must assess the performance of the ship. A governing parameter then, is the current total ship resistance. Ship resistance may be divided into pressure and frictional components. Then the total ship resistance may be regarded as a sum of the tangential shear force (friction) and normal pressure forces acting on the wetted surface of the hull. By considering the ship resistance from an energy dissipation point of view, the resistance is considered as the sum of the energy scattered in the wake and the energy used to create propagating waves (Molland et al., 2011). The latter is known as ship wave making resistance. See figure 2.1 for a detailed overview of ship resistance coefficients.

The viscous forces (mainly friction) dominate over the pressure forces in magnitude. This is especially true for tankers and container ships, which operate at a low Froude number and large submergence. For these vessels frictional forces comprise about 60-70 % of the total resistance (Larsson et al., 2010). Ship performance will not be treated much further in this report, however it is important to be aware of the magnitude of the frictional resistance relative to other resistance components. The theoretical aspects dealing with frictional resistance is also important to grasp, as this is extensively used throughout this report. For a more in-depth description of ship resistance and performance see for instance Molland et al. (2011) or Tupper (2013).

To predict the full scale resistance of a ship, model tests are carried out in towing tanks or ship model basins. The in-depth description of a ship model test procedure and extrapolation of results to full scale will not be considered thoroughly here, see e.g Steen (2014b) for a more extensively description of this. Some aspects related to determination of resistance components is however worth mentioning. When extrapolating the model resistance to full scale it is convenient to use dimensionless resistance coefficients. By neglecting air and base drag resistance, the total ship resistance could be represented in the following way (see also

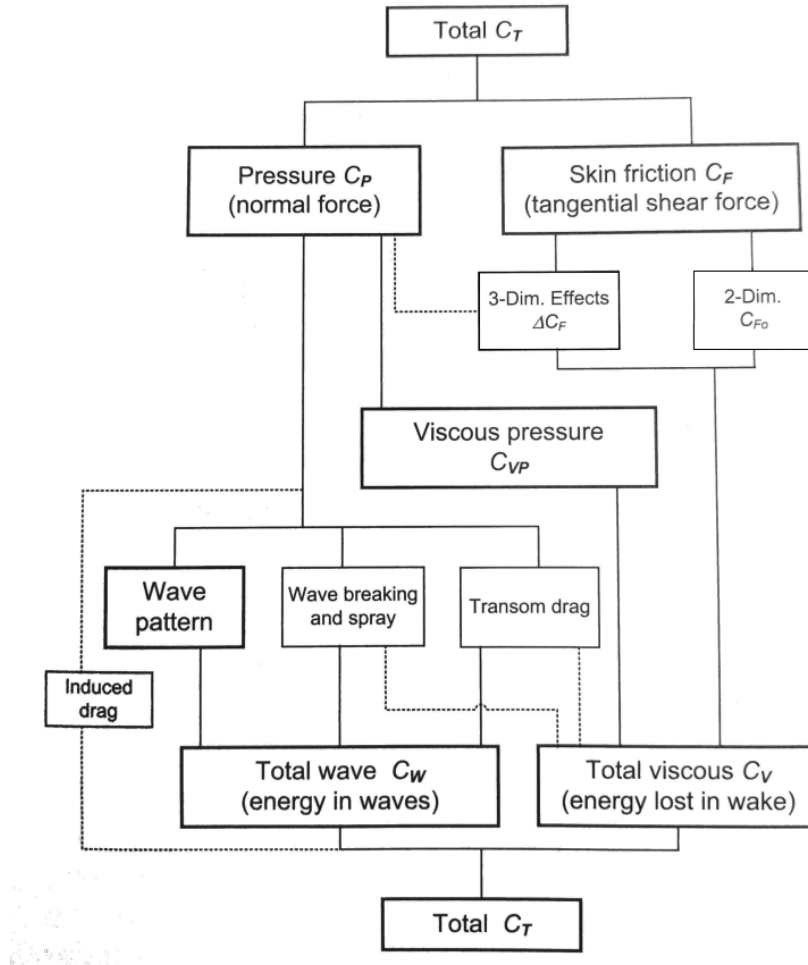


Figure 2.1: Resistance components of a ship, from Molland et al. (2011).

figure 2.1)

$$C_{Ts} = (C_{Fs} + \Delta C_F)(1 + k_f) + C_R + C_A \quad (2.1)$$

Where C_{Fs} is the frictional coefficient of the ship, ΔC_F is the roughness allowance of the hull, k_f is a form factor that accounts for three dimensional effects of the ship hull, C_R is the residuary resistance coefficient determined from model tests and is mainly due to energy dissipation through wave making. C_A is an empirically determined correlation allowance which aim is to correct the result for any scale effects or other uncertainties connected to the model testing. Then, the total full scale resistance is now determined as

$$R_{Ts} = \frac{1}{2} \rho S U^2 C_{Ts} \quad (2.2)$$

Where S represents the wet surface of the ship hull, U corresponds to the ship speed.

The frictional coefficient, C_F , greatly depends on whether the flow is laminar, turbulent or transitional. This physical phenomenon is more carefully discussed in later sections, but

from an engineering point of view it is of importance to be aware of the large difference in expected skin friction between a laminar and turbulent flow field. See figure 2.2 for an illustration of this difference. Here friction lines for laminar flow (Blasius line) and turbulent flow (Prandtl-Von Karman line) is shown, as well as typical lines for a transitional flow characteristic. The friction line mostly used today, both in model and full scale, is the ITTC-57 friction line given by

$$C_F = \frac{0.075}{(\log Rn - 2)^2} \quad (2.3)$$

Where Rn is the length based Reynolds number given by equation 1.3, corresponding to either full scale or model scale values. The ITTC-57 friction line is valid for a fully turbulent flow field, emphasizing the importance of a turbulent flow field in model testing. For the discussion and full derivation of this formula see ITTC (1957). It is worth to mention that this friction line is intended as an interim solution for practical engineering purposes only, such as ship power predictions from model experiments. The ITTC-57 line is specially designed to give a good correlation between model scale and full scale (Steen, 2014b). It is therefore believed that the Prandtl-Schlichting line given by Schlichting (1968) is better in order to capture the physical effects. Therefore the Prandtl-Schlichting turbulent friction coefficient is further used in this report. This friction line is calculated as

$$C_{F_{turb}} = \frac{0.455}{(\log Rn)^{2.58}} \quad (2.4)$$

For comparison the Blasius total skin friction coefficient is given by

$$C_{Flam} = \frac{1.328}{\sqrt{Rn}} \quad (2.5)$$

This laminar friction line is according to Larsson et al. (2010) one of the few viscous flow cases where an analytic solution exists.

2.2 Viscous flow and transition to turbulence

In order to fully comprehend what the frictional resistance really is, one should be aware of the fundamental fluid mechanics at play. Some of this basic theory might seem trivial, however it is of great importance in order to fully describe the environment experienced by a ship model. This present section aims to define some key concepts of viscous fluid flow and determine parameters used in further flow description. Most of the knowledge presented herein is obtained from the introductory fluid mechanics book by Munson et al. (2013), or from the somewhat more advanced book on viscous fluid flow by White (2006).

Viscosity is defined as the fluid property that relates shear stress, τ , to fluid motion, u , v and w . The shear stresses occur both between fluid particles themselves, and a particle and the

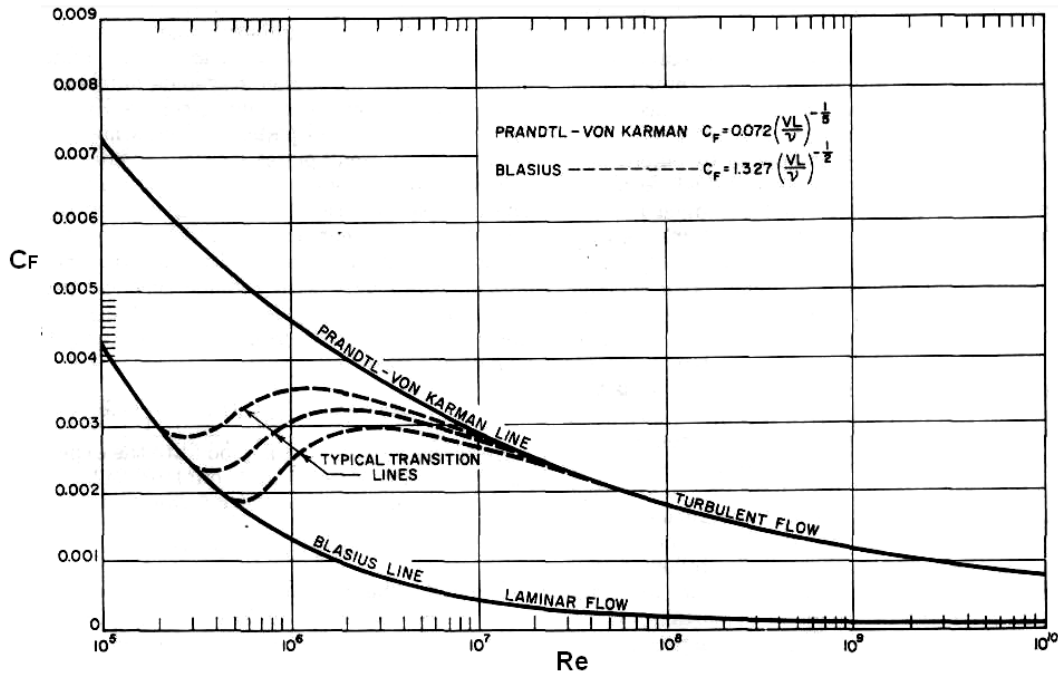


Figure 2.2: Friction lines as function of Reynolds number, for laminar and turbulent flow, from Lewis (1988).

surface of a body subjected to the viscous flow. A physical consequence of this is the *non-slip condition* which states that for a body in a viscous flow there is no fluid particle velocity at the surface of the body. Then, as a consequence of the stream velocity and the shear stress between the particles a rotation in the flow will occur as adjacent particles along the y -axis (normal to the wall) will experience different velocities. At a certain point along the y -axis there will be a negligible rotation, and the flow velocity at this point will be more or less equal to the free stream velocity. The distance between the body surface and this specific point is known as the *boundary layer*, with a boundary layer displacement thickness noted δ . Inside this layer viscous effects are of great importance. Outside the boundary layer viscous effects plays a minor role. In general, for large Reynolds number the boundary layer is relatively thin, and according to Molland et al. (2011) the boundary layer of a ship model is about twice as thick as the corresponding full scale boundary layer when allowing for scale of course. Hence, models are more prone to boundary layer effects than full scale ships. See figure 2.3 for a definition of the axes in play, as well as illustrations of typical velocity profiles in a boundary layer. The turbulent boundary layer velocity profile is both flatter at the wall and slightly thicker than in the case of a laminar boundary layer.

The shear stress created between the body surface and the viscous flow will lead to what is known as friction drag, D_f . This will together with pressure drag give the total drag of the

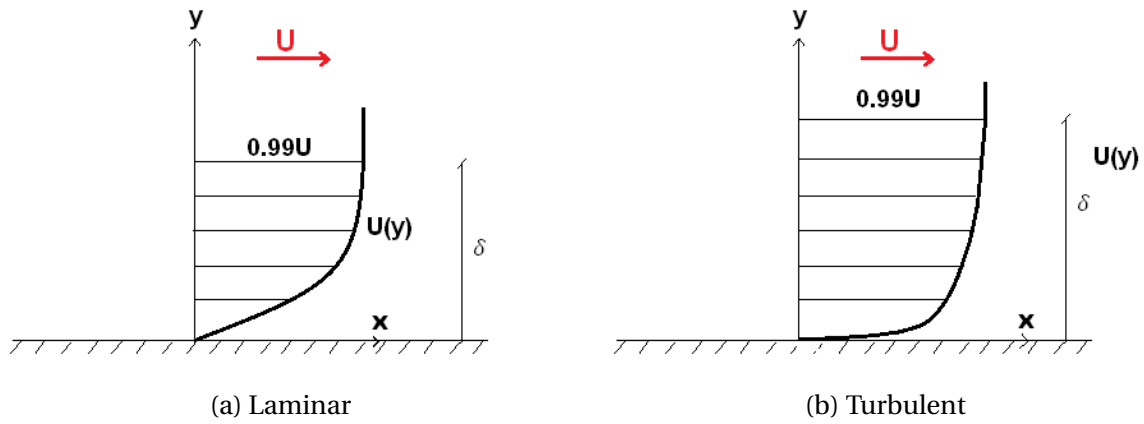


Figure 2.3: Typical velocity profiles of a laminar and turbulent boundary layer.

body, given in the following equation

$$D = \int dF_x = \int p \cos \theta dA + \int \tau_w \sin \theta dA \quad (2.6)$$

Where F_x is the total force component in the longitudinal direction, θ is the inflow angle relative to normal of the body surface, p is the pressure that causes normal stress on the surface and dA is an area element on the body surface. According to White (2006) the shear stress in a two dimensional steady flow is given by

$$\tau = \mu \left(\frac{\partial u}{\partial y} + \frac{\partial v}{\partial x} \right) \quad (2.7)$$

Where μ is the dynamic viscosity, u is the fluid velocity in longitudinal direction (x-direction) and v is the fluid velocity in outward direction (y-direction). Assuming a more or less steady flow it is now fair to say that $\frac{\partial u}{\partial y}$ is much larger than $\frac{\partial v}{\partial x}$ (see also figure 2.3), according to White (2006) it will be two orders larger. Thus, it is reasonable to write the shear stresses at the wall as

$$\tau_w = \mu \left(\frac{\partial u}{\partial y} \right)_{y=0} \quad (2.8)$$

2.2.1 Laminar and turbulent flow

Under almost any real life conditions the flow situation is a rather complex three-dimensional and time-dependent situation. The velocity of a fluid particle at a certain position (x, y, z) and time t may be expressed as

$$V = V(x, y, z, t) = ui + vj + wk \quad (2.9)$$

Here u, v and w is the flow velocity components in respectively x, y and z direction. The assumption that one of the velocity components is smaller relative to the other two is often a reasonable approach. In this way the problem is reduced to a two dimensional flow. Now,

as an expression for the velocity is established, it is natural to assign the flow into the two categories steady or unsteady flow. For a steady flow the velocity components at a certain point does not vary in time, thus $\frac{\partial V}{\partial t} = 0$. Most flow situations however tend to be unsteady with either a periodic or random variation in velocity.

This leads to the more useful classification of a flow as either turbulent, laminar or transitional. If the unsteadiness is of a random, irregular and non repeatable character the flow is said to be turbulent. As opposed to a laminar flow that flows smoothly, with only minor fluctuations in velocity if any at all. The first distinguishing between laminar and turbulent flow was documented by Reynolds (1883), in his later so famous experiment involving flow in a pipe. Reynolds established that the characteristics of a flow is dependent on a dimensionless parameter giving the relationship between inertia and viscous forces, previously defined in equation 1.2 as the Reynolds number. The properties of laminar and turbulent flows and their different effect on a body subjected to the flow is further discussed in the following subsections.

Laminar flow

As described in the previous section laminar flow is characterized as a "smooth and steady" flow. More theoretically, laminar flow occurs when the fluid flows in parallel layers and there is no cross-currents perpendicular to the direction of the flow. In the case of a ship model, water particles will flow entirely parallel to the model hulls surface. Thus, the flow velocity only varies from one streamline to the next. This variation in velocity, known as the velocity gradient, combined with the water viscosity will generate wall shear stress and following drag force as described in equations 2.6 to 2.8. In the laminar boundary layer the velocity gradient is close to constant, causing the velocity profile in the boundary layer to resemble a straight line. This is also indicated in figure 2.3a.

Turbulent flow

Turbulence in a flow regime is characterized by a chaotic and random fluctuation in several flow parameters including the dynamic pressure and all three velocity components. It is in such a way a contrast to the ordered laminar flow. In any practical situation turbulent flow is more likely to occur than laminar flow. However, due to its complexity, turbulence still remains the least understood area of fluid mechanics, at least according to Munson et al. (2013). In figure 2.4 the time dependent axial velocity component of a typical turbulent flow $u(t)$ is shown. Evidently random fluctuations occur, thus in order to describe the flow velocity at any given time a mean value must be established. This is done in the following way

$$\bar{u} = \frac{1}{T} \int_{t_0}^{t_0+T} u(x, y, z, t) dt \quad (2.10)$$

Where T is the time interval considered. Then the value u' is defined as the fluctuating part of $u(t)$, see again figure 2.4 for an illustration of these parameters. According to White (2006) these fluctuations may be up to 11 % of the free stream speed. Following, the axial velocity component of the flow may be written as

$$u = \bar{u} + u' \quad (2.11)$$

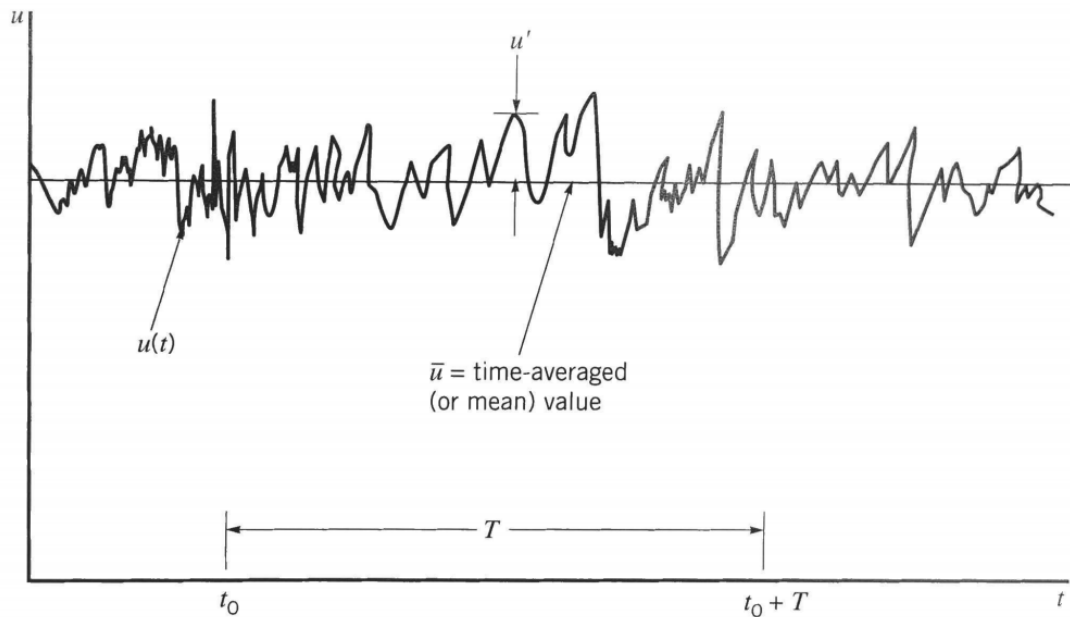


Figure 2.4: A realization of the velocity in a turbulent flow (Munson et al., 2013).

As the structure of a turbulent flow often varies, it could be useful to define certain parameters describing the turbulent flow in addition to the mean and fluctuating values. One such parameter is the *turbulence intensity*, describing the level of turbulence in a flow. This is defined as

$$\rho = \frac{\sqrt{\overline{(u')^2}}}{\bar{u}} \quad (2.12)$$

Thus, a larger turbulence intensity yields higher fluctuations in velocity or any other flow parameters such as pressure and shear stresses. According to Munson et al. (2013) typical values are $\rho \geq 0.1$. Another parameter describing turbulence is the velocity fluctuating period. The frequency of fluctuations will differ from a flow situation to another, but is estimated to be in the order of 10, 100 or 1000 cycles per second for a flow regime involving water at moderate speeds (Munson et al., 2013).

As a turbulent flow consists of several turbulent eddies or vortices, the fluid particles will be transported across several velocity layers inside the boundary layer. A fluid particle moving from a low axial velocity layer outward in y -direction to a higher velocity will be accelerated by the fluid in the upper plane. Similarly, a particle moving downwards in the boundary layer

will be slowed down. This will cause a momentum flux in the axial direction across these layers, giving rise to a shear force between the layers. In a turbulent flow the mixing of flow layers is certainly greatly increased compared to a laminar flow, where mixing only occurs on a molecular level, hence turbulent shear stress greatly exceeds the one found in a laminar flow.

The velocity components responsible for the mentioned momentum transfer and following shear stress, are u' and v' . Where v' is the fluctuating velocity component in the direction perpendicular to the flow (y-direction), thus this is the most important parameter for the rate of mass transfer crossing each plane. The shear stress on a plane in a turbulent boundary layer is then expressed as

$$\tau = \mu \frac{\partial \bar{u}}{\partial y} - \rho \overline{u'v'} \quad (2.13)$$

The latter term, known as the *Reynolds stress*, will always be positive as u' and v' have opposite signs. It is clear that if either u' and v' (or both) are zero, corresponding to a laminar flow, equation 2.13 is reduced to equation 2.8 providing the shear stress in a laminar flow. Near the body surface one might be tempted to think that the velocity fluctuations is dropping rapidly towards a zero value considering the non-slip condition. This is however only true for \bar{u} , as turbulence is quite resistant to wall damping effects. According to White (2006) studies have shown that significant fluctuations occur even at $y/\delta = 0.0001$.

Considering equation 2.6 it is obvious that an object placed in a turbulent flow will, due to the increase in flow shear stress, experience larger frictional force than in the case of laminar conditions. The laminar wall shear stress, τ_w , is clearly given from equation 2.8. The wall shear stress in a turbulent flow however has no precise expression. This is due to a lack of knowledge concerning the velocity gradient close to the the wall in a turbulent flow. It is therefore necessary to make use of certain empirical relationships when predicting or otherwise dealing with turbulent wall stresses and following drag force. Such an expression would be the friction lines given in equations 2.4 and 2.3.

2.2.2 Transition from laminar to turbulent flow

In this section the transition in flow characteristics, from laminar to turbulent, over an immersed body will be discussed. In available literature regarding laminar-turbulent transition a flat plate submerged in a fluid is often preferred as an example explaining the physical aspects of the process. This is comparable to several practical situations, including that of a ship model in a towing tank. The parameter governing transition to a turbulent flow is the Reynolds number based on a distance, x , starting from the leading edge of the plate (or any other structure). The Reynolds number is then given by

$$Rn_x = \frac{Ux}{\nu} \quad (2.14)$$

The value of Rn_x where transition occurs is referred to as Rn_{xcrit} . The determination of this value is not straight forward, and according to White (2006) there is no theory of transition. However several experimental approaches have been carried out aiming to predict the onset of turbulence and distinguish how different flow parameters affect the transition. However, the value of Rn_{xcrit} is found to be a function of the following parameters: pressure gradient, freestream turbulence, wall roughness, Mach number, wall suction/blowing and wall heating/cooling. According to Schlichting and Gersten (2016) the parameters of most importance are the pressure distribution of the outer flow, traits of the wall (roughness and curvature) and level of disturbances in the outer flow. These parameters may easily be thought of as conditions that may be subject to change in ship model experiments. For instance the pressure distribution is given by the model geometry and background turbulence could be a function of waiting time between runs. According to Munson et al. (2013) the value of Rn_x which turbulent transition occurs is given in the interval of

$$2 \cdot 10^5 < Rn_{xcrit} < 3 \cdot 10^6 \quad (2.15)$$

According to White (2006) any laminar-turbulent transition is a consequence of an instability in the flow field. These instabilities are due to small disturbances imposed on the laminar boundary layer flow and will be further discussed in the following sections. However, this leads to the fact that laminar-turbulent transition is not instant, but occurs over a region of the immersed body. According to Schlichting and Gersten (2016) the regions may be divided into a laminar flow region, instability region, intermittency region and, at last, a fully turbulent region.

Natural transition

Based on the mentioned existence of Rn_{crit} any initially laminar flow around a body, with a free stream velocity and kinematic viscosity, will eventually become turbulent provided that the body's dimensions are large enough. This process without any form for turbulence enhancement is referred to as a natural transition to turbulence, and is briefly elaborated in the following section. For an in-depth analysis of the turbulent transition process see e.g Schlichting and Gersten (2016) or White (2006), these are also the main literature upon which the present brief discussion is based.

Again the example of an immersed flat plate, this time of infinite length, with an incoming freestream velocity, U , parallel to the plate is utilized. Close to the leading edge the boundary layer will always be laminar due to low Rn_x values. Then further downstream as Rn_x ap-

proaches Re_{crit} the almost infinitesimal initial disturbances always present in a laminar flow will develop into initial flow instabilities. These instabilities will occur as two dimensional waves known as Tollmien-Schlichting waves, named after the scientists who first studied them. These first indications of laminar flow instability will quickly start to show a span-wise variations and thus three dimensional effects occur. One should note that at this point the flow is still mainly laminar, with the disturbances superimposed in the flow. Then as three dimensional waves develop, vortices are formed. These are simply known as Λ -vortices due to their shape (see region 2 in figure 2.5). From now on the transition process is more of a breakdown than a growth process as the Λ -vortices begins a cascading collapse into smaller units. This collapse happens with a random frequency and leads to an intense change in local velocity and pressure. The next step is now the formation of so called turbulent spots. These spots are growing and spreading rapidly in time and will eventually entrain the laminar flow. The flow is said to be fully turbulent when the spots continually exists and prosper in time. A consequence of transition to turbulence is a strong increase in boundary layer thickness and change in velocity gradient. Meaning that the time averaged velocity profile illustrated in figure 2.3 will cast aside the almost linear shape valid for a laminar flow.

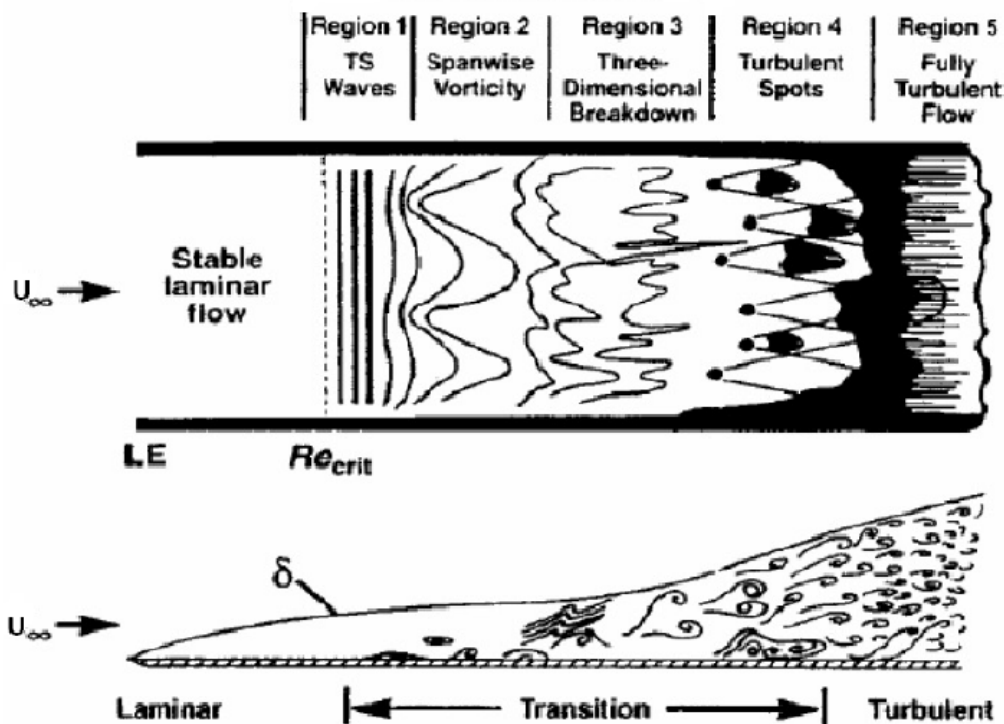


Figure 2.5: The process of transition to turbulence from Schlichting and Gersten (2016)

As mentioned, there is no theory of transition, thus the described process is solely based on observations from experiments. However, it is now clear that transition is due to disturbances in the laminar flow. When assessing the onset of transition, the question is then if

these disturbances will die out (flow remains laminar) or grow in time (transition could occur). By utilizing this fact, a stability theory of laminar flow can be developed. This theory is then used to determine Re_{crit} , also named the indifference Reynolds number in Schlichting and Gersten (2016).

The instability of the laminar boundary layer may be assessed by the so called *Orr-Sommerfeldt* equation.

$$(U - c)(\phi'' - \alpha^2 \phi) - U'' \phi = -\frac{i\nu}{U_m \delta} (\alpha^4 \phi - 2\alpha^2 \phi'' + \phi''''') \quad (2.16)$$

Where $U = U(y)$ is the mean component of the velocity in x-direction within the boundary layer, U_m is the maximum velocity of the main flow. As δ represent the boundary layer thickness, it is clear that the term $\frac{i\nu}{U_m \delta}$ may be written as $\frac{i}{Re_\delta}$. The dimensionless disturbance is given by $\phi = \phi(y)$. The disturbances are described as waves with wave number α and phase velocity c given by

$$c = c_r + ic_i = \frac{\beta}{\alpha} \quad (2.17)$$

Where $\beta = \beta_r + i\beta_i$ is the complex frequency of the disturbance, thus β_r is the circular frequency. When β only consists of the real part ($\beta_i = 0$) the disturbance travels with constant amplitude. When $\beta_i > 0$ the wave (disturbance) amplitude grows exponentially, meaning that we have an unstable flow and transition will occur. If $\beta_i < 0$ the disturbances will decay and the flow is said to be stable. These disturbances are interpreted as either disturbances purposely initiated or naturally present in the flow, the latter will always be true for a laminar flow although the initial disturbances are infinitesimal. In equation 2.16 Re_δ is considered to be given and α to be specified. Then by applying the boundary conditions $\phi(y=0) = \phi(\infty) = \phi'(0) = \phi'(\infty) = 0$ (due to the presence of the boundary layer) the equation may be solved to obtain $\phi(y)$ and the complex phase velocity c , corresponding to each pair of Re_δ and α . Then from the value of c_i it is possible to investigate the stability in a similarly way as for β_i .

The derivation of equation 2.16 is based on Reynold's hypothesis that the laminar solution of the Navier-Stokes equation always is a possible solution, but becomes unstable above a definite limit. The reader is advised to consult White (2006), Schlichting and Gersten (2016) or Kristiansen (2017) for the complete derivation of equation 2.16. In this report the Orr-Sommerfeldt equation is not further discussed, however, it serves as an example of how transition to turbulence may be assessed on a higher and more complex level than the approach utilized in this study.

Stimulated transition

As mentioned in previous sections, there are several parameters affecting the laminar-turbulent transition. The by far most practical and efficient parameter one could alter in a ship model experiment is the wall roughness. According to Schlichting and Gersten (2016) the wall

roughness is of considerable practical importance, but unfortunately rather inaccessible to theoretical treatment. However, its effects on transition are well studied through experiments. Results show, as one could expect, that the introduction of a roughness element will in general cause earlier transition due to the additional disturbance imposed to the boundary layer flow (Kristiansen (2017)).

According to White (2006) roughness elements should be categorized into two-dimensional and three-dimensional geometries. Examples of the first are a wire or a cylinder stretched across the flow, the latter category includes a sphere, a spike or just a single grain of sand. Two- and three-dimensional roughness elements will affect the flow quite differently. In the case of the two-dimensional wire, vortex shedding will cause a wake similarly to that behind a cylinder in a flow (see figure 2.6). Then the wire wake will cause disturbances which increases the growth rate of the Tollmien-Schlichting waves, thus shortening the transition length drastically compared to a natural transition. As a two-dimensional roughness element will produce disturbances only in its immediate wake, the wake behind a three-dimensional element will cause a larger zone of disturbances spreading in space. If the roughness height is sufficiently large the flow downstream of a three-dimensional roughness will resemble a wedge of continuous turbulence (White (2006))

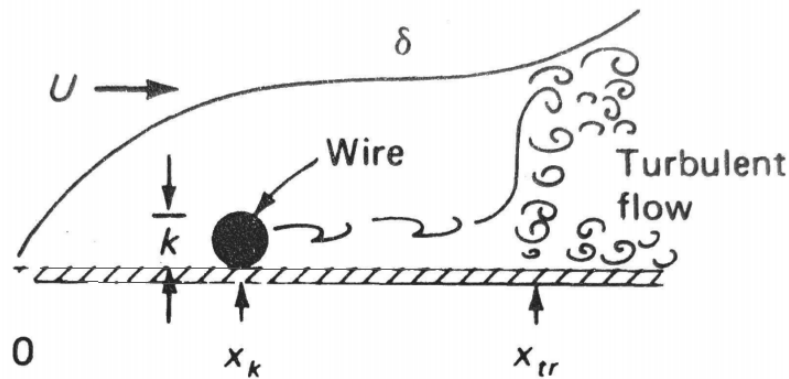


Figure 2.6: Tripwire in flow, from White (2006).

When assessing a stimulation device certain parameters describing the roughness are useful. The ratio between wire diameter, k , and local boundary layer thickness δ at the location of the roughness is such a parameter. If the wire diameter is much smaller than δ the device will have little or no effect on the transition process. According to White (2006) a tripwire will not have a significant effect until either the free stream velocity or wire diameter increases to produce $\frac{\delta}{k} > 0.3$, then the point of transition for a smooth wall will move towards the location of the tripwire. Another parameter describing the roughness' ability to generate turbulence is the roughness based Reynolds number defined as

$$Rn_k = \frac{u(k)k}{\nu} \quad (2.18)$$

Where $u(k)$ is the longitudinal velocity component at the roughness height. In the available literature regarding turbulence stimulators a limit for Rn_k is often given for each stimulation device to be fully effective. Therefore, this seems as a good indication of each turbulence stimulators ability to generate turbulence. In this way the roughness Reynolds number allows for a theoretical comparison of different stimulation mechanisms.

Chapter 3

Turbulence Stimulation

As thoroughly described by Gad-el Hak (2000) there are several ways to either suppress or enhance turbulence in a flow field, and both active or passive methods may be used for this purpose. Active methods such as wall vibration, sound wave injection or flow acceleration is not feasible in ship model testing as they would either be too complicated or interfere with the experimental set up in a too large extent. Passive methods such as change in pressure gradient by altering geometry is obviously not appropriate as the geometry in question is the very subject of the experiment. Thus, additional roughness is the only acceptable method of turbulence enhancement in ship model testing. This section will cover the existing routines connected to turbulence stimulation used in test facilities today, as well as present the main stimulation mechanisms.

According to Van Manen and Van Oossanen (1988) the use of turbulence stimulation on ship models was first recorded in 1925 by the towing tank in Berlin. Here a tripwire with 0.9 mm diameter was placed vertically around the hull at 5 percent of the ship's length behind the forward perpendicular. By 1933 this had come into general use in the Berlin tank. Since then turbulence stimulation research developed several different stimulation mechanisms. When searching for literature enclosing this subject, one will find that extensive research was done on turbulence stimulation both in towing tanks and wind tunnels in the 1950's. However, still today the type of stimulator utilized and the corresponding placement on the model hull seem to vary from a ship model testing facility to another. This is supported by Murphy (2010) who states that there is no firm procedure for determining the location, type or amount of turbulence stimulation used in ship model testing today. Available guidelines are further limited and primarily based on empirical approaches at best.

3.1 ITTC-guidelines

The current ITTC recommendations regarding turbulence stimulation on ship models and propellers is the third revision of the model manufacture procedures found in ITTC (2011).

The recommendation is somewhat vague as it states that all models should be fitted with *recognized* turbulence stimulator devices. Three kinds of such devices are then mentioned as tripwires, studs and sand strips. These stimulation devices will together with the Hama strip be thoroughly presented in the following sections.

The recommendations gives a location of 5 % of the ship L_{PP} aft of the leading edge as the preferred location. Also, ship models with a bulbous bow should be fitted with additional stimulators, typically at $\frac{1}{3}$ of the bulb length from its fore end. The bulb shape should also be taken in consideration as, in the case of an S-formed bulb, stimulators should be applied short before the pressure gradient becomes positive. An expectation from the mentioned ITTC-guidelines is when high-speed models are tested. Then, according to ITTC (2017a) great care has to be taken in the placement of the stimulators. It is even recommended that a set of test runs is carried out if there are any doubts about the placement of the stimulators.

There are currently no recommendations for turbulence stimulation in the case of propellers. However a remark of the necessity of turbulence stimulation in cavitation tests is found in the guidelines.

3.2 Studs

Studs are small cylindrical or square objects pinned to the ship model hull, as seen in figure 3.1 and 3.2. The basic principle is that the studs will generate three dimensional unsteady vortex structures which then rapidly grows into turbulence. See figure 3.2b for the three dimensional vortex structures created by a stud. The effect of size and spacing of the studs was

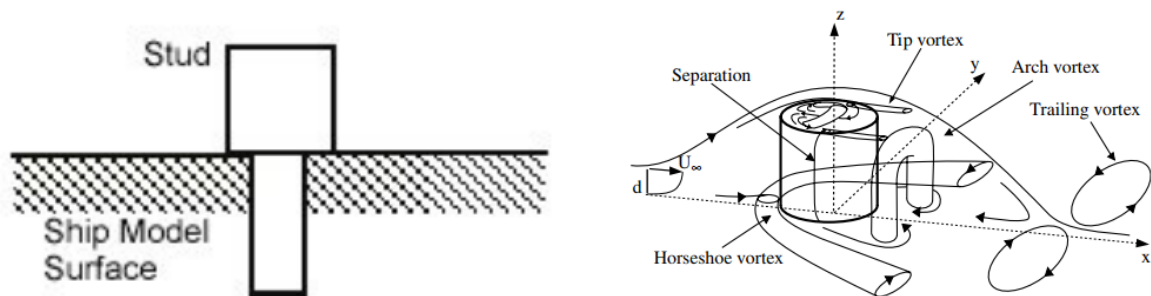


Figure 3.1: Studs on a ship model (Murphy (2010)).

comprehensive studied by Hughes and Allan (1951). They concluded that the diameter and

projection of the pins should be relatively large in order to ensure that turbulence is established immediately. Murphy and Hearn (2007) reports that the roughness based Reynolds number should at least exceed 500 for a stud to be effective in causing a turbulent transition. According to Larsson et al. (2010) a typical stud height is 2.5 mm with a diameter of 3 mm. This corresponds well with the recommendations given in ITTC (2017b) where the typical stud diameter is put to between 1.6 and 3.2 mm with a height of 0.5 to 3 mm.

Following, the studs should be placed parallel to the stem of the ship model or the otherwise leading edge of the test subject. When it comes to the location of the studs ITTC guidelines refer to Hughes and Allan (1951) which presented a figure where the location is given based on model length and bow geometry (see figure 3.3). Larsson et al. (2010) states that if studs are placed too close to the stem there is a risk of relaminarization of the boundary layer if the pressure gradient is favorable. This phenomenon could also come about if the spacing between the studs is too large. In Hughes' experiments a spacing of 25 mm was utilized and, in general, recommended by ITTC for the further use of studs.



(a) Normal installation of studs on a ship model (Murphy and Hearn, 2007). (b) Flow around a stud from Pattenden et al. (2005).

Figure 3.2

As all turbulence stimulation devices the pins will introduce an additional drag resistance known as parasitic drag. This leads to another parameter to consider when assessing the location of the stimulators. As described by Van Manen and Van Oossanen (1988) and ITTC (2017b) the object is to ensure that the parasitic drag is balanced out by the loss in resistance due to a laminar region in front of the stimulation device, as the friction drag will be less here compared to a fully turbulent flow. This is exactly what Hughes and Allan (1951) tried to do when constructing figure 3.3. For a more analytic calculation method of induced drag by studs see Molland et al. (1994).

Studs are in general considered as a good device for turbulence stimulation. As it is an efficient turbulence enhancer, due to the immediate three dimensionality. However the mounting is somewhat more demanding than other mechanisms as a penetration of the model hull

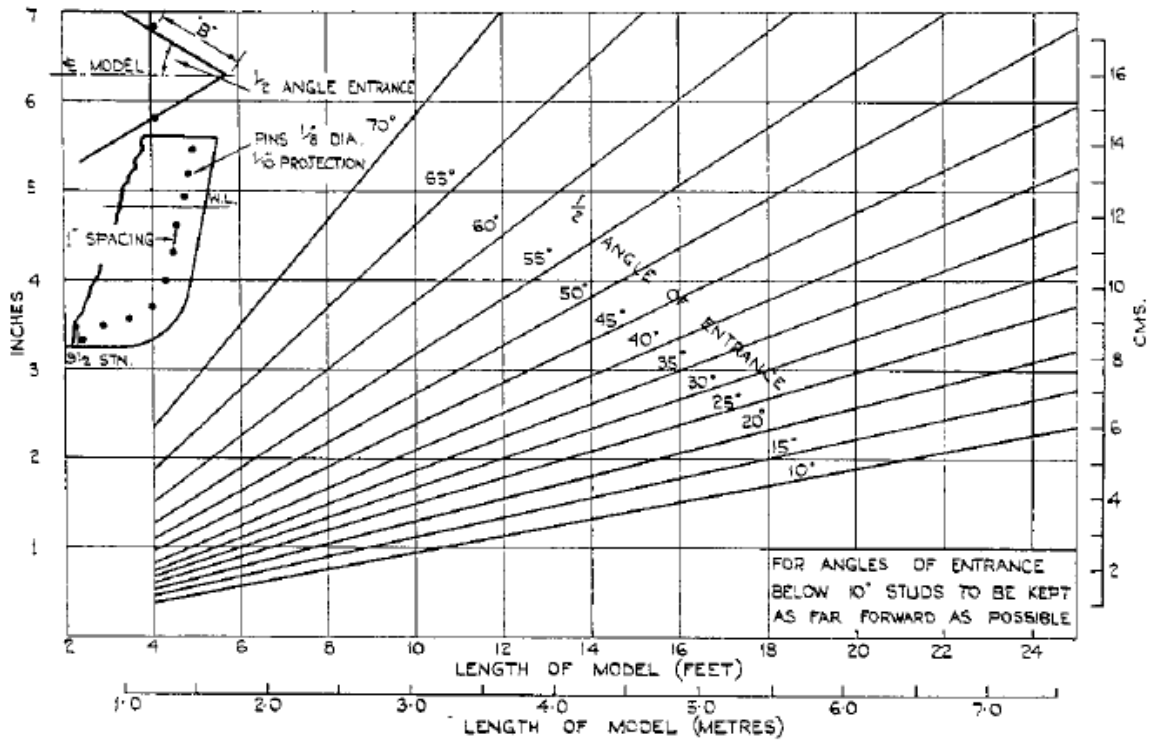


Figure 3.3: Recommended location of studs based on model length and bow angle of entrance (Hughes and Allan, 1951).

is required. The application of studs also includes the consideration of more parameters than other mechanisms, as the height, diameter and spacing must be assessed for each ship model.

3.3 Tripwire

The idea behind a tripwire is to *trip* the laminar flow with a wire perpendicular to the inflow. The ITTC guidelines states that wires should typically be 0.5 to 1 mm in diameter, depending on model speed and location. The wire will generate a two dimensional disturbance which eventually develops into turbulence. (See also section 2.2.2 and figure 2.6).

Several papers has been published regarding the efficiency of tripwires with different size and location, see e.g Hughes and Allan (1951), Smith and Clutter (1959) or Tani and Sato (1956). In the latter the roughness ratio k/δ_k , was found to be the parameter governing the wire's effectiveness in generating turbulence. Here k is the height of the roughness element (wire diameter) and δ_k is the thickness of the boundary layer at the roughness element location. When k/δ_k is small (<0.15), the flow will separate at the wire, but reattach to the model surface at some distance back hardly generating any disturbance. When the roughness ratio is large however (>0.6), transition to turbulence will occur in the separated boundary layer causing the disturbed flow to reattach after only a short distance. A fully turbulent boundary layer is then established soon after the reattachment. See figure 3.5 for the development of the boundary layer velocity profile in each case, along with the developing disturbances

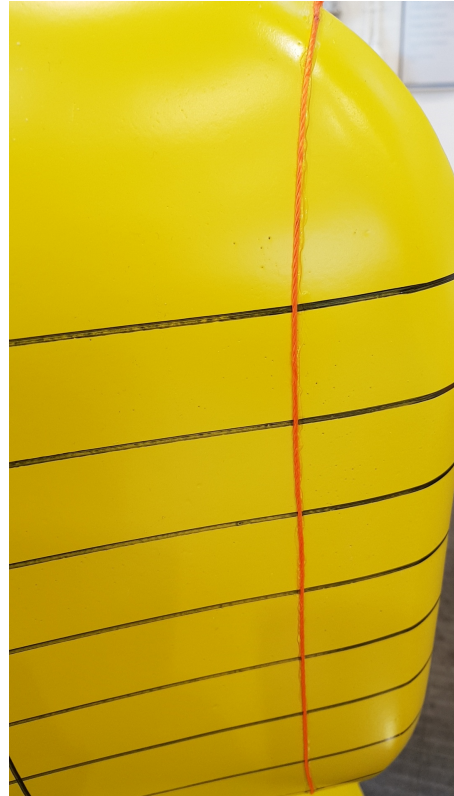
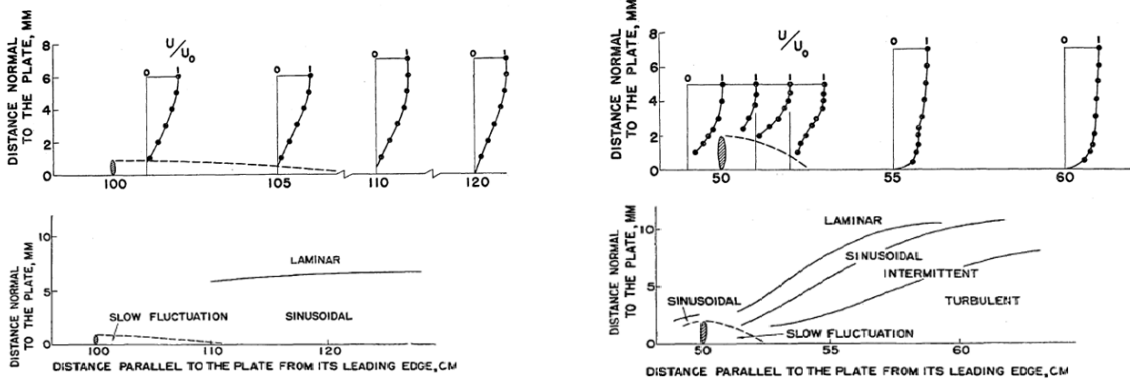


Figure 3.4: Tripwire on a model ship bulb.



(a) Small roughness ratio.

(b) Large roughness ratio.

Figure 3.5: Disturbance and development of boundary layer due to a tripwire (Tani and Sato, 1956).

A wire with a diameter of approximately 1 mm placed around the hull at station 5 percent of the model length is today the standard practice of turbulence stimulation in most towing tanks (Larsson et al., 2010). This is mainly due to the easy mounting procedure, and small required variations from model to model. Thus, not much consideration from the user is required in each case. The tripwire efficiency compared to other devices is an interesting topic to discuss. As the wire introduces two dimensional disturbances, a longer transition region is required before a fully turbulent boundary layer is established, compared to other three dimensional devices. Gibbings (1959) gives the following requirement for a trip wire to be fully effective

$$\frac{Uk}{\nu} \geq 850 \quad (3.1)$$

Where U now is the free stream velocity (outside the boundary layer) and k is the wire diameter. This is supported by McCarthy et al. (1976) who reports that a free stream based Reynolds roughness number between 600 and 1200 will provide a sufficient rise of Tollmien-Schlichting waves to cause a turbulent transition. In Hama (1957) and ITTC (1990) the application of a tripwire on foils is discussed. Both these reports gives $Rn_k > 200$ as a requirement for an effective tripwire, here however, the fluid velocity at the roughness height $u(k)$ is utilized, corresponding to equation 2.18. Similarly, Shen et al. (2015) performed tests on in general axis-symmetric bodies and found $Rn_k = 400$ to be sufficient to trip the flow. This value corresponds well with equation 3.1 as the ratio $\frac{u(k)}{U}$ is given as approximately 0.5 for a wire of 0.9 mm (Shen et al., 2015).

When model velocity increases to the high-speed range the efficiency of a tripwire will reduce. This is because the wire could be a source to ventilation as it provides an open channel to the free surface (ITTC, 2017a). Resulting in fields along the model surface covered by air, undoubtedly leading to a false resistance prediction if experimental results are extrapolated to full scale. Therefore, tripwires are not frequently used on high-speed models. Also, if the

wire diameter is too large, it will affect the global flow. This is of special concern for smaller models such as hydrofoils or other appendages. Therefore tripwires are mostly used on larger ship models of a conventional nature.

3.4 Sand strips

Another three-dimensional turbulence stimulation method is to apply a strip of sand grains or a larger field of sand to the model surface. The term *sand* could seem a bit too general in this case, as according to ITTC (1990) carborundum is often used. Carborundum is also known as silicon carbide, and can be produced to form hard ceramic structures with high endurance (Faltinsen (2006)). This is favorable when it comes to turbulence stimulation as the sharp edges of the grains will increase the three-dimensionality of the disturbances and hence enhance turbulence stimulation. The sand grain strip is usually 5-10 mm wide with grain size of about 0.5 mm and attached to the model surface with a strip of glue (see figure 3.6a). Strips of sand as turbulence stimulator are most frequently used on smaller high speed craft models and appendages (Steen, 2014a). The stimulation method associated with a larger field of distributed roughness is showed in figure 3.6b. A more extensive description of this method proved to be difficult to obtain based on available literature. However, a similar behavior and effect (in terms of the roughness Reynolds number) as the carborundum grain strip may be reasonable to assume as both methods may be classified as distributed sand based three dimensional roughness types.

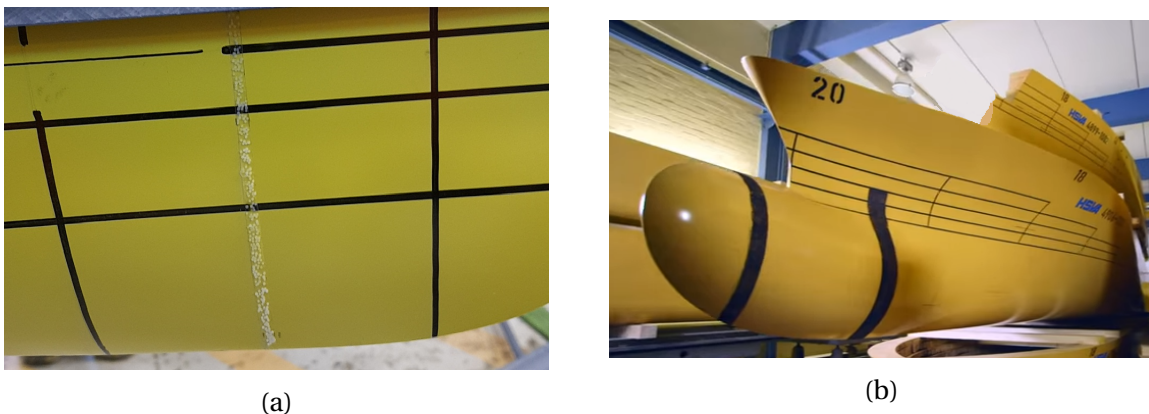
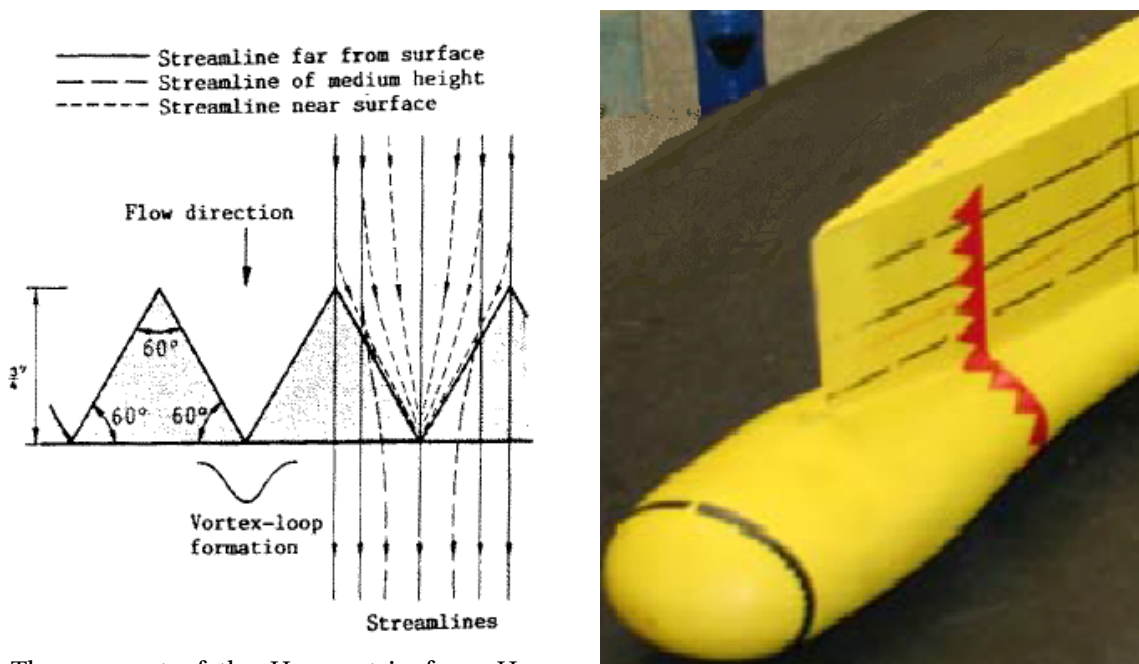


Figure 3.6: Sand strips as turbulence stimulation for two ship models.

The effect of three dimensional roughness distributed over an area has been less studied than the application of tripwires and studs. However an interesting result was reported by Feindt (1957), showing that little or no effect on transition occurs before $Rn_k = \frac{u(k)k}{\nu} \geq 120$. Where k now represents the sand grain height.

3.5 Hama strip

The Hama strip was first introduced by Hama (1957) and consists of tape with a saw tooth edge on the upstream side. This tripping device is often made by using several layers of normal adhesive tape, see figure 3.7 for illustrations of the Hama strip. In ITTC (1990) this mechanism was described as a lesser known, but most efficient turbulence stimulator. The principle of the Hama strip is to directly produce a three-dimensional disturbances in the form of a three dimensional vortex loop. As streamlines close to the model surface will converge to each other due to the triangular shape of the device the fluid velocity will be increased. This increment results in a larger capability to shed vortices, contributing to increased disturbance in the boundary layer. In figure 3.7a streamlines with different height from the model surface is shown, by studying this figure one is able to get an impression of how the three-dimensional vortex loops are created. According to Hama (1957) the roughness Reynolds number required to efficiently cause turbulence is $Rn_k = 45$ when using this device, indicating a superior effect compared to other stimulation techniques.



(a) The concept of the Hama strip from Hama (1957).

(b) Hama strip fitted on model from Harrington and Wells (2011).

Figure 3.7

As the Hama strip is capable of triggering turbulence with only small changes in model profile it is frequently used on foils and, on some occasions, on propeller models. According to Faltinsen (2006) an advantage with the Hama strip is the almost constant drag coefficient for both high and low Reynolds numbers, as opposed to other tripping devices where this is a function of both roughness height and velocity (Shen et al., 2015). Due to its efficiency in causing turbulence, its constant drag coefficient and in general small parasitic drag

the Hama strip has been deemed an effective tripping device for foils (Lewandowski, 1989). However, any use on Hama strip beyond foils and appendices has been reported in a much smaller extend. An exception is the experiment conducted by Harrington and Wells (2011) where a trimaran type model fitted with Hama strips was tested in a towing tank, however no assessment of the Hama strip as a turbulence stimulation device was made.

Chapter 4

Experimental Setup and Procedure

The procedure utilized to provide a thorough experimental study regarding various turbulence stimulation techniques is described in this chapter. Amongst others this includes the choosing of appropriate ship models, design of turbulence stimulation and waiting times between runs in the towing tank. All ship model tests were carried out in the large towing tank operated by SINTEF Ocean.

4.1 Ship models

In the choosing of appropriate ship models in which experiments were to be performed on, several aspects were considered. Firstly, the total ship model resistance should as much as possible consist of frictional resistance. This is because the difference in a turbulent or laminar flow around the hull as previously discussed, affects the frictional resistance to a large extent. According to Larsson et al. (2010) this is particularly true for tankers and large bulk carriers, as these have a large submergence and operate at low to moderate speeds. Therefore, by utilizing ships with fuller lines and a large wetted surface, any discrepancies in frictional resistance would be prominent. Also, by choosing a model with little or no wet surface in the transom stern any vortex shredding in the stern leading to viscous pressure resistance may be eliminated. In addition, at least one model should be sufficiently large so that any discrepancy in laminar-or turbulent frictional resistance coefficients will have a significant magnitude in measured model resistance. In the experiments carried out within this thesis it was decided to perform tests on two ship models. The main difference between these models was model scale factor, thus one relatively large and one small ship model were tested.

A large model previously used in commercial testing by SINTEF Ocean seemed to fit the requirements for an appropriate model to use in the experiment. This model is referred to as model A throughout this report, see figure 4.1a. The chosen small model was also deemed appropriate considering the mentioned requirements, however with a drastically increased model scale compared to the large model. See figure 4.1b for the smaller model referred to as model B. In table 4.1 data describing the two models are presented. In this present thesis



(a) Model A, fitted with a Hama strip for the occasion.



(b) Model B, no stimulation device applied.

Figure 4.1: Ship models used in turbulence stimulation experiments.

only model scale values are of interest, thus full scale data is more or less omitted from this study. As a curiosity however, it should be mentioned that the full scale equivalent of model A is a 175 m long bulk carrier. Model B represents a 270 m long Panamax oil tanker.

Although, model A had been stored in a warehouse for approximately two years, the surface was still uniform and relatively smooth. Model B however was lacquered once more shortly before testing due to a decay in surface smoothness over several years without a refurbishment. Another potential downfall for a stored model is twisting of the model itself, due to the natural tendency inherited in wood to curl over time. However, in this case little or no displacement of the material could be registered on any of the models. Previous transportation and use of the two models had caused minor damages in the model surface. A plastic filler was carefully applied to fill in any cracks or holes present. These areas were then again lacquered to retain a smooth surface.

<i>Note</i>	<i>Symbol</i>	<i>Unit</i>	<i>Model A</i>	<i>Model B</i>
Model scale	λ	[-]	28.327	105
Length waterline	L_{WL}	[m]	6.02	2.52
Breadth waterline	B_{WL}	[m]	1.059	0.394
Draught	T	[m]	0.353	0.169
Block coeff.	C_b	[-]	0.780	0.805
Displacement	Δ	[ton]	1.765	0.135
Wet surface	S	[m^2]	8.92	1.587
Wet surf. transom stern	A_T	[m^2]	0.00	0.002

Table 4.1: Model data for ship models utilized in experiments.

4.2 Placing of turbulence stimulation

In the tests conducted with model A all turbulence stimulators were placed on the same location in order to produce comparative results between the different test conditions. The standard procedure at the current towing tank facility was to apply the stimulation at section "19.5" for models of this size. Considering that the ship model consist of 20 sections, the stimulation device is thus placed at 2.5 % of L_{PP} aft of the fore perpendicular. As opposed to the ITTC recommendations of 5%. The significance of this discrepancy will be thoroughly discussed in later sections of this thesis. In the case of model B, any previous stimulation devices had been located at 5 % of L_{PP} aft of the stem. Implying a difference in location of stimulation device for the small and large model. Thus, in order to investigate the effects of different placement of stimulation mechanisms one stimulation condition, the Hama strip, was tested at three different locations for model B. These locations were 2.5 %, 5 % and 10 % of L_{PP} , as illustrated in figure 4.3.

From a fluid dynamic point of view the physical length from the ship model fore perpendicular to the turbulence stimulation, l_s , is of interest. Firstly, because the Reynolds number based on this length will provide an approximation of the flow characteristics at the stimulator. Secondly l_s decides how thick the boundary layer will be at the turbulence stimulators. This is of great importance when considering necessary roughness height and parasitic drag of the stimulator. In figure 4.2 l_s is illustrated for model A. Evidently it is important to account for the ship hull curvature when determining this length. In table 4.2 l_s is given for both models corresponding to each location of the turbulence stimulation device tested.

<i>TS location, of L_{PP}</i>	2.5%	5%	10%
<i>Model A</i>	0.28 m	-	-
<i>Model B</i>	0.11 m	0.175 m	0.31 m

Table 4.2: Length from FP to stimulator along the model surface.

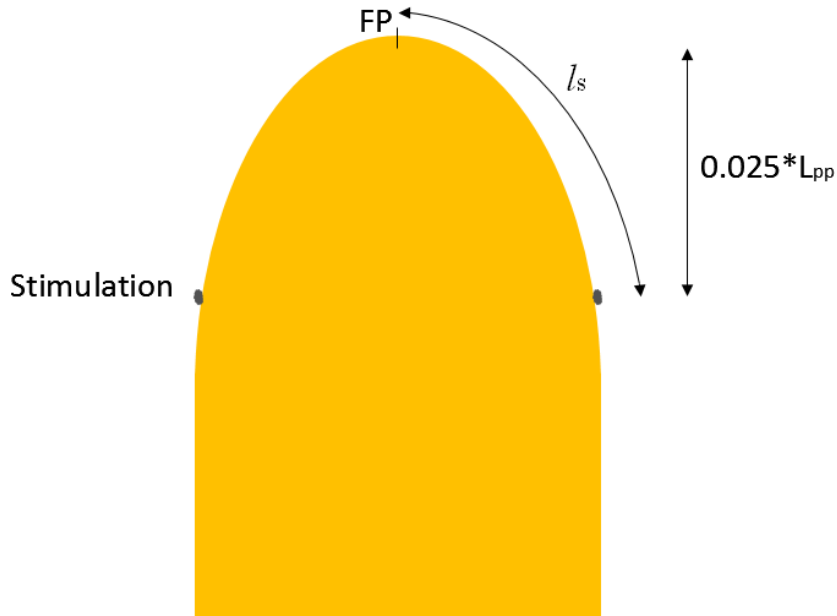


Figure 4.2: Sketch indicating l_s and the turbulence stimulation location on model A.

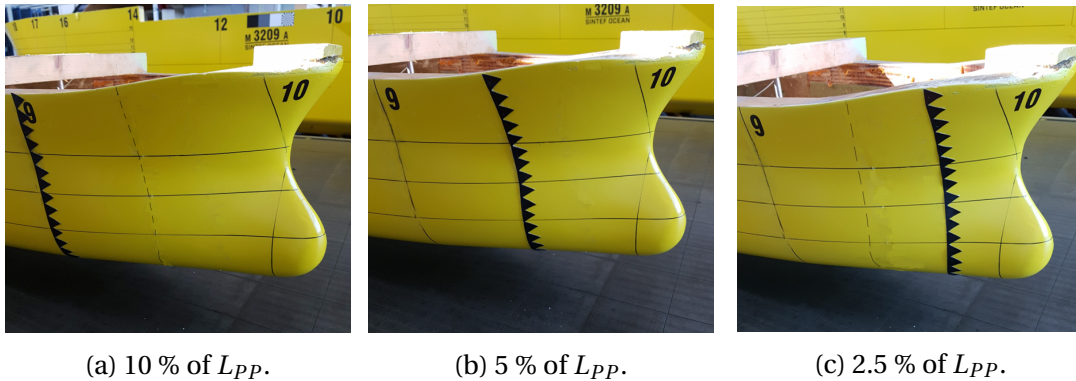


Figure 4.3: Hama strip located at the different location on model B.

4.3 Calculation of roughness height

The determination of effective roughness height for each turbulence stimulation was calculated based on the given effective roughness Reynolds number, Rn_k , for each stimulation type. for a quick recap of these values see table 4.3. Following, equation 4.1 was used to determine the required roughness height.

$$k = \frac{\nu Rn_k}{u(k)} \quad (4.1)$$

As the chosen stimulation height should be effective at both low, moderate and high model speeds, a roughness height sufficient even at the lowest speed was utilized in the experiments. The reader should therefore be aware that model tests performed at higher speeds

	Rnk
<i>Hama strip</i>	45
<i>trip wire</i>	400
<i>sand strip</i>	120

Table 4.3: Required roughness Reynolds number for each stimulation device tested.

will require a smaller height of the turbulence stimulation. Thus, with respect to the ability to generate turbulence the roughness height was for the majority of the speeds excessive.

By definition Rn_k is computed with respect to the fluid velocity at the roughness height, $u(k)$. Therefore, in order to perform an accurate approximation of the necessary roughness height, k , the presence of a boundary layer had to be accounted for. To obtain a decent velocity profile a laminar boundary layer was assumed at the turbulence stimulation. Several approximations for the velocity profile of a laminar boundary layer exists. As this present roughness calculation is based on rather crude estimates of Rn_k , the different velocity profile approximations gave little or no deviation in the final result. However, a sine approximation presented in equation 4.2 was chosen for further calculations, as according to Munson et al. (2013) this is fairly close to Blasius' analytical results.

$$\frac{u(y)}{U} = \sin\left[\pi \frac{y}{2\delta}\right] \quad (4.2)$$

Here U is the free stream velocity (equal to ship model velocity) and δ is the boundary layer thickness. By inserting equation 4.1 in equation 4.2, setting $y = k$ and consider the boundary layer thickness at the stimulation, δ_s , an expression for the required roughness height was obtained as

$$k = \frac{\nu Rn_k}{U \sin\left[\pi \frac{k}{2\delta_s}\right]} \quad (4.3)$$

This expression can either be solved by iteration or analytically by use of a simple spreadsheet. For simplicity the latter method was utilized. The following results are presented in table 4.4. At this stage the effects of increased local flow velocity due to pressure gradients along the hull was not included. Thus, this presented method only serves as a rough decision making process. The effects of pressure gradients is more thorough investigated in later calculations concerning induced drag by the stimulation devices.

4.4 Test conditions

4.4.1 Stimulation devices

The aim of this thesis is to investigate any differences in total resistance for a ship model that might occur due to various use of turbulence stimulation. Thus, a wide selection of

stimulation devices had to be included in the study to give an adequate quantitative basis for comparability. Amongst the stimulation mechanisms presented in chapter 3 all mechanisms were tested, with the exception of studs. The use of studs would require penetration and corruption of the model surface, as well as a rather time consuming application procedure. As the experiments were being performed on a tight time schedule and since models were subjected to reuse, the drawbacks connected to studs as turbulent stimulation were deemed too large. Therefore, studs were not included in the experimental part of this present study. Leaving the remaining turbulence stimulations to be tested as: trip wire, sand grain strip and Hama strip. In addition, tests were conducted on both models without any stimulation device.

As tripwire was the most used mechanism at SINTEF Ocean, two wires with different diameter were tested on model A. This was done to give a benchmark regarding model resistance when no turbulence enhancement is applied. And based of this, provide an approximation of when the flow around the model hull naturally becomes turbulent. To summarize: a total of five different stimulation conditions were performed on model A. On the smaller model B only one trip wire and a Hama strip was tested. The Hama strip however was as previously mentioned tested at different locations for model B.

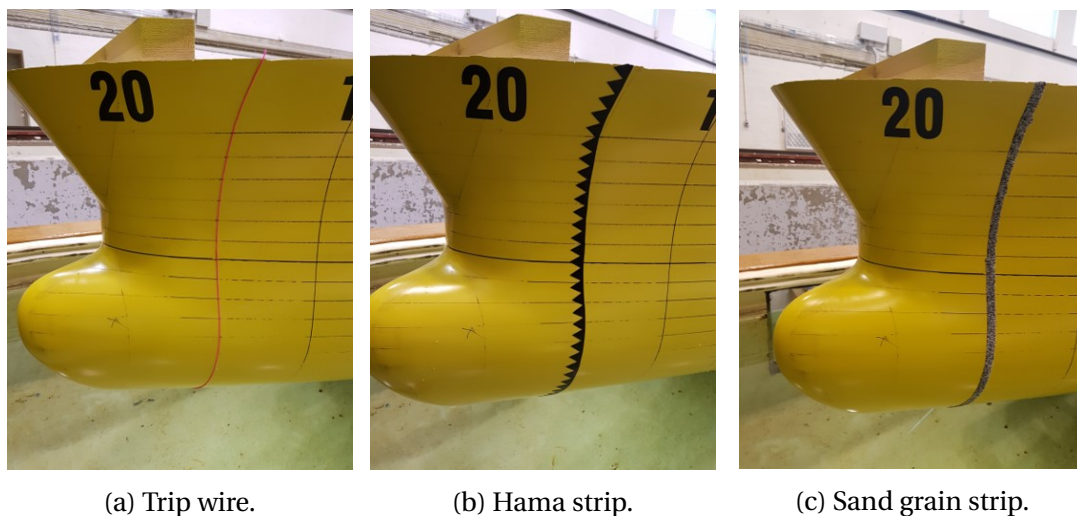


Figure 4.4: Different turbulence stimulation devices applied on the large model.

In figure 4.4 the three different turbulence stimulation techniques tested on model A are shown. The required roughness height for the stimulation to be effective in causing turbulence, k_{req} , was determined from the procedure previously described. See table 4.4 for a description of each conditions required roughness height compared with the actual roughness height implemented in the experiments, k_{exp} . The roughness height used in the experiment differ from the required value due to practical issues such as availability in material thickness. For the trip wires, this height is equal to wire diameter. Thus any application of excessive glue used in the mounting of the wire is omitted. This is a fair assumption for the

present experiments as only small fractions of extravagant glue was present.

	k_{req} [mm]	k_{exp} [mm]
Trip wire 1	1.22	1.2
Trip wire 2	1.22	1.5
Hama strip	0.57	0.61
Sand strip	0.94	0.9 - 1.2

(a) Large model.

	k_{req} [mm]	k_{exp} [mm]
Trip wire	1.11	1.5
Hama strip 1	0.52	0.53

(b) Small model.

Table 4.4: Calculated required roughness height and actually applied roughness height.

The tripwires were simply made from available cotton thread according to common routines at the towing tank facility. Two different standard thread diameters were available, consequently these two were tested to quantify any possible discrepancy between them. Leaving only the Hama strip and sand strip to be shaped according to calculated values for required roughness height. To reach the necessary height in tests including model A, the Hama strip consisted of two layers of standard duct tape (0.23 mm each) and one layer of insulation tape (0.15 mm). In the case of model B a Hama strip consisting of one layer of duct tape and two layers of insulation tape was necessary. The triangular shapes characterizing the Hama strip were cut out utilizing a sharp wallpaper knife. The sand strip consisted of sand grains originally intended for use in aquariums. These grains had a rather sharp and rough surface, and according to the manufacturer they came in a diameter between 0.7 and 1 mm. Considering this, the sand grains met the requirements for an acceptable turbulence stimulator in our case. In order to largely simplify the mounting and dismantle procedure, the sand grains were attached to a piece of tape about 0.2 mm thick and 10 mm wide.

4.4.2 Model velocities

As previously discussed, the flow around an object becomes naturally turbulent at high Reynolds numbers. Consequently, any investigation regarding each turbulence stimulation's ability to generate turbulence should be carried out in the low Re regime. However, this study should also aim to provide applicable results regarding day to day ship model testing. Hence, somewhat more relevant speeds with respect to the full scale ship were chosen as opposed to a deep study in the low Re regime. The significance of testing different turbulence stimulators at higher speeds should not be neglected. This could be especially useful to determine any differences in parasitic drag induced by the stimulators. Due to a very small measurable resistance compared to the force oscillations inherent in the towing carriage, the lowest speed was omitted for the small model B. Instead a higher speed was added to the test schedule. This was also done to obtain more information about any differences in parasitic drag. Otherwise the two models were tested at same Froude numbers to possibly determine any

scale effects connected to turbulence stimulation. See table 4.5 for the lists of speeds tested for each model. To make results comparable, obviously all model speeds were the same for each turbulence stimulation condition.

$U_{model} [m/s]$	0.4	0.6	0.8	1.0	1.2	1.5
Fn	0.052	0.078	0.104	0.130	0.156	0.195
Rn_m	$2.23 \cdot 10^6$	$3.34 \cdot 10^6$	$4.46 \cdot 10^6$	$5.57 \cdot 10^6$	$6.69 \cdot 10^6$	$8.36 \cdot 10^6$
$U_{full\ scale} [kts]$	4.14	6.21	8.28	10.35	12.41	15.52

(a) Model velocities for model A.

$U_{model} [m/s]$	0.39	0.52	0.65	0.78	0.97	1.09
Fn	0.078	0.104	0.130	0.156	0.195	0.219
Rn_m	$9.1 \cdot 10^5$	$1.21 \cdot 10^6$	$1.52 \cdot 10^6$	$1.82 \cdot 10^6$	$2.26 \cdot 10^6$	$2.54 \cdot 10^6$
$U_{full\ scale} [kts]$	7.77	10.36	12.95	15.54	19.32	21.71

(b) Model velocities for model B.

Table 4.5: Ship model velocities utilized in experiments.

4.4.3 Waiting times

Unless otherwise stated the waiting time between runs for model A was 15 minutes. This was chosen based on existing routines in the towing tank. However, another aspect of the present study was to investigate if any variations in waiting time between runs could affect the measured resistance. As this objective was of a secondary importance and such a study could be largely time consuming only two of the conditions connected to model A were subjected to such tests. Because tripwire was the preferred turbulence stimulation mechanism at the current towing tank, this was the first subject to such tests with a waiting time variation. Further, one might assume that a model with no turbulence stimulation would be more sensitive towards any fluid disturbances in the tank. Therefore, also the condition with no stimulation was repeated for different waiting times. Due to time schedule constraints only shorter waiting periods between runs was performed for this condition. Thus, in addition to the standard 15 minutes waiting period, one short period of 5 minutes and one long period of 60 minutes were tested for the trip wire condition. For the condition without stimulation tests with 15 and 5 minutes waiting time were performed. Again due to time restrictions only two speeds, one low and one high, were run on the non-standard waiting times. See table 4.6 for conditions and speeds connected to the waiting time experiments.

The required waiting time between runs for the smaller model B, was determined based on the standard waiting time for model A by assuming an equality in waiting times if time were scaled to full scale. According to Steen (2014a) time is scaled by the factor $\sqrt{\lambda}$. Then if waiting

Waiting periods	5 min	15 min	60 min
Speeds trip wire 1 [m/s]	0.6 & 1.5	all speeds	0.6 & 1.5
Speeds w/o stimulation [m/s]	0.6 & 1.5	all speeds	-

Table 4.6: Speeds tested for each condition with different waiting time for model A.

time for model A was to be scaled to full scale and then scaled down to the scale utilized in tests on model B, the following equation may be applied to determine the waiting time for model B.

$$t_{waitB} = \frac{\sqrt{\lambda_A} t_{waitA}}{\sqrt{\lambda_B}} \quad (4.4)$$

By inserting the respective model scales and the standard waiting time of 15 minutes for model A, a required waiting time of 8 minutes was estimated for model B. This claim is supported by considering the problem from a more practical perspective: As the decrement in water plane area and draft between model A and model B is large, it would be fair to assume that a much smaller water disturbance would occur in the case of model B. Thus the assumption of almost halving the waiting time without affecting the test environment seemed as a good approach.

If no activity in the tank occurred for more than two hours, a *dummy* was conducted. Meaning that a test run was completed without making use of the following data. This was done to ensure that all other runs were performed under similar conditions, and was according to the standard routine at SINTEF Ocean. The measured resistance of the dummy runs were still recorded. These results are briefly discussed in chapter 8.

4.5 Experimental setup

All experiments considered in this thesis were conducted at the large towing tank at SINTEF Ocean's laboratories in Trondheim. The tank actually consists of two tanks with different depths and a dock gate between them. In order to obtain a satisfying amount of sample data to give a reliable mean value, the dock gate was lowered so the combined tank length could be fully utilized. The ship models were towed over a total distance of 172 meter. See figure 4.5 for a sketch of the tank with length, breadth and depth dimensions.

For all tests conditions the models were towed at a constant speed and zero yaw angle. As in most other ship model towing tests the models were free to pitch, roll and heave, thus allowing for sinkage and trim. In sway and yaw however, the model was restrained and the respective sway force and yaw moment measured. The trim posts used to constraint the sway and yaw displacements were connected at the fore and aft perpendicular. The resistance measurements themselves were carried out through a force transducer, also referred

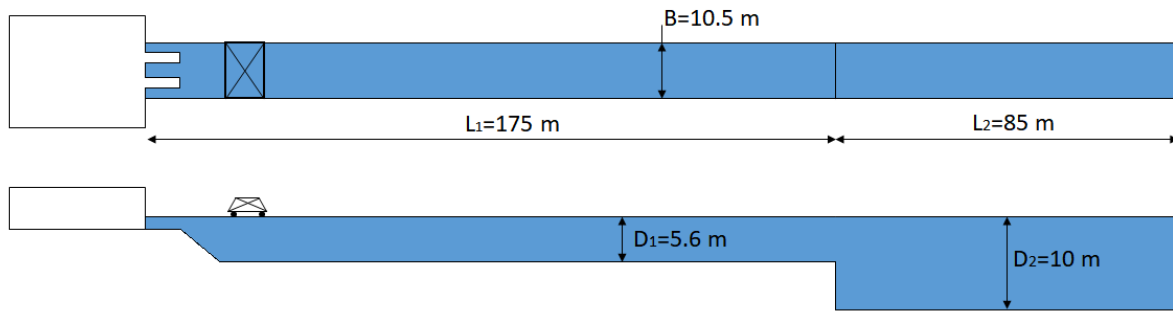


Figure 4.5: Sketch of the large towing tank at SINTEF Ocean in Trondheim.

to as a resistance dynamometer, which connects the model to the towing carriage. Figure 4.6 gives an overview of the mounting of the resistance dynamometer as well as the clamp used to unload the dynamometer during acceleration and deceleration of the ship model. To minimize oscillations in measured resistance due to vibrations in the towing carriage a dampener was mounted between the ship model and the resistance dynamometer.

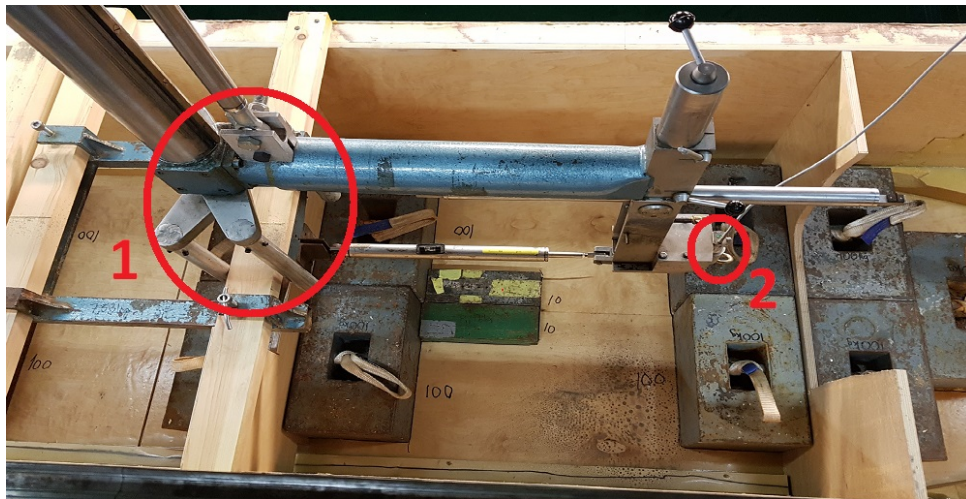


Figure 4.6: 1) Clamp used to accelerate and decelerate the model. 2) Resistance dynamometer. The dampener is clearly showed connecting the dynamometer to the ship model.

4.6 Determination of uncertainty

In every physical experiment an inherent uncertainty will be connected to the measured values. To fully describe any discrepancies in measured resistance due to turbulence stimulation, as is the goal of this study, it is crucial to have firm control of the uncertainty. According to Steen (2014a) uncertainty is just a statistical representation of error. An *error* may be divided into bias and precision error. The former being systematic errors and following may not be quantified with repeated tests. As the experimental setup is equal for all conditions, it would be fair to neglect any bias errors when comparing results in this experiment. The

precision error may be described as the scatter in the result. For the present study this is of great importance as it will define the accuracy of the experiments. Now, the precision limit may be defined. This is a description of how large the range of error we can expect is. In the following section the procedure used to calculate the accuracy, referred to as precision limit from now on, is described. The calculation is largely based on the proposed procedure by Ersdal (2004).

Firstly, it was assumed that if a measurement is repeated an infinite number of times the measured values will be normal distributed around a mean value. The normal, or *Gaussian*, distribution is given on the form

$$f(X) = \frac{1}{\sigma\sqrt{2\pi}} \exp\left[-\frac{(X - \bar{X})^2}{2\sigma^2}\right] \quad (4.5)$$

Where σ is the standard deviation and \bar{X} is the mean value of a series consisting of N measurements. The mean value of N measurements was now, as usually, determined as

$$\bar{X} = \frac{1}{N} \sum_{j=1}^N X_j \quad (4.6)$$

with the following standard deviation

$$S_x = \sqrt{\frac{1}{N-1} \sum_{j=1}^N (X_j - \bar{X})^2} \quad (4.7)$$

Where X_j represents a single measurement. Now the precision limit for a single sample may be expressed as

$$P_x = S_x t \quad (4.8)$$

Where t is a weighting factor which is a function of degree of freedom, $N - 1$, and confidence interval, γ . The latter defined as the probability of a measurement to be within the precision limit. According to Steen (2014a) a typical value for ship model testing would be $\gamma = 0.95$. As N increases the value of t will converge to a finite value dependent of the assumed confidence interval. As the convergence rate is asymptotic, only increasing the number of samples slightly will largely decrease the precision limit. From figure 4.7 it is clear that only small reductions of t occurs by increasing the number of samples beyond 10.

When the precision limit is determined one can easily calculate the uncertainty of the model test. As this will be equal to the ratio between precision limit and mean value. The uncertainty of a single measurement given in percent may then be written as

$$P_{x\text{percent}} = \frac{P_x}{\bar{X}} \cdot 100 \quad (4.9)$$

From a ship model testing facility's point of view this is interesting enough as usually only

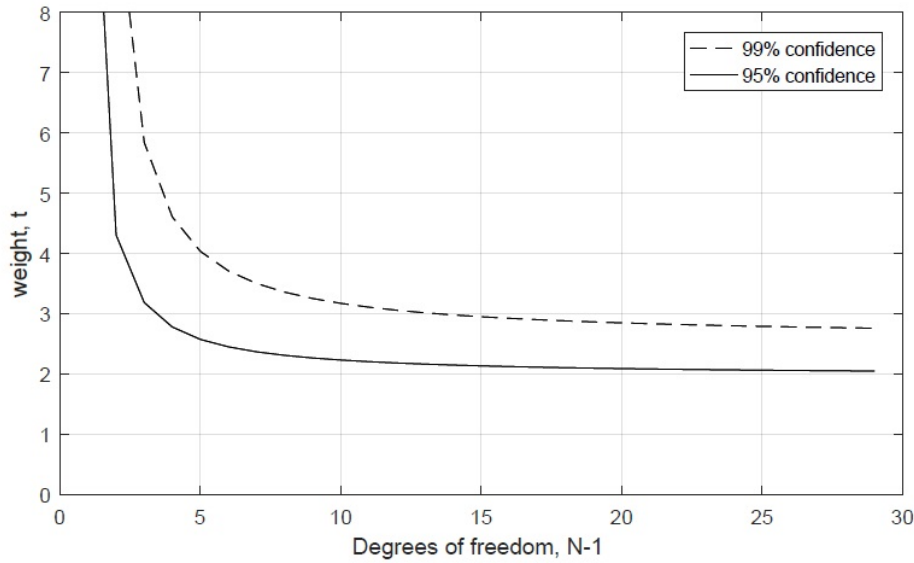


Figure 4.7: The weighting factor t as a function of degrees of freedom.

one repetition is conducted in day to day ship model testing. In this current study however, large efforts were made to minimize the uncertainty. Thus, several repetitions were carried out for all model velocities. Then the uncertainty of the mean of these repetitions is determined as

$$P_{\bar{x}} = t \frac{S_x}{\sqrt{N}} \quad (4.10)$$

Where N is the number of repetitions.

To determine the uncertainty and accuracy of the current experiments one low speed and one high speed were repeated ten times. Thus, the precision limits for one single test were based on this measurements. Then to obtain relevant values for the intermediate speeds, interpolation procedures were carried out. The intermediate speeds were repeated twice for model B. Consequently, the precision limit further utilized in this report corresponds to the precision limit for one single test divided by $\sqrt{2}$. For model A the different conditions were repeated different times, due to changes in the time schedule underway. Resulting in a somewhat different precision limit of the mean between conditions. See table 5.1 for an overview of the number of repetitions for each stimulation.

A large number of runs was necessary to obtain such a thorough estimate of the accuracy. In between the two models a total of 300 runs were completed. Luckily, an automatically driven towing carriage was available during the model testing, easing the use of resources drastically.

Chapter 5

Experimental Results

The results from the ship model experiments are presented in this chapter. For the most, mean values are presented herein. For a complete description of the measured resistance corresponding to each runs see appendix A.

5.1 Model A

5.1.1 Uncertainty analysis

In this section the calculated uncertainty and accuracy of the model experiments are presented. The quantification of this uncertainty was obtained by implementing experimental result into the procedure described in section 4.6.

In figure 5.1 the precision limits for one single measurement for each of the test conditions are shown, corresponding to equation 4.9. Evidently, the uncertainty is substantially larger at lower speeds. The smallest trip wire gave a substantially lower precision limit. Also, the precision limit is considerably larger for the sand strip condition. It should however be mentioned that the runs for this condition were performed in a random order. The results in figure 5.1 were obtained by repeating the lowest and highest speed 10 times each.

As this study aims to quantify rather small discrepancies several repetitions were conducted to decrease the precision limit. According to equation 4.10 the precision limit is decreased by a factor of \sqrt{N} by repeating the experiment N times. In table 5.1 the uncertainty of the mean of N repetitions is shown for each stimulation technique. It is important to note the difference in number of repetitions for each stimulation condition when comparing the different rows in the table. Also, the values presented in table 5.1 must be kept in mind when assessing further results regarding the discrepancies in measured resistance for model A with different turbulence stimulation.

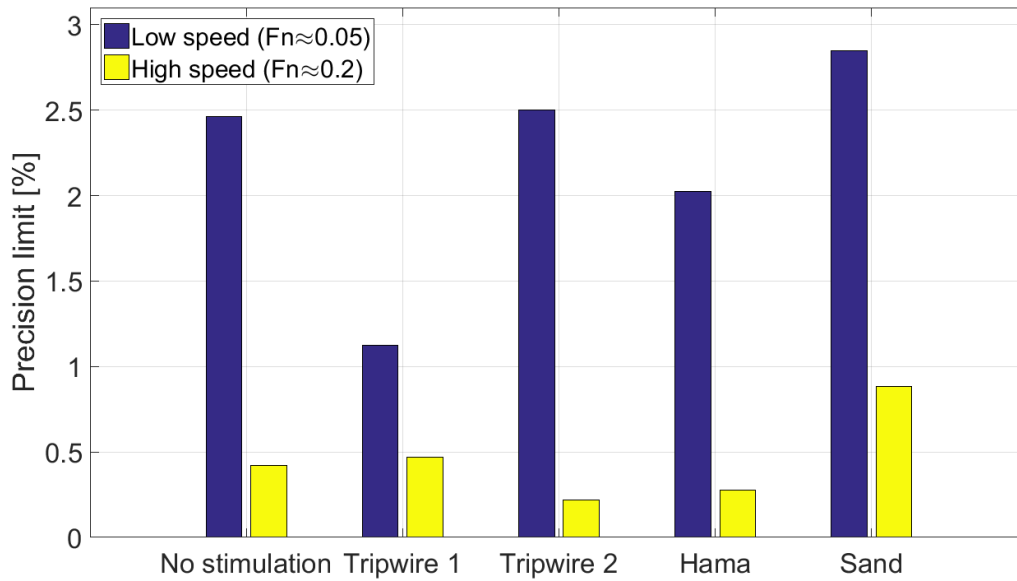


Figure 5.1: Precision limit of one single measurement for different turbulence stimulation, model A.

F_n	0.052	0.078	0.104	0.13	0.156	0.195
<i>w/o stimulation (3 reps)</i>	±1.42%	±1.21%	±0.99%	±0.78%	±0.56%	±0.24%
<i>tripwire 1 (2 reps)</i>	±0.80%	±0.71%	±0.63%	±0.54%	±0.46%	±0.33%
<i>tripwire 2 (4 reps)</i>	±1.25%	±1.04%	±0.84%	±0.63%	±0.42%	±0.11%
<i>Hama strip (4 reps)</i>	±1.01%	±0.85%	±0.69%	±0.54%	±0.38%	±0.14%
<i>sand strip (5 reps)</i>	±1.27%	±1.11%	±0.95%	±0.79%	±0.63%	±0.40%

Table 5.1: Precision limit of the mean for different speeds and stimulation conditions for the large model.

5.1.2 Measured resistance

In this section the mean value of the measured resistance for each turbulence stimulation condition on model A is presented. When assessing the following results, one should keep the already presented precision limits in mind. In table 5.2 the mean values of the measured resistance for each condition are given. Utilizing equation 2.2 the total model resistance may be expressed on a non-dimensional form as the total resistance coefficient, C_T . This is more convenient when comparing the measured resistance as any discrepancy will be made much more clear on a non-dimensional form. See figure 5.2 for the following results on a non-dimensional form. To indicate the accuracy of the results the precision limit for one of the tripwire conditions as well as the condition without stimulation is included in the figure as errorbars.

From figure 5.2 and table 5.2 it is clear that the ship model fitted without any sort of stimulation gives the lowest resistance. This difference is especially clear in the low speed range.

F_n	0.052	0.078	0.104	0.130	0.156	0.195
<i>w/o stimulation</i>	3.07 N	6.70 N	11.77 N	17.68 N	25.76 N	41.01 N
<i>tripwire 1</i>	3.37 N	7.08 N	12.08 N	18.10 N	26.37 N	41.95 N
<i>tripwire 2</i>	3.37 N	7.11 N	12.12 N	18.22 N	26.46 N	42.12 N
<i>Hama strip</i>	3.11 N	7.03 N	12.06 N	18.10 N	26.24 N	41.80 N
<i>sand strip</i>	3.35 N	7.13 N	12.17 N	18.26 N	26.56 N	42.55 N

Table 5.2: Mean values of measured resistance for model A with different turbulence stimulators.

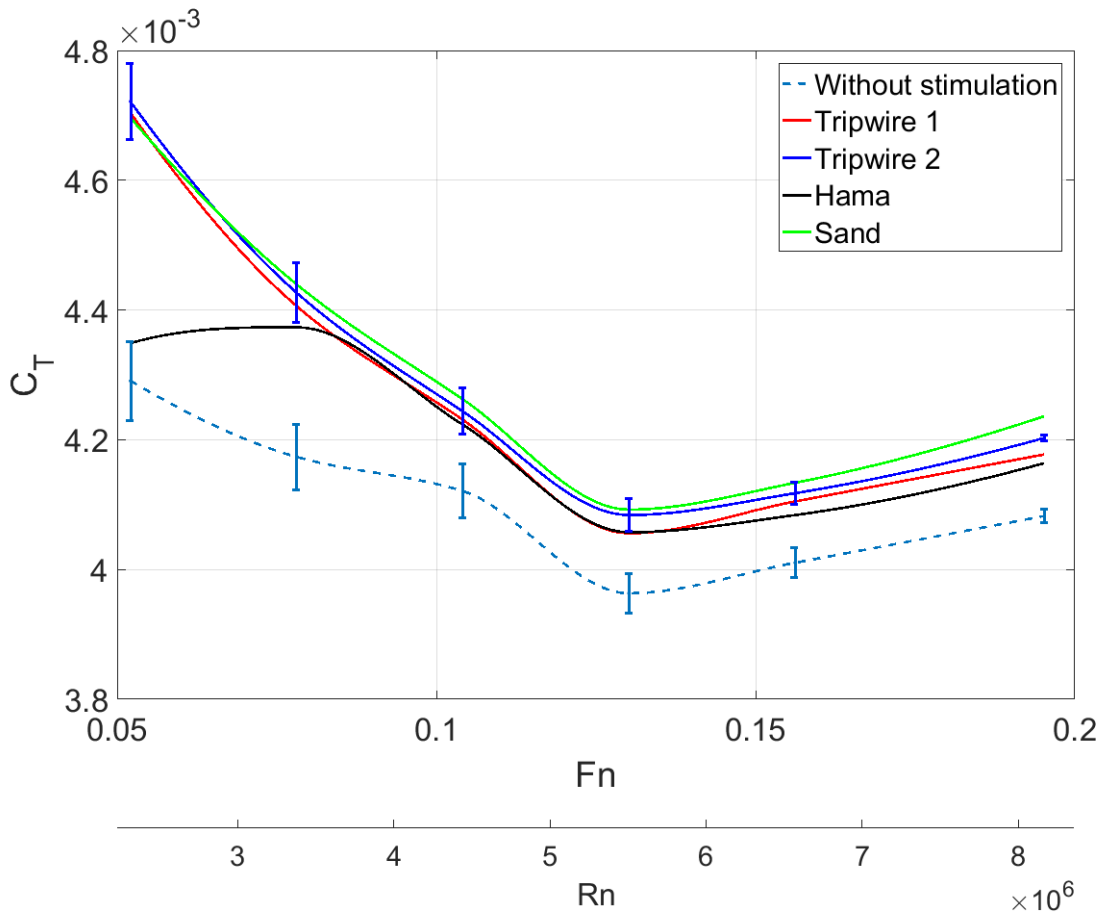


Figure 5.2: Total resistance coefficient for model A with different stimulation conditions with precision limits of the mean value for the two condition.

For low speeds it is also evident that the Hama strip used in the experiment gave lower total resistance than the other stimulation devices. The results for the other turbulence stimulators are not easily separated in this speed range. This is due to both a large precision limit as well as small differences in measured mean values. For higher speeds however, the precision limit is much lower. This, combined with a larger relative difference make it possible to distinct between the different conditions in this speed range. Here, it is clear that the sand strip causes the highest total resistance, and the Hama strip again causes the lowest amongst the stimulation techniques. The measured resistance for the two tripwire conditions seem

to be in-between these to extremities. From a more general point of view it is worth to note the sudden bend of the curve that occurs at $Fn \approx 0.13$. For a complete comparison of the difference in measured resistance between the different stimulation conditions see section B.1.

5.1.3 Variation in waiting time

The measured resistance with different waiting times between runs is given in table 5.3. Here two speeds were tested, one low and one high. The results show little or no significant discrepancy for the low speeds tested at the different waiting times. For the tripwire condition no significant differences were detected at low speed even when varying the waiting time from 5 to 60 minutes. When the speed was increased however, the differences in measured resistance between the different waiting time are considerable. From table 5.3 it is indicated that decreasing the waiting time from 15 to 5 minutes will increase the total ship model resistance with about 1% for high speeds. Also, the standard deviation is increased when decreasing the waiting time. When a waiting time of 60 minutes was applied for high speeds, the measured resistance experienced a somewhat similar increase as the 5 minute wait relative to a 15 minute waiting time. However, the standard deviation was now substantially smaller than both 5 and 15 minutes. Note that the 15 minutes waiting time runs were performed 10 times for high speeds.

Stimulation type	Waiting time	Fn	no. of reps	std [%]	Mean [N]	dev. from 15 min [%]
Trip wire 1	5 min	0.078	4	0.35	7.07	-0.14
		0.195	3	0.28	42.31	+0.91
	15 min	0.078	3	0.37	7.08	-
		0.195	10	0.21	41.93	-
	60 min	0.078	3	0.23	7.06	-0.28
		0.195	3	0.12	42.25	+0.76
w/o stimulation	5 min	0.078	3	0.63	6.70	+0.15
		0.195	3	0.20	40.98	+0.98
	15 min	0.078	3	0.81	6.71	-
		0.195	10	0.17	41.38	-

Table 5.3: Results from tests with variation in waiting time, model A.

5.2 Model B

5.2.1 Uncertainty analysis

In an identical way as for model A the precision limit is now presented regarding the experiments conducted with model B. In figure 5.3 the precision limits when performing one measurement are given. As for model A it is clear that the precision limit is much larger for

low speeds. Also, the precision limits for both the Hama strip and tripwire were calculated to be somewhat equal. In the case of no applied stimulation the precision limit is considerably smaller relative to the other two conditions.

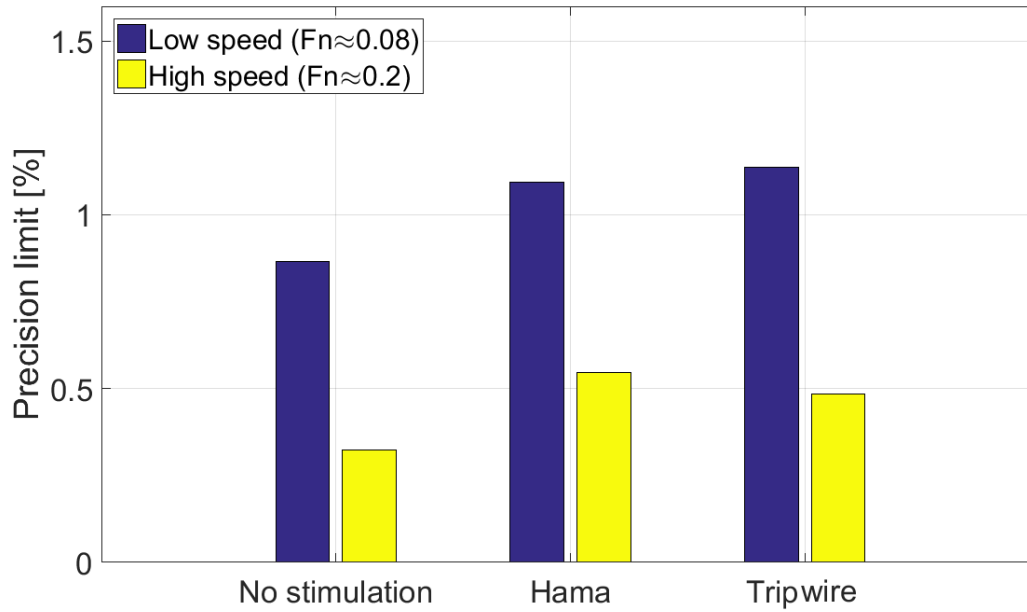


Figure 5.3: Precision limit of one single measurement for different turbulence stimulation, model B.

For the experiments conducted on model B the number of repetitions on intermediate speeds were repeated twice. Thus the precision limit of the mean value corresponds to the values from figure 5.3 divided by a factor equal to $\sqrt{2}$. This following result is presented in table 5.4. They are further used to indicate the accuracy of these present experiments.

F_n	0.078	0.104	0.13	0.156	0.195	0.22
<i>w/o stimulation (2 reps)</i>	±0.61%	±0.54%	±0.47%	±0.40%	±0.29%	±0.23%
<i>Hama strip (2 reps)</i>	±0.85%	±0.77%	±0.68%	±0.59%	±0.47%	±0.39%
<i>tripwire (2 reps)</i>	±0.88%	±0.80%	±0.73%	±0.66%	±0.55%	±0.49%

Table 5.4: Precision limit of the mean for different speeds and stimulation conditions for model B.

5.2.2 Measured resistance

The mean values of measured model resistance for model B fitted with different turbulence stimulators is given in figure 5.5. The total model resistance coefficient was determined in the same way as for model A, and is depicted with corresponding precision limits in figure 5.4. From these results it is clear that a serious disagreement in measured resistance is

present between all three stimulation conditions. As for model A, the difference is largest in the low speed regime. However, the difference between the Hama strip and tripwire does not seem to decrease when the speed is increased, as was the case for model A. In case of the condition without any stimulation the results indicate a decrease in relative difference with the other two conditions as the speed is increased. For all three conditions a dramatic increase in total resistance coefficient occurs at $Fn \approx 0.16$. For a complete description of the difference in resistance between the current stimulation techniques see section B.2.

Fn	0.078	0.104	0.13	0.156	0.195	0.22
<i>w/o stimulation</i>	0.61 N	1.09 N	1.68 N	2.38 N	4.00 N	6.04 N
<i>Hama strip</i>	0.66 N	1.16 N	1.77 N	2.52 N	4.19 N	6.21 N
<i>trip wire</i>	0.69 N	1.20 N	1.83 N	2.60 N	4.34 N	6.46 N

Table 5.5: Mean values of measured resistance for model B with different turbulence stimulators.

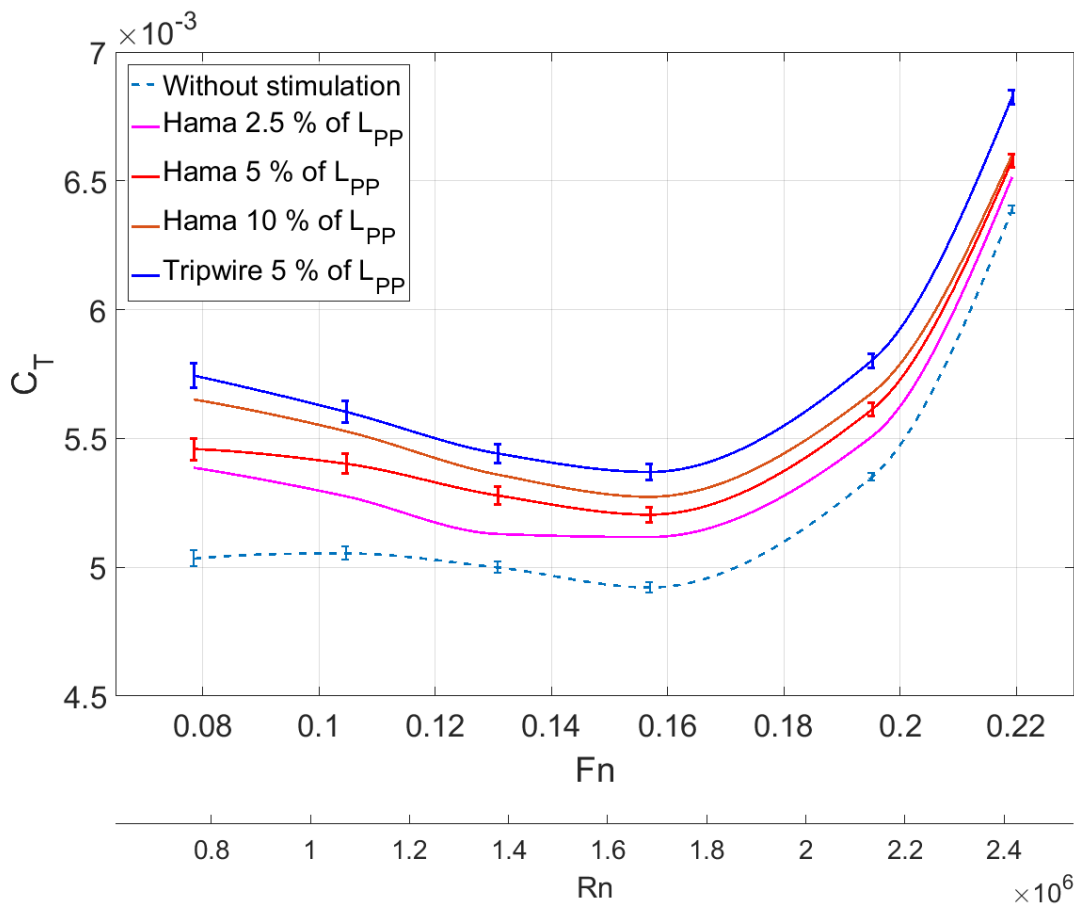


Figure 5.4: Total resistance coefficient for model B with different stimulation conditions and precision limits for the mean value.

5.2.3 Variation in location of stimulation

In addition to testing of different turbulence stimulators, model B was subjected to tests with different placement of the turbulence stimulation. The Hama strip was utilized as the stimulation device subjected to these tests. In table 5.6 the measured resistance for the three different locations, stimulator at 2.5 %, 5 % and 10 % of L_{PP} aft of FP is given. The corresponding total resistance coefficients are also presented in figure 5.4.

Fn	0.078	0.104	0.13	0.156	0.195	0.22
2.5 % of L_{PP}	0.65 N	1.13 N	1.72 N	2.47 N	4.12 N	6.15 N
5 % of L_{PP}	0.66 N	1.16 N	1.77 N	2.52 N	4.19 N	6.21 N
10 % of L_{PP}	0.68 N	1.19 N	1.80 N	2.55 N	4.24 N	6.24 N

Table 5.6: Mean values of measured resistance for different locations of the Hama strip.

The results show that the greatest resistance is achieved by placing the Hama strip at 10 % of L_{PP} . Then, the decrease in length between FP and the stimulation device results in a smaller measured resistance. Again the discrepancy between the different conditions is largest for low speeds. When the ship model velocity is increased the relative differences generally diminish.

Chapter 6

Theoretical Resistance Predictions

In this section rough estimates and simple calculations are used to illustrate certain physical aspects regarding total ship model resistance and the role of turbulence stimulation in this context. The theoretical results provided by this section are later compared to the experimental results presented in chapter 5.

6.1 Drag induced by turbulence stimulation

Of great interest in this study is the hydrodynamic drag induced by the turbulence stimulation device itself. This resistance contribution is referred to as *parasitic drag*, as it essentially only serves as excessive model resistance compared to a full scale condition where obviously the stimulation device and its following drag force is not present. However, according to Hughes and Allan (1951) an important hypothesis in ship model testing is that the parasitic drag cancels out the loss in frictional resistance due to a laminar flow upstream of the turbulence stimulation. This implies that the parasitic drag should not be below a certain value. In the following section the procedure utilized to quantify the parasitic drag of each turbulence stimulation technique is described. This current method is heavily based on the procedure proposed by Shen et al. (2015) for a similar problem.

Firstly, let R_{trip} denote the parasitic drag, and C_{trip} the drag coefficient corresponding to each stimulation. Then the parasitic drag is expressed as

$$R_{trip} = \frac{\rho}{2} C_{trip} S_{trip} u(k)^2 \cos \alpha \quad (6.1)$$

Where $u(k)$ is the velocity at the roughness height. S_{trip} represents the projected area of the tripping device, set equal to the length of the device submerged in water times the roughness height. The parameter α is the angle between the centerline of the ship model and a vector tangent to the body, thus the term $\cos \alpha$ decomposes the total force to only contain the longitudinal force component, as only this is of interest.

Studies by Hughes and Allan (1951) and Tagori (1963) indicate that the drag coefficient is a function of the boundary layer thickness compared to the roughness height and obviously the geometry of the stimulator. McCarthy et al. (1976) states that $C_{trip} = 0.75$ gives a good approximation in the case of a tripwire. In Hoerner (1965) a variety of shapes and their drag coefficients are discussed. From this the drag coefficient for a sand grain strip may be estimated to 1.2. According to Tagori (1963) the drag coefficient for the Hama strip is significantly larger than the trip wire, and an assumption of a value around 2 seems to be a good approximation for C_{trip} .

When determining $u(k)$ a similar procedure as presented in section 4.3 was utilized, however two important additional aspects were included in the calculation. Firstly it was accounted for the change in hydrostatic pressure around the hull and the following change in local flow velocity. Secondly, the use of a turbulent boundary layer profile at the stimulation device was included in some of the calculations.

The change in pressure along the hull could be of particular interest when assessing the different location of the Hama strip on model B, as the local velocity would differ significantly dependent on the current location. As an example, the ship stem could represent a stagnation point where flow velocity by definition is zero, leading to a high pressure. Along the ship shoulder the pressure is decreasing and the following local speed increased. To identify where and how large the variations in speed were, a similar ship hull was used as reference, see figure 6.1. This is the hull of the crude carrier *KVLLC 2* which has been a subject to extensive numerical investigations of flow patterns around the hull (Larsson et al., 2013). As this ship has a good resemblance with the models tested in this thesis, it was assumed that the pressure coefficients from figure 6.1 also was valid for models A and B.

The pressure coefficient, C_p , is defined as

$$C_p = \frac{P_s - P_\infty}{P_0} \quad (6.2)$$

Where P_s is the hydrostatic pressure at the ship hull surface, P_∞ is the hydrostatic pressure far away, while P_0 is the hydrodynamic pressure far away from the hull. Thus, by assuming $P_\infty = 0$ the static pressure at the hull surface may then be expressed

$$P_s = P_0 \cdot C_p \quad (6.3)$$

Further, Bernoulli's equation states that the total pressure far away of the hull equals the local total pressure. Leading to the following equation

$$P_s + P_d + P_a = P_0 + P_\infty + P_a \quad (6.4)$$

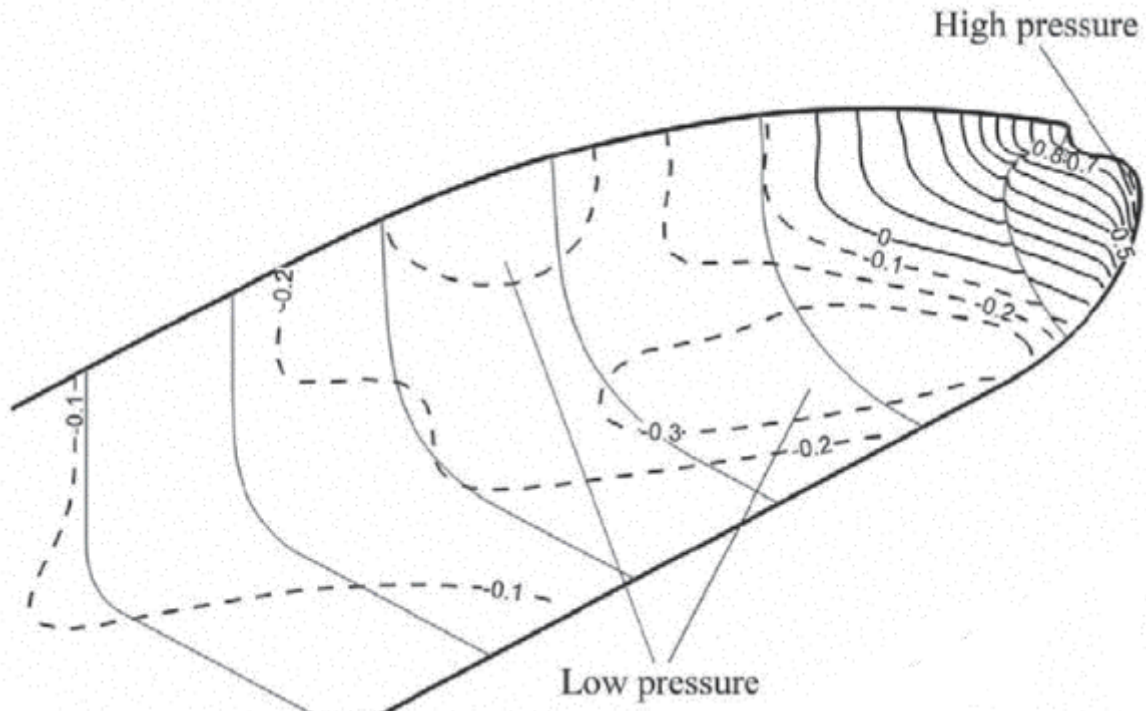


Figure 6.1: Pressure distribution around the hull of KVLCC2. Contours labeled with C_p , from Larsson et al. (2010).

Where P_a is the atmospheric pressure and P_d is the local dynamic pressure given by

$$P_d = \frac{\rho}{2} u_L^2 \quad (6.5)$$

Here u_L is the local flow velocity. Thus by inserting equations 6.5 and 6.3 into equation 6.4 the following expression is obtained

$$P_0 \cdot C_p + \frac{\rho}{2} u_L^2 = \frac{\rho}{2} U^2 \quad (6.6)$$

Where U is the ship model speed. Then, by solving equation 6.6 with respect to u_L the following expression was established to determine the local flow velocity at the ship model hull

$$u_L = U \cdot \sqrt{1 - C_p} \quad (6.7)$$

The assumed pressure coefficients for the respective locations based on figure 6.1 are given in table 6.1 together with the respective projected area of the Hama strip and α values. The following effect of pressure gradients along the hull in terms of local velocity is illustrated in figure 6.2a. As expected the velocity is significantly decreased closer to the stem, which serves as a stagnation point in the flow.

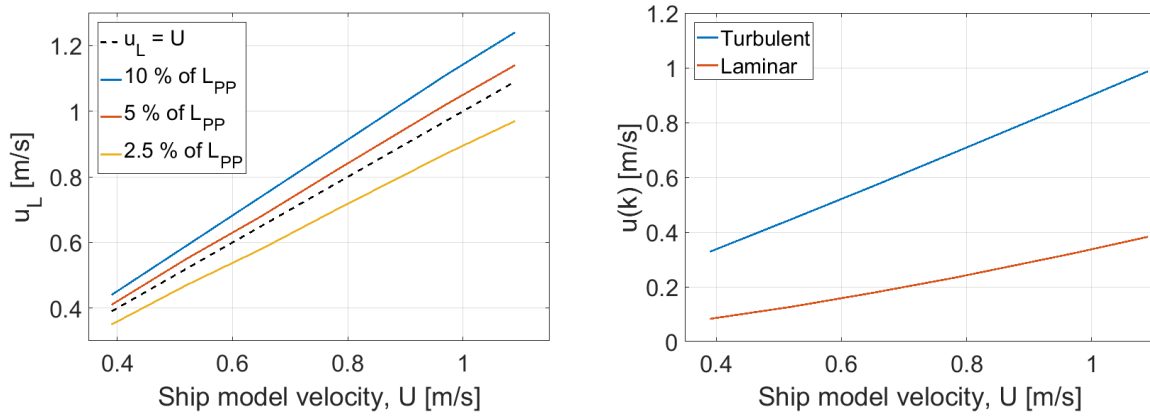
The second feature affecting the flow velocity at the stimulation height is the onset of a turbulent or laminar boundary layer. The difference between the two velocity profiles was pre-

	C_p	S_t	α
2.5 %	0.2	$2.5 \cdot 10^{-4} m^2$	8°
5 %	-0.1	$2.7 \cdot 10^{-4} m^2$	4°
10 %	-0.3	$3.4 \cdot 10^{-4} m^2$	0°

Table 6.1: Describing values for Hama strips at different locations, in percent of L_{PP} aft of FP.

viously illustrated in figure 2.3. The flow velocity in laminar boundary layer profile is mathematically described in equation 4.3. According to Munson et al. (2013) the following expression may be used in the case of a turbulent boundary layer.

$$u(k) = u_L \cdot \left[\frac{k}{\delta} \right]^{1/7} \quad (6.8)$$



(a) Effects of pressure gradients in terms of local flow velocity, u_L , at different locations along the hull.

(b) Differences in $u(k)$ when assuming a laminar or turbulent boundary layer. Valid for a Hama strip located at 10 % of L_{PP} on model B

Figure 6.2

This equation was further used to assess $u(k)$ when the flow was assumed to already have a turbulent characteristic at the stimulation device. From figure 2.3 it is clear that when this is the case a significantly larger flow velocity is present at the stimulation height assuming $k < \delta$. Note that the local velocity u_L given from the pressure coefficient calculations is used in equation 6.8, thus the most accurate estimate for $u(k)$ is provided. Naturally, this is also the case when a laminar boundary layer is assumed at the stimulation which is by far the prevailing approach in this thesis. In figure 6.2b the effect of a turbulent versus a laminar velocity profile is shown, regarding the velocity at the roughness height, $u(k)$. Evidently, a turbulent flow leads to an increase in $u(k)$ leading to a substantial enlargement of the induced drag.

From equation 6.1 it is clear that both the effects of pressure gradients and boundary layer velocity profiles is of great importance when assessing the parasitic drag, as they both largely

affect $u(k)$. Therefore, they are widely included when predicting the parasitic drag of the Hama strip at 2.5 %, 5 % and 10 % of L_{PP} . This is again essential when assessing the optimal location of the turbulence stimulation. Now, by inserting values from table 6.1, drag coefficients, relevant speeds and roughness heights, estimates for the parasitic drag corresponding to each stimulation condition were found. In figures 6.3 and 6.4 the calculated parasitic drag for each stimulation condition is shown. Note that these values are, with one exception, based on the assumption of a laminar boundary layer at the stimulation device. Due to an increased length from the stem to the stimulation in the case of a Hama strip located 10 % of L_{PP} from FP, one might expect a turbulent transition upstream of the turbulence stimulator. Hence, a turbulent boundary layer profile should be used to determine the parasitic drag. This is illustrated in figure 6.4 by the dashed line.

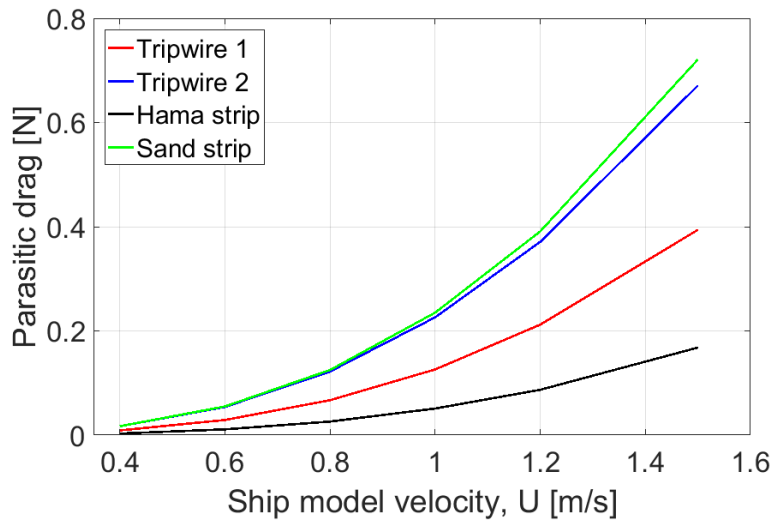


Figure 6.3: Parasitic drag for different turbulence stimulators, Model A.

From the figures it is clear that the determined parasitic drag described in this thesis is absolutely smallest for the Hama strip. Even though this was assigned the largest drag coefficient. Then, drag is increasing as roughness height increases. Thus, a significantly discrepancy exists between the two tripwires tested on model A. From the calculation regarding induced drag on the Hama strip at different location, only small differences are evident between the locations. However, this is only true when a laminar boundary layer is assumed at the stimulator. In the case of a turbulent flow over the stimulator the induced drag is drastically increased.

To be able to investigate the magnitude of parasitic drag on a non-dimensional level the resistance coefficient was defined as

$$C_{Rtrip} = \frac{R_{trip}}{\frac{\rho}{2} S U^2} \quad (6.9)$$

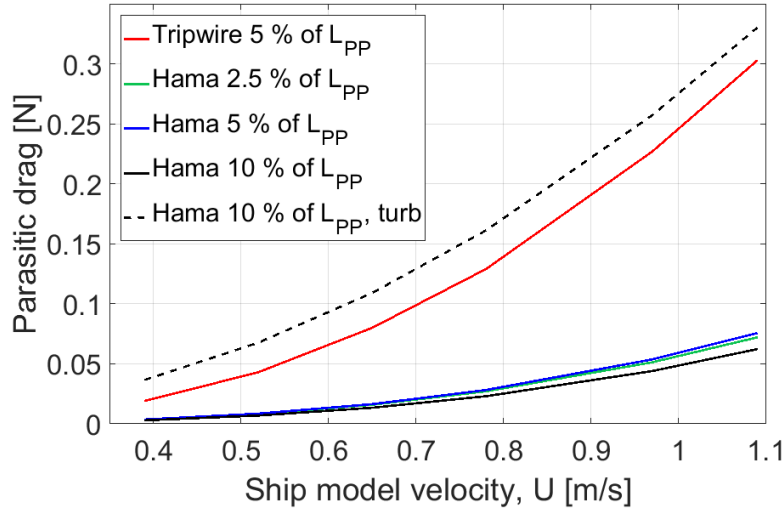


Figure 6.4: Parastic drag for different turbulence stimulators, Model B.

Where R_{trip} denotes the parasitic drag. This allows for a comparison across the two models. In figure 6.5 C_{Rtrip} for the tripwire conditions are shown both for model A and B. Evidently the smaller model B is subjected to a dimensionless parasitic drag in the order of 5 - 6 times larger than for model A.

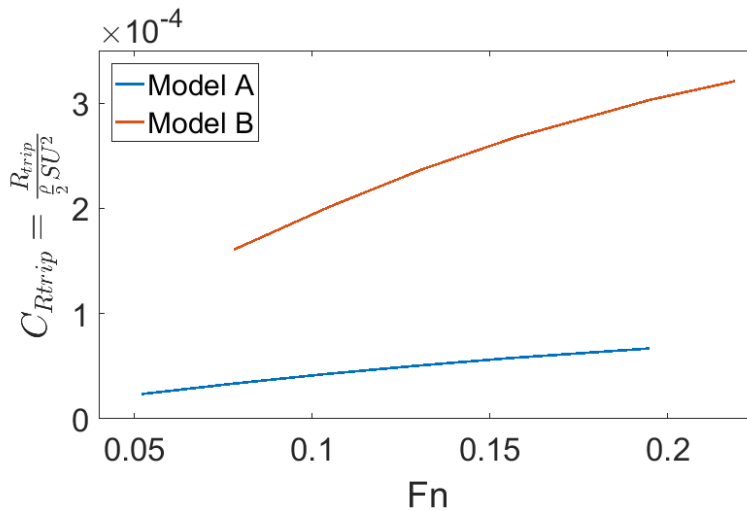


Figure 6.5: Comparison of dimensionless parasitic drag for the tripwire conditions between the two models.

6.2 Frictional resistance

The scope of this section is to provide a theoretical estimate of the ship model resistance. This is mainly done by assuming different extent of a partly laminar and partly turbulent flow over the hull.

According to Larsson et al. (2010) the wave making resistance is negligible when $Fn < 0.15$. Thus the total resistance consists mainly of viscous components and may be expressed as

$$C_T = C_V = (1 + k_f) \cdot C_F \quad (6.10)$$

Hence, to capture the effect of a partly laminar flow over the ship model in terms of ship resistance the frictional coefficient C_F could be somewhat altered. This was done by utilizing the previously presented friction lines for laminar and turbulent flow characteristics. This requires the rather rough assumption that it is possible to superpose the resistance contributions from a partly laminar and partly turbulent flow, thus neglecting the intermittency region. Following, a combined friction coefficient may be expressed as

$$C_{Fc} = p_{turb} \cdot C_{Fturb} + (1 - p_{turb}) \cdot C_{Flam} \quad (6.11)$$

Where p_{turb} is a number from 0 to 1 describing the extent of the turbulent flow region ($p=1$ corresponds to a fully turbulent flow, while $p=0$ corresponds to a fully laminar flow over the hull). The turbulent friction line, C_{Fturb} , is represented by the Prandtl-Schlichting line presented in equation 2.4. C_{Flam} is Blasius' solution for a laminar friction line given by equation 2.5. Then the total resistance coefficient is given as

$$C_{Tf} = (1 + k_f) \cdot C_{Fc} \quad (6.12)$$

Further the total frictional resistance may be expressed by

$$R_{Tf} = \frac{1}{2} \rho S U^2 \cdot (1 + k_f) C_{Tf} \quad (6.13)$$

Where S is the wetted surface of the model.

6.2.1 Determination of form factor

This section aims to determine the form factor, k_f , for the two models featured in this thesis. As presented in previous chapters, the form factor is crucial information when estimating or otherwise dealing with theoretical aspects of viscous resistance for ships. Several methods to determine this exists, both a priori and based on experimental results. In the following section a selection of form factor calculation procedures is performed in order to give a certain estimate of the true value.

Empirical methods

Several studies have tried to construct closed form equations in order to give a good estimate of the form factor. An assortment of such methods and their results are presented in the following section.

From Grigson (1999) the following expression for the form factor is proposed

$$k_f = 0.028 + 3.3 \cdot \left[\frac{S}{L^2} \sqrt{C_B \frac{B}{L}} \right] \quad (6.14)$$

and in Molland et al. (2011) the *Watanbe* form factor is given as

$$k_f = -0.095 + 25.6 \cdot \left[\frac{C_B}{\left(\frac{L}{B}\right)^2 \sqrt{\frac{B}{T}}} \right] \quad (6.15)$$

According to Conn and Ferguson (1967) the following approximation of a form factor was determined by a series of geosim tests

$$k_f = 18.7 \cdot \left[C_b \cdot \frac{B}{L} \right]^2 \quad (6.16)$$

In addition Steen (2014b) gives the *MARINTEK* form factor to be

$$k_f = 0.6 \cdot \Phi + 75 \cdot \Phi^3 \quad (6.17)$$

where

$$\Phi = \frac{C_B}{L} \cdot \sqrt{B(T_{FP} + T_{AP})} \quad (6.18)$$

By inserting the data corresponding to each model from table 4.1 the results given in table 6.2 were obtained. As this is not a study of different form factor calculation procedures, these results will not be heavily discussed in this thesis. When assessing these results one should note that the *MARINTEK* formula is know within the towing tank community to underestimate the form factor to a large extent. However, these presented values, as well as the mean value of the methods are worth to notice.

	Model A	Model B
k_f Grigson	0.329	0.321
k_f Watabe	0.262	0.235
k_f Conn	0.353	0.296
k_f MARINTEK	0.173	0.189
k_f mean	0.279	0.261

Table 6.2: Calculated ship model form factors based on proposed equations.

Experimental methods

According to Molland et al. (2011) there are mainly two methods to determine the form factor based on ship model resistance measurements. The first method involves a low speed

towing tests, while the other contains an extrapolation of the wave resistance coefficient. The latter is referred to as *Prohaska's* technique. Both methods together with their results are in the following sections thoroughly described.

The method of low speed testing requires the model to be towed at speeds so small that the total resistance coefficient curve is parallel to the frictional resistance coefficient curve. As previously described, this is approximately the case when $Fn \leq 0.15$, as wave-making resistance may be neglected at such speeds. Hence, by assuming that the measured resistance only consists of frictional contributions the total resistance coefficient may be expressed as

$$C_T = (1 + k_f) \cdot C_F \quad (6.19)$$

In this thesis however, an attempt to obtain the most accurate results as possible were carried out. Thus, the presence of a laminar flow upstream of the turbulence stimulator was accounted for in this calculation. Subsequently the form factors were determined by

$$k_f = \frac{C_T}{C_{Fc}} - 1 \quad (6.20)$$

where C_{Fc} is a combined laminar-turbulent friction line calculated similarly as in equation 6.11. Hence, by assuming transition to turbulence at the stimulation device the loss in frictional resistance due to a laminar flow is accounted for. The experimental results for C_T was for both models chosen from the trip wire conditions, as these represents the most widely used stimulation technique. Also the trip wire was believed to be efficient in causing turbulence immediately due to its relatively large diameter compared to calculated required roughness height. Results from the two lowest Froude numbers tested were utilized. This was done to ensure that friction was by far the largest resistance contribution. The following results from equation 6.20 is presented in table 6.3.

Fn	Model A		Model B	
	0.052	0.078	0.078	0.104
C_T	$4.7 \cdot 10^{-3}$	$4.44 \cdot 10^{-3}$	$5.75 \cdot 10^{-3}$	$5.60 \cdot 10^{-3}$
C_{Fc}	$3.76 \cdot 10^{-3}$	$3.50 \cdot 10^{-3}$	$4.32 \cdot 10^{-3}$	$4.09 \cdot 10^{-3}$
k_f	0.251	0.258	0.329	0.30

Table 6.3: Results from the determination of form factor based on low speed test results.

According to ITTC (2002) Prohaska's method is the recommended procedure for estimating the ship form factor. In this method it is now assumed that the wave-making resistance, represented by the non-dimensional coefficient C_W , is proportional to Fn^n , where n is a

number between 4 and 6. Hence, the non-dimensional total resistance may be expressed as

$$C_T = C_F \cdot (1 + k_f) + A \cdot F n^n \quad (6.21)$$

Where A is a constant. Again, by utilizing a combined friction line equation 6.21 may be rearranged to give

$$\frac{C_T}{C_{Fc}} = (1 + k_f) + \frac{A \cdot F n^n}{C_{Fc}} \quad (6.22)$$

Which resembles a straight line on the form $y = b + ax$. Thus, by plotting C_T/C_F against $F n^n / C_F$ on the x-axis the y-axis interception point equals $(1 + k_f)$. Again the tripwire conditions were utilized in this calculation. The factor $n = 4$ was found to provide a line which had good correspondence with the experimental results. See figure 6.6 and 6.7 for the plot as well as the linear function for respectively model A and B. The resulting form factors for the two ship models are presented in table 6.4.

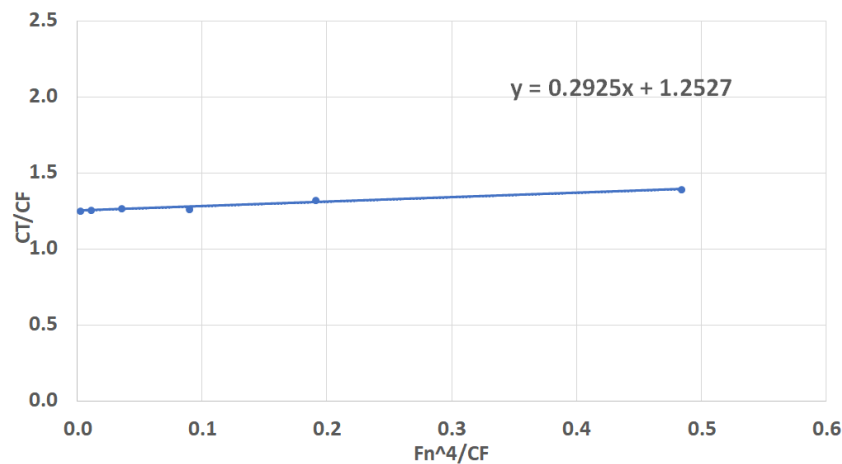


Figure 6.6: Prohaska plot with corresponding linear function when $n=4$ for model A.

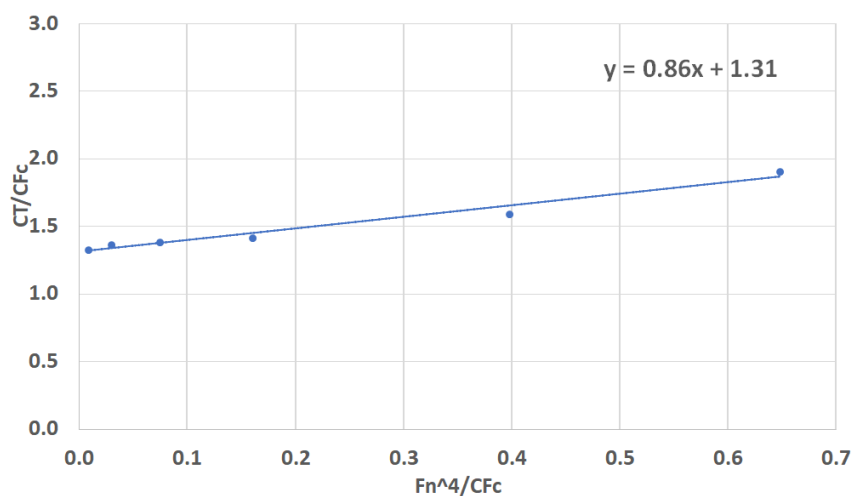


Figure 6.7: Prohaska plot with corresponding linear function when $n=4$ for model B.

	Model A	Model B
k_f	0.253	0.31

Table 6.4: Form factors calculated with Prohaska's method.

As the empirical methods do not take the current hull lines into account, they have a limited accuracy (Larsson et al., 2010). Because of this the experimental estimates for the form factor are believed to be more accurate and closer to the true value. However, some of the empirical results were found to have a remarkable agreement with the experimental results. For model A the results from low speed tests and Prohaska's method corresponds well, and $k_f = 0.245$ is further assumed in this report. In the case of model B the scatter in estimated form factor is somewhat larger between the methods. The empirical methods, with the exception of Grigson's method and Conn's method, gave a low value compared to the experimental results. Nonetheless, a form factor of $k_f = 0.31$ seems to agree well with both low speed tests and Prohaska's method and is therefore further assumed as the true value.

6.2.2 Resistance predictions

Now, as the ship model form factors are defined further frictional resistance predictions may be carried out. A total frictional resistance coefficient, C_{Tf} , given from equation 6.11 is still assumed to be valid. Thus, by performing calculations with different p_{turb} values, an expected frictional resistance based on where the turbulent transition occurs is obtained. These results are shown in figures 6.8 and 6.9. As expected the frictional resistance is greatest when a turbulent flow is assumed over the entire hull ($p_{turb} = 1$), and then decreasing as the wetted surface covered by a laminar flow is increased.

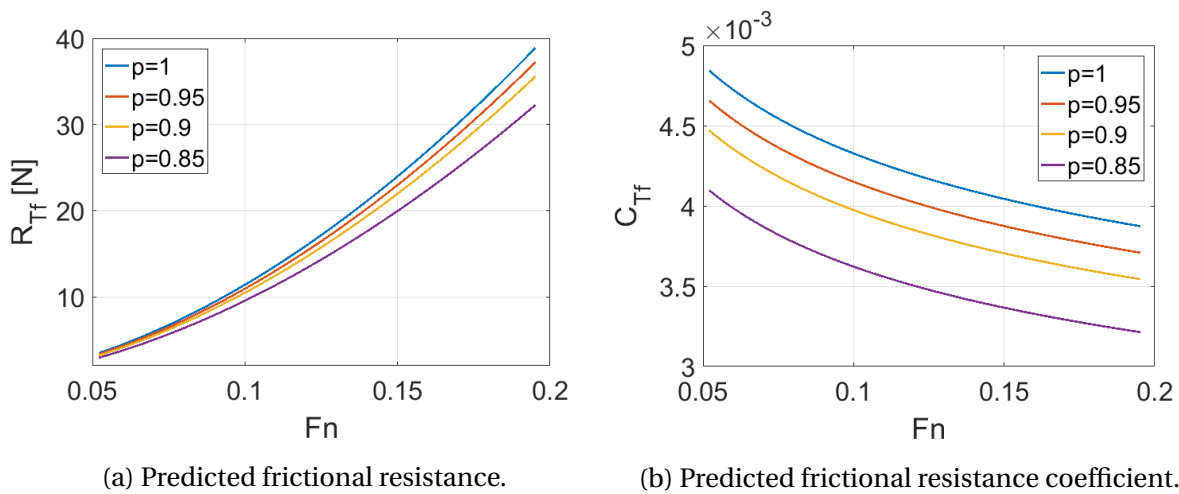


Figure 6.8: Model A.

This allows for the definition of the parameter ΔR_T which represents the loss in resistance

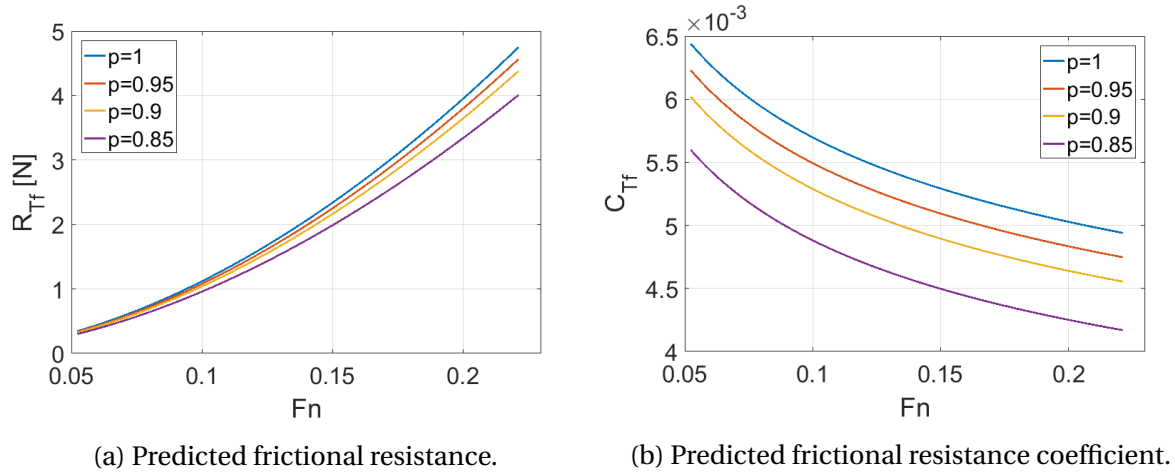


Figure 6.9: Model B.

due to a partly laminar flow compared to a fully turbulent flow surrounding the submerged hull. Following, ΔR_T is defined as

$$\Delta R = \frac{\rho}{2} S U^2 \cdot [(1 + k_f) \cdot C_{F_{turb}} - C_{Tf}] \quad (6.23)$$

This is a useful expression as it allows for an assessment of the hypothesis that the parasitic drag equals the loss in frictional resistance due to a laminar flow upstream of the stimulation device. This resistance is made dimensionless when written on the form

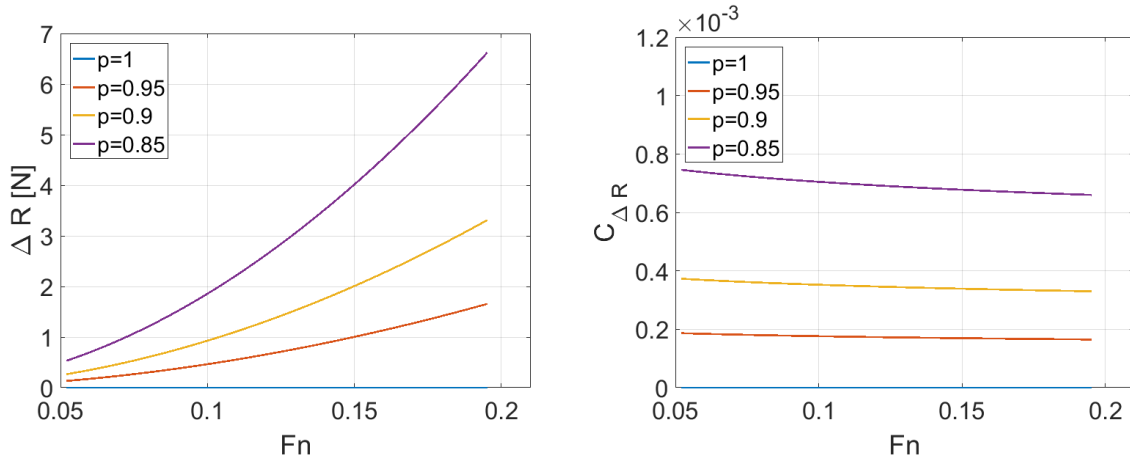
$$C_{\Delta R} = \frac{\Delta R}{\frac{\rho}{2} S U^2} \quad (6.24)$$

For the results regarding ΔR and $C_{\Delta R}$ for different p_{turb} values see figures 6.10 and 6.11 respectively. Clearly the loss in frictional resistance is increased when the part of the hull covered with laminar flow increases. The dimensionless loss in resistance is slightly larger for model B with the same p_{turb} values, implying that frictional resistance plays a somewhat larger role for this smaller model.

6.3 Total ship model resistance

6.3.1 Theoretical

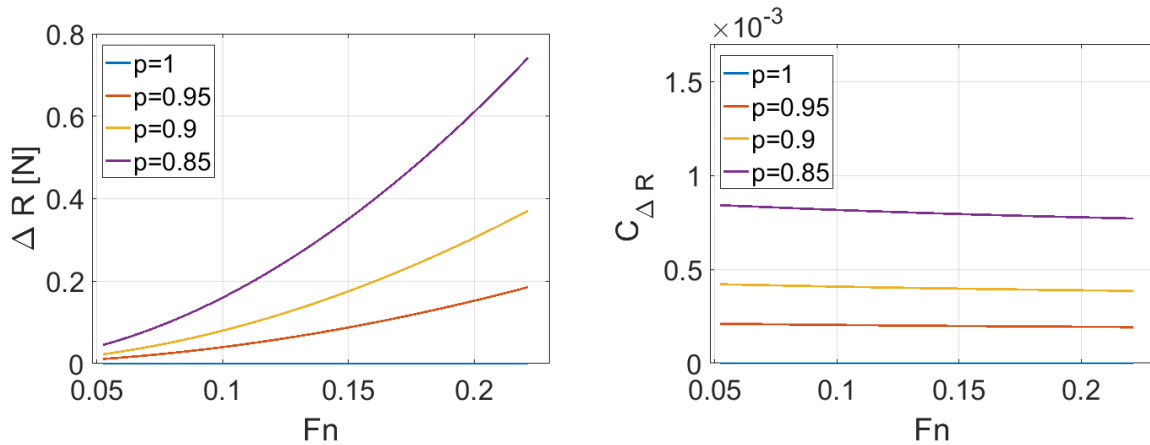
When determining the total ship model resistance only the viscous components and the parasitic drag due to the stimulation device is included in this theoretical approach. Residuary resistance such as wave-making resistance is following omitted in this approach. Consequently, the theoretical solution is only comparable with experimental results in the low Froude number range ($Fn < 0.15$). A plausible assumption made in this approach is that the turbulent transition occurs at one specific location, neglecting the intermittency region and any differences in point of transition along the hull. The point of transition was again



(a) Loss in frictional resistance due to partly laminar flow.

(b) Dimensionless loss in frictional resistance due to a partly laminar flow.

Figure 6.10: Model A.



(a) Loss in frictional resistance due to partly laminar flow.

(b) Dimensionless loss in frictional resistance due to a partly laminar flow.

Figure 6.11: Model B.

put to the same location as the turbulence stimulators. Following, the wetted surface upstream of the turbulence stimulator was assigned to a laminar friction line. In table 6.5 the surface upstream of the stimulator are given for the different conditions.

Now, by letting the parameter p_{turb} in equation 6.11 be equal to the part downstream of the stimulation, a corresponding resistance coefficient is determined. Then, the parasitic drag coefficient is superposed to give the total theoretical dimensionless resistance as

$$C_T = C_{Tf} + C_{Rtrip} \quad (6.25)$$

The results from this approach is thoroughly compared to experimental results in section 7.

	<i>Location</i>	<i>Surf. upstream</i>	<i>Part lam</i>	<i>Part turb</i>
Model A	2.5 % of LPP	0.31 m^2	0.035	0.965
Model B	2.5 % of LPP	0.067 m^2	0.042	0.958
	5 % of LPP	0.113 m^2	0.071	0.929
	10 % of LPP	0.215 m^2	0.135	0.865

Table 6.5: Wetted surface upstream of stimulators.

6.3.2 Semi theoretical

A scope of this chapter is to provide a basis on which the proposed method to determine total resistance by a combined friction coefficient and parasitic drag may be assessed. Therefore, a comparison between theoretical and experimental results over the entire speed range was sought after. However, to obtain such results the residuary resistance must be included. According to Molland et al. (2011) the determination of this is the sole purpose of conducting ship model tests. Hence, it is clear that no theoretical or empirical results would provide a liable approximation. So, to get an estimate of the residuary resistance coefficient, C_R , the experimental result for one of the conditions were utilized. Hence, it is assumed that C_R is equal for all turbulence stimulation conditions.

For both models the tripwire conditions were chosen to provide the experimental results in the calculation of C_R . This was done as the tripwire was believed to be efficient in causing immediate transition. Also the drag coefficient for a tripwire is well documented, providing a reliable approximation of the parasitic drag. Consequently, the following expression was utilized when estimating the residuary resistance component for the two ship models.

$$C_R = C_{Te} - (1 + k_f) \cdot [p_{lam} \cdot C_{Flam} + p_{turb} \cdot C_{Fturb}] - C_{Rtripwire} \quad (6.26)$$

Where C_{Te} is the experimental result for total resistance coefficient. p_{lam} and p_{turb} corresponds respectively to the part of wetted surface upstream and downstream of the stimulator (given in table 6.5). The final term, $C_{Rtripwire}$, is the dimensionless parasitic drag for a tripwire with diameter 1.5 mm. Then, as the residuary resistance component was determined, the total resistance coefficient for the other stimulation conditions was estimated as

$$C_T = C_R + (1 + k_f) \cdot [p_{lam} \cdot C_{Flam} + p_{turb} \cdot C_{Fturb}] + C_{trip} \quad (6.27)$$

Where C_{trip} now represents the parasitic drag of the current stimulation device in question. The results from this semi theoretical approach are carefully presented in chapter 7.

Chapter 7

Comparison of Theoretical and Experimental Results

As no determination of flow characteristics was conducted in connection with this thesis, only the measured resistance compared to available theory may be used in the assessment of each turbulence stimulation device. The purpose of this chapter is to provide such a comparison. To do so the theoretical and semi theoretical approach given in section 6.3 are compared to the experimental values presented in chapter 5.

7.1 Resistance

7.1.1 Model A

In figure 7.1 the experimental results are plotted together with the predictions described in section 6.3.1. In addition, the calculated total theoretical resistance by utilizing the fully turbulent ITTC-57 friction line is given for comparison.

The discrepancy between experimental results and the present theoretical approach are small, and well within the precision limits for the model test results at low speeds. Therefore, no certain conclusion could be made as the differences are smaller than the accuracy of the test results. However, the differences between the theoretical and experimental results seem to be consistent over the entire speed range. It is therefore assumed that a comparison of the two is credible, even though differences are within the precision limit.

From figure 7.1 it is clear that the Hama strip produce the smallest ship model resistance, while the sand strip provides the largest both theoretically and experimentally. In the low speed regime the experimental results for the Hama strip deviates drastically from the assumed friction line. Also, one should note that the measured values for the condition without turbulence stimulation only is parallel to the friction line in the range $0.1 < Fn < 0.13$.

Otherwise, the theoretical approach seems to be able to portray the differences in measured resistance to a decent extent. This is made clear when comparing the relative difference between the theoretical and experimental approach. Evidently, the use of the ITTC-57 friction line largely overestimates the frictional resistance, by utilizing the current form factor.

For a more clean and easily read figure, see figure 7.2 where only the two different trip wire conditions are shown. Here, the differences in theoretically determined resistance are solely due to a discrepancy in calculated parasitic drag. This theoretically determined difference seem to agree relatively well with the experimental results.

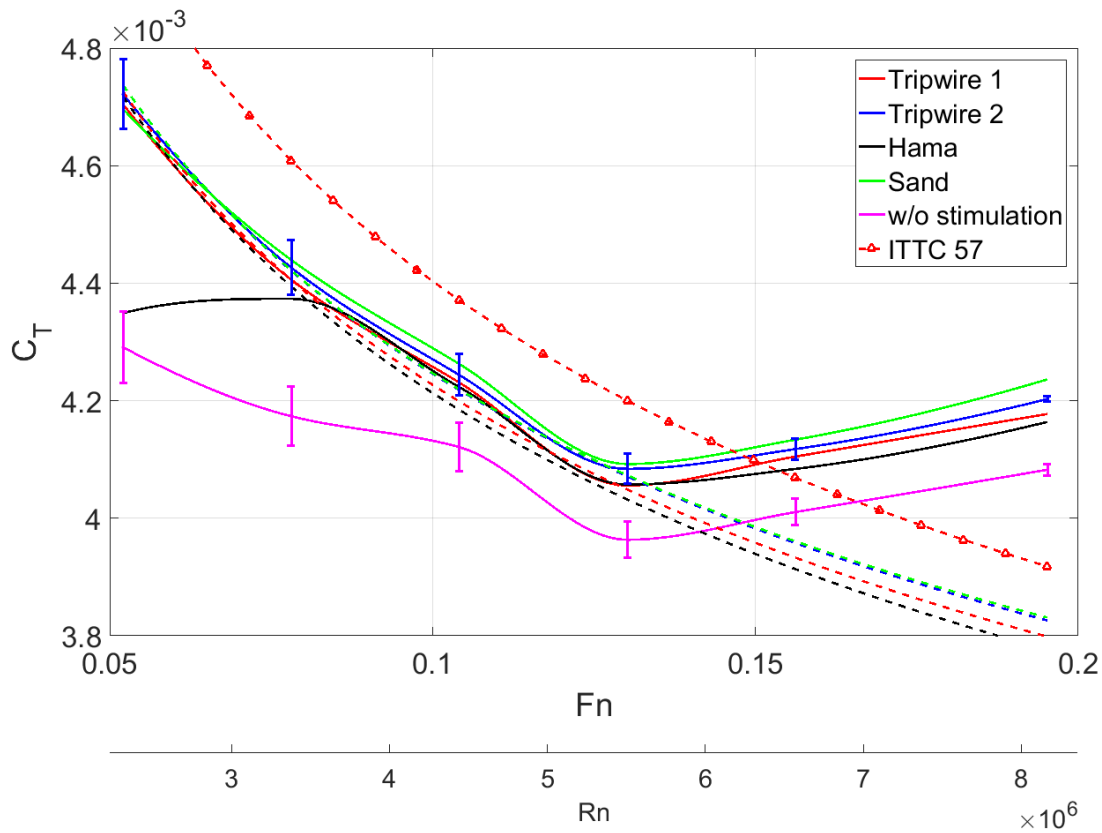


Figure 7.1: Comparison between theoretical and experimental results for model A, all stimulation techniques. Dashed lines represents the theoretical approach with a combined friction line, while triangles represents the ITTC-57 approach with calculated parasitic drag for tripwire 1.

The theoretical approach given in these two figures are solely based on friction lines and dimensionless parasitic drag. Consequently, the method is not capable of following the total resistance curve through any bumps or valleys naturally present in the experimental results and certainly not when the residuary resistance component kicks in for $Fn < 0.13$. Thus, by following the procedure described in section 6.3.2 the experimental results could be measured against the now *semi theoretical* resistance prediction. This is done in figure 7.3. Where the residuary resistance is found by utilizing the experimental results for the tripwire con-

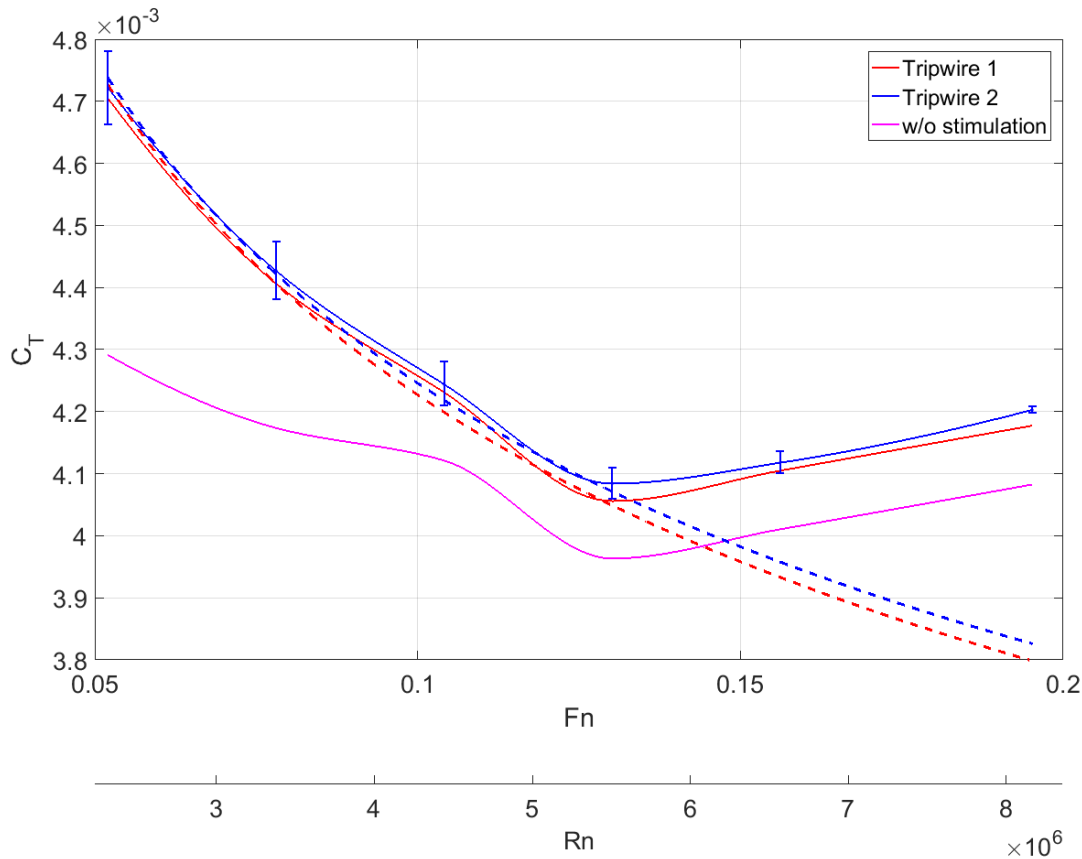


Figure 7.2: Comparison with analytical results for model A, trip wires. Dashed lines represents the theoretical approach with a combined friction line.

dition with the largest diameter, known as *tripwire 2*. This condition is consequently not included in the figure as the semi theoretical prediction would equal the experimental result. From this comparison a similar agreement as for the theoretical approach is evident. Underlining that the proposed method to determine parasitic drag is, to a certain degree, consistent with experimental results although the total resistance is somewhat underestimated.

7.1.2 Model B

Similarly as done for model A a comparison between experimental and theoretical result was performed for the smaller model B. In figure 7.4 the measured total resistance coefficient is presented together with the predicted frictional resistance superimposed with the calculated parasitic drag. Again, the theoretical approach is able to capture the measured discrepancy between the stimulation techniques. However, as speed increases the measured difference in resistance between the stimulation conditions decreases. This is in opposition with the theoretical approach, where the discrepancy in parasitic drag only expands as speed is increased. However, these deviations between the measured and theoretical results are fairly precise when considering the total resistance coefficient values. To illustrate this table 7.1

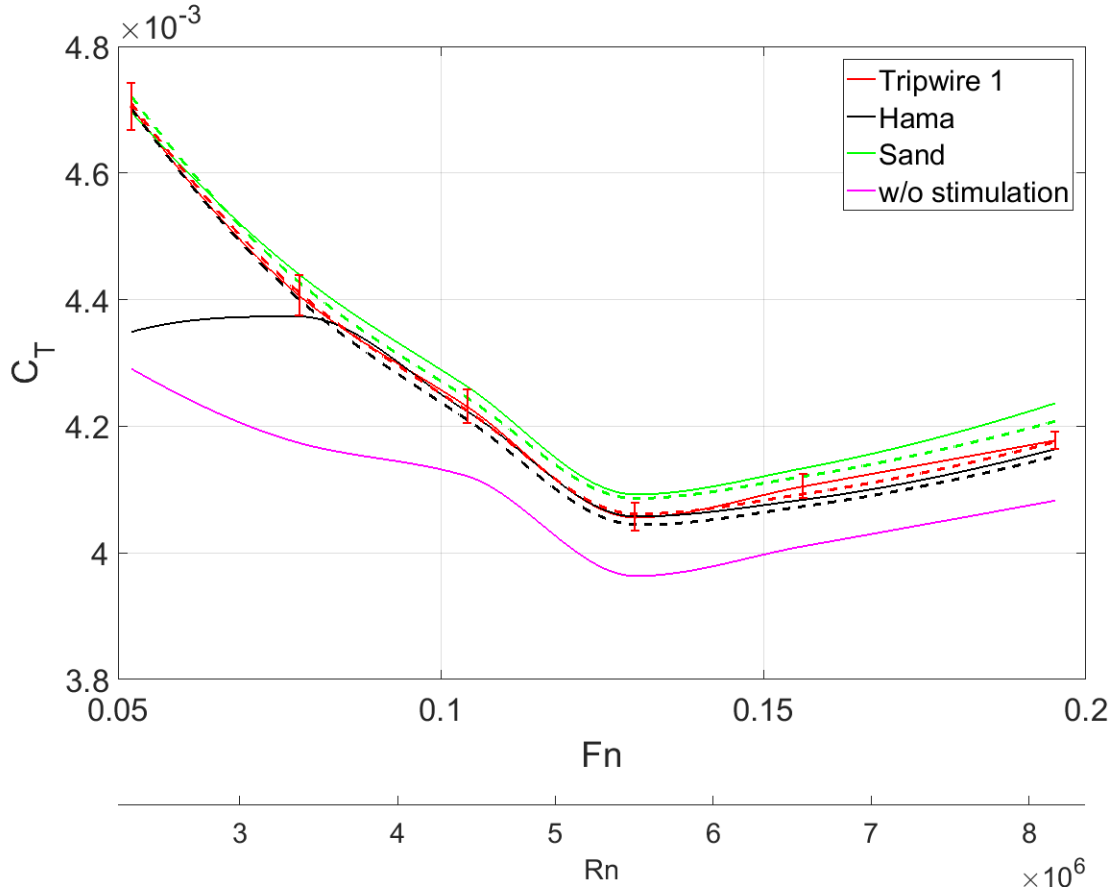


Figure 7.3: Comparison with semi theoretical results for model A. Dashed lines represents the semi theoretical approach.

was constructed, showing the difference in percent between the trip wire and Hama strip for both experimental and theoretical results on low and high speed. Similarly as for model A the ITTC-57 approach overestimates the resistance to a large extent.

For low speeds, the experimental results for the Hama strip shows a somewhat similar deviation from theoretical calculations as for model A. Even the tripwire condition seems to deviate from the predicted resistance at the very lowest speed. In the speed range of $0.1 < F_n < 0.14$ the predicted resistance for the tripwire condition follows the experimental C_T -curve to a large extent. In case of the Hama strip deviations from the theoretical approach are larger in the same speed interval.

	<i>Low speed</i>	<i>High speed</i>
<i>Theoretical</i>	1.9 %	4.3 %
<i>Experimental</i>	3.7 %	3.0 %

Table 7.1: Differences in total resistance between the Hama strip and trip wire on model B.

In figure 7.5 comparisons of results from the conditions with Hama strip at different locations are shown.

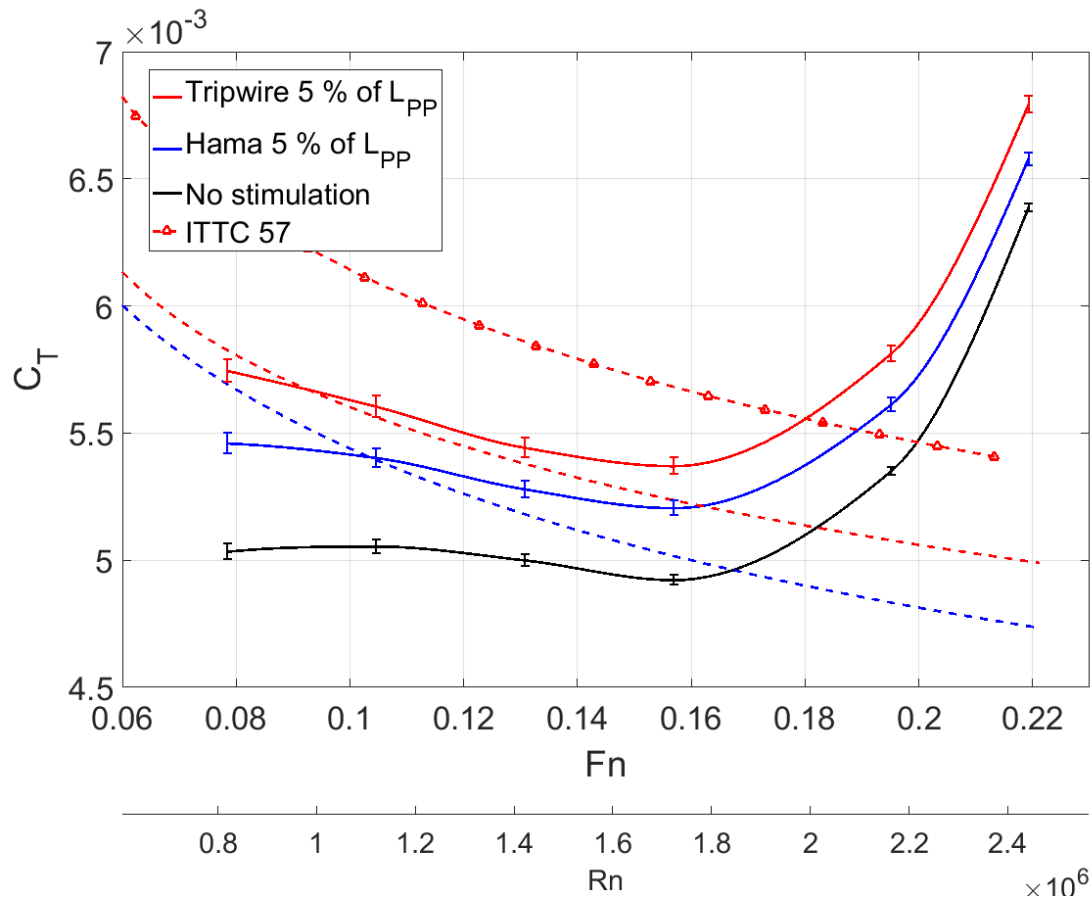


Figure 7.4: Comparison between theoretical and experimental results for model B. Dashed lines represents the theoretical approach with a combined friction line, while triangles represents the ITTC-57 approach with calculated drag for the tripwire.

Now, as transition to turbulence is assumed at the stimulation, the theoretical approach predicts a larger frictional resistance when the tripping device is located closer to the model FP. This is clearly shown in the theoretical results where the condition with a stimulator at 2.5 % gives the largest resistance, for then to decrease as the Hama strip is located further aft. However, when comparing this to the measured resistance from the model tests quite the opposite outcome was evident. From figure 7.5 it is clear that the largest experimental resistance was produced when the Hama strip was placed furthest aft, and then decreasing as the turbulence stimulator moves closer to the stem. Such a large discrepancy between theoretical and experimental results could imply that the assumptions made in the theoretical calculations are not appropriate. As expected, by including the residuary resistance component similar characteristics are manifested along the entire speed range. This is illustrated in figure 7.6.

As shown in figure 6.4 the parasitic drag increases when a turbulent boundary layer is present compared to a laminar boundary layer. The calculated naturally extent of the laminar regions for the two models are presented in the next section, however based on these results indications are made to that transition occurs upstream of a stimulator when located at 10

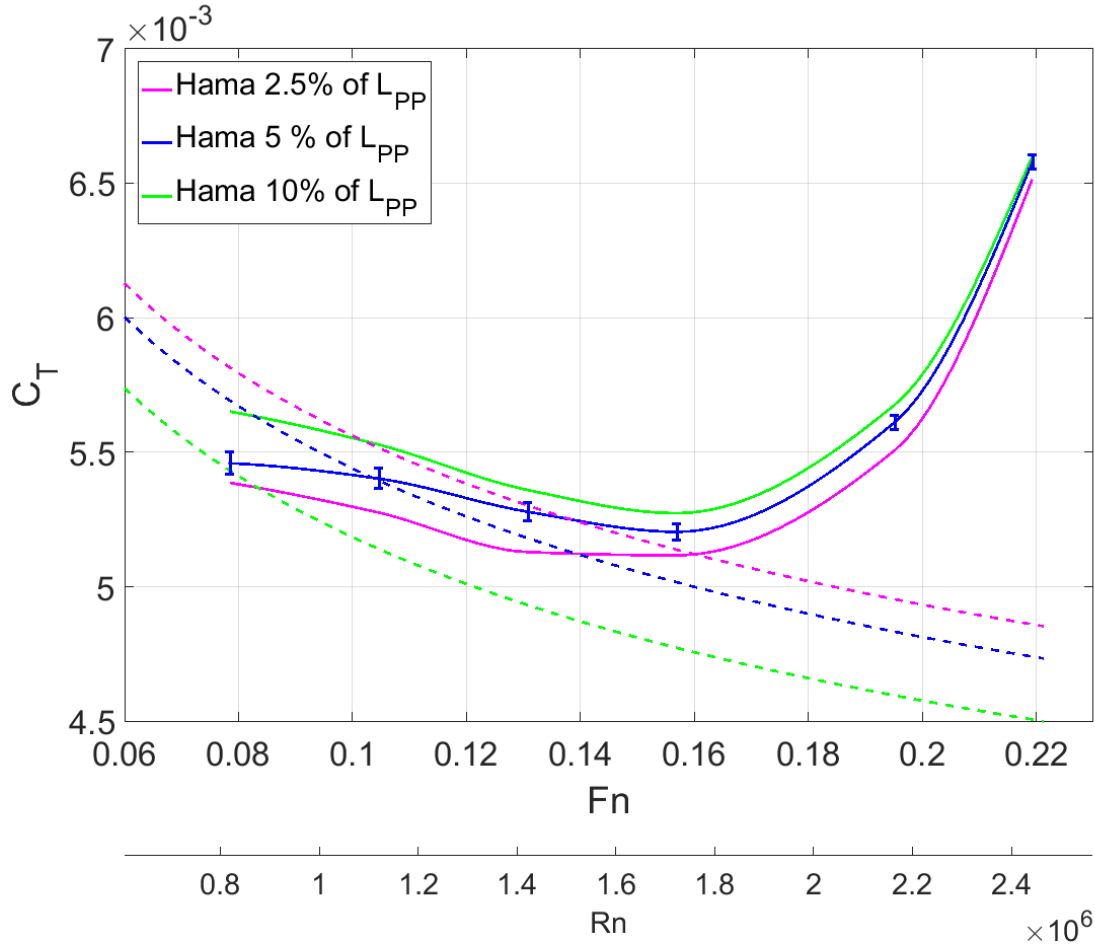


Figure 7.5: Comparison between theoretical and experimental results with turbulence stimulation at different locations for model B. Dashed lines represents the theoretical approach.

% of L_{PP} . Then, 12 % of the wetted surface is exposed to laminar flow, as opposed to 13.5 % when transition is assumed at the stimulator. Thus both the parasitic drag and the assumed friction coefficient should be altered in the theoretical approach to obtain accurate predictions. This is done in figure 7.7 where a natural transition to turbulence is assumed upstream of the stimulator. Evidently the consequences are an increased parasitic drag and increased frictional resistance compared to when transition is assumed at the stimulation device. The approach assuming a transition to turbulence shortly upstream of the stimulator provides a remarkable resemblance with the experimental results.

7.2 Naturally extent of laminar region

As no methods of flow characteristics determination was performed, only the measured resistance compared to theoretical calculations could reveal where transition to turbulence actually occurred naturally in the experiments. This was attempted by setting the experimentally determined total resistance coefficient for the conditions without any turbulence

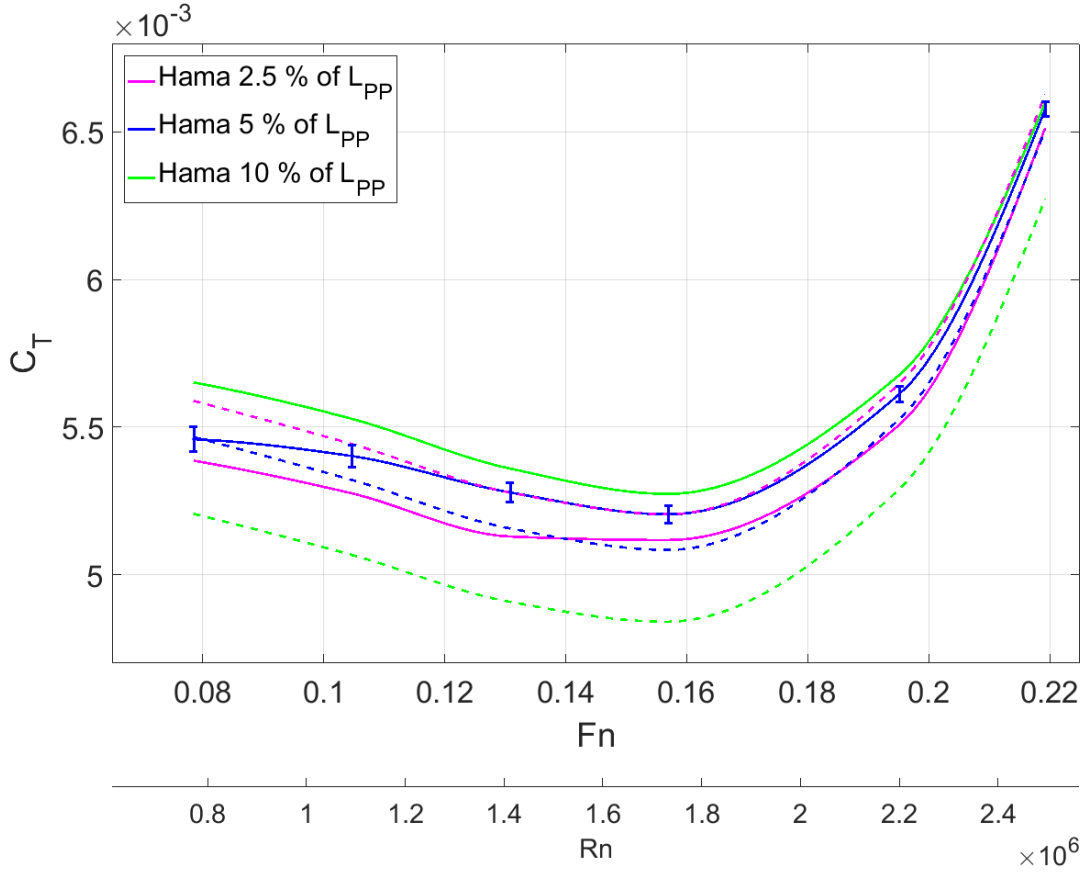


Figure 7.6: Comparison between semi theoretical and experimental results for model B. Dashed lines represents the semi theoretical approach.

stimulation equal to equation 6.27. Thus, the following expression was obtained

$$C_{Texp} = C_R + (1 + k_f) \cdot [p_{lam} \cdot C_{Flam} + (1 - p_{lam}) \cdot C_{Fturb}] + C_{trip} \quad (7.1)$$

Where C_{Texp} is the experimental total resistance coefficient for the conditions without any turbulence stimulation. Consequently $C_{trip} = 0$ as no stimulation device was applied. Thus, by solving equation 7.1 with respect to p_{lam} the extent of the laminar region based on the experimental results was obtained as

$$p_{lam} = \frac{\left[\frac{C_T - C_R}{1 + k_f} - C_{Fturb} \right]}{C_{Flam} - C_{Fturb}} \quad (7.2)$$

The theoretical predictions which is further compared to the results from equation 7.2 are based on the critical Reynolds number for transition to turbulence, Rn_{crit} given by

$$Rn_{crit} = \frac{U \cdot x_{crit}}{\nu} \quad (7.3)$$

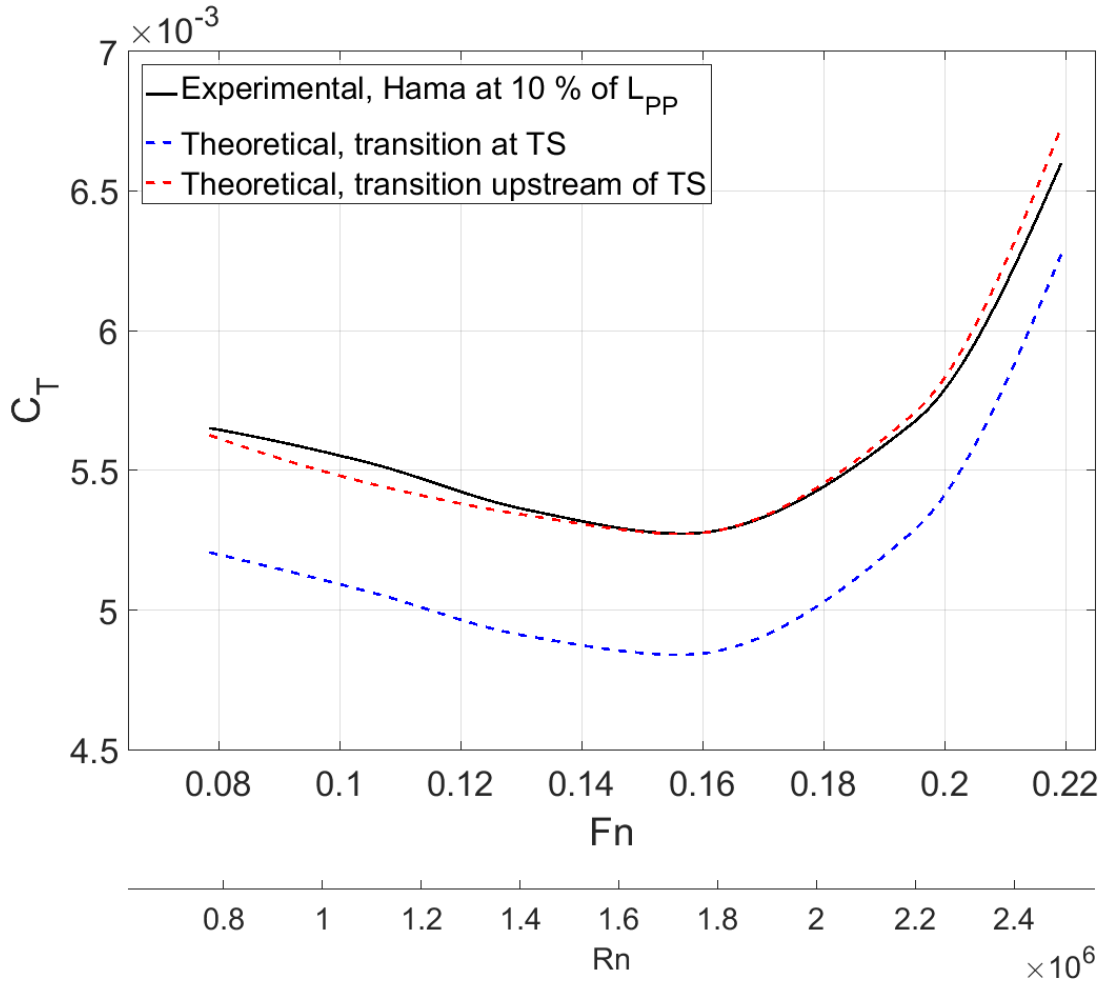


Figure 7.7: Theoretical and experimental results for model B with Hama strip located at 10 % of L_{PP} . Indicating the difference in assuming transition to turbulence upstream or at the location of stimulator.

Where x_{crit} now represents the length from the ship model FP to the point where turbulence naturally occurs somewhere along the hull. By solving equation 7.3 with respect to x_{crit} and assuming a value for Rn_{crit} a prediction of the laminar extent was obtained. From the definition in equation 2.15, the assumption of $Rn_{crit} = 3 \cdot 10^5$ was made. Thus the x_{crit} is given on the form

$$x_{crit} = \frac{3 \cdot 10^5 \cdot \nu}{U} \quad (7.4)$$

Now, in order to compare the theoretical estimates to the experimental results a relation between x_{crit} and p_{lam} is required. This was done by measuring l_s (as defined in section 4.2) and its corresponding wetted surface at several points along the hull. Then, by plotting the results a regression line was constructed to give the relationship between l_s and wetted surface, or in this case x_{crit} and p_{lam} . As no measurements of wetted surface was performed

in the aft part of the models the following results are assumed to be valid when $\frac{p_{lam}}{S} < 0.5$. Suitable regression lines were found from relatively simple quadratic equations. These are given on the following form for model A and B respectively

$$x_{critA} = -3 \cdot 10^{-5} \cdot p_{lamA}^2 + 0.058 \cdot p_{lamA} + 0.08 \quad (7.5)$$

$$x_{critB} = 2 \cdot 10^{-4} \cdot p_{lamB}^2 + 0.013 \cdot p_{lamB} + 0.08 \quad (7.6)$$

Then, by solving these equations with respect to p_{lam} the following expressions were obtained for model A and B

$$p_{lamA} = \frac{20}{3} \left[\sqrt{21085 - 750 \cdot x_{critA}} + 145 \right] \quad (7.7)$$

$$p_{lamB} = \frac{5}{2} \left[\sqrt{800 \cdot x_{critB} + 105} - 13 \right] \quad (7.8)$$

In figure 7.8 the theoretical estimates given from equation 7.7 and 7.8 is compared to the experimental values given from equation 7.2.

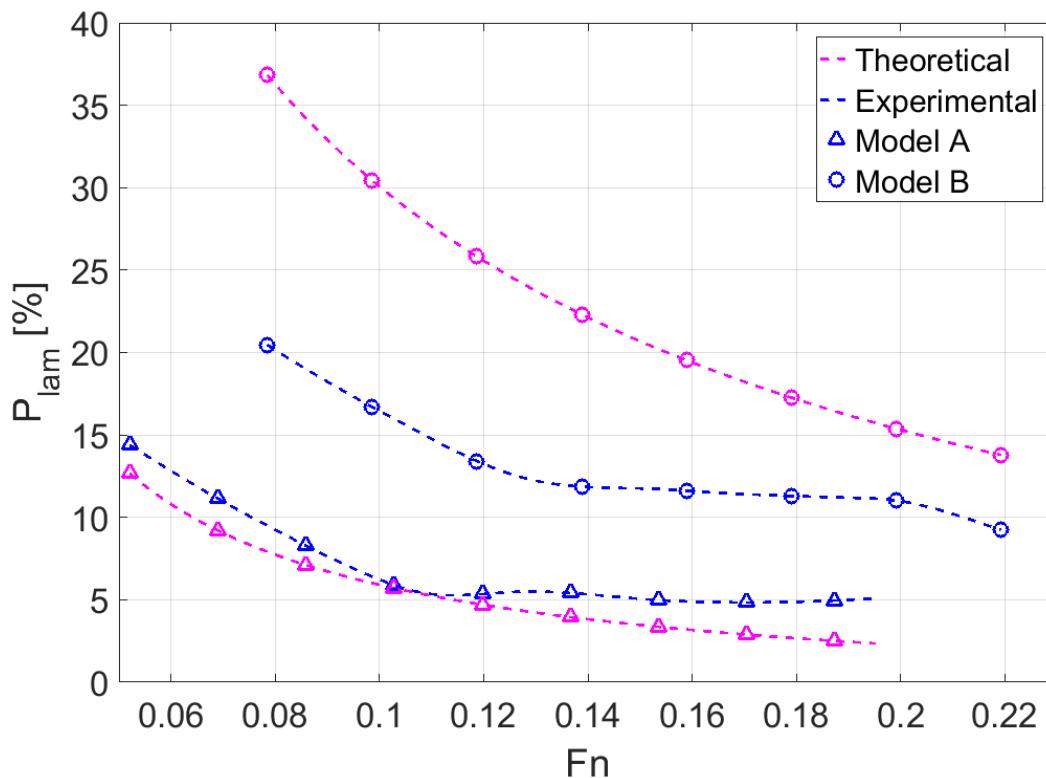


Figure 7.8: Comparison of theoretical and experimental results regarding naturally extent of laminar flow given in percent of total wetted surface.

From figure 7.8 it is clear that the laminar region decreases with increasing speed, as should be expected from equation 7.4. Clearly model B is experiencing a laminar flow over a larger

region relative to its wetted surface than model A. The difference between the two models on this subject are however much larger when following the theoretical approach compared to the measured values. This should lead to a discussion regarding the assumed constant value for Rn_{crit} . Figure 7.8 indicates that the assumption of $Rn_{crit} = 3 \cdot 10^5$ is a somewhat low, but decent estimate for model A. For model B on the other hand, it is not a particularly good assumption as it predicts a way too high extent of the laminar region.

This may further be compared to certain visual observations made during the ship model testing. Figure 7.9 shows close up pictures taken of the model hull traveling at the lowest speeds tested. In the pictures a wave pattern is clearly visible at a point along the model surface. Although not clear from the pictures, the wave formation did to a certain extent move between sections 14 and 15 for model A and sections 7 and 8 for model B. As no other pressure gradient was present here, the surface waves could originate from turbulent eddies present in this area due to a laminar-turbulent transition. This would in that case agree well with the experimentally determine extent of laminar region given in figure 7.8.

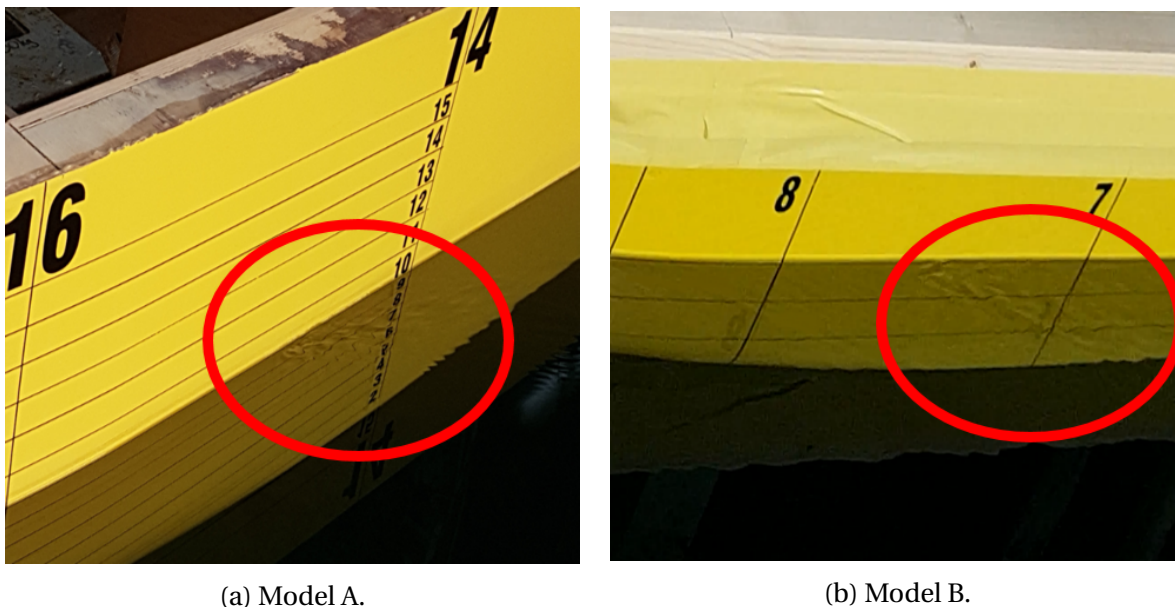


Figure 7.9: Picture showing what seems to be surface waves generated by turbulent eddies due to a laminar-turbulent transition.

To determine Rn_{crit} from the experimental results equation 7.2 was utilized together with equations 7.5 and 7.6. These results are presented in figure 7.10. Evidently neither results for model A nor model B seems to have a constant Rn_{crit} , as values are increasing with increased speed. However $Rn_{critB} = 2 \cdot 10^5$ seems to be a fair estimate for model B. For model A values for Rn_{crit} varies with speed to a larger extent and the determination of a constant value is more difficult. Nonetheless, $Rn_{critA} = 3.7 \cdot 10^5$ could serve as a good approximation. Considering that Munson et al. (2013) in general gave Rn_{crit} to be within the interval $2 \cdot 10^5 < Rn_{crit} < 3 \cdot 10^6$, it is indicated that in the case of ship model testing transition occurs relatively early compared to other situations within fluid dynamics.

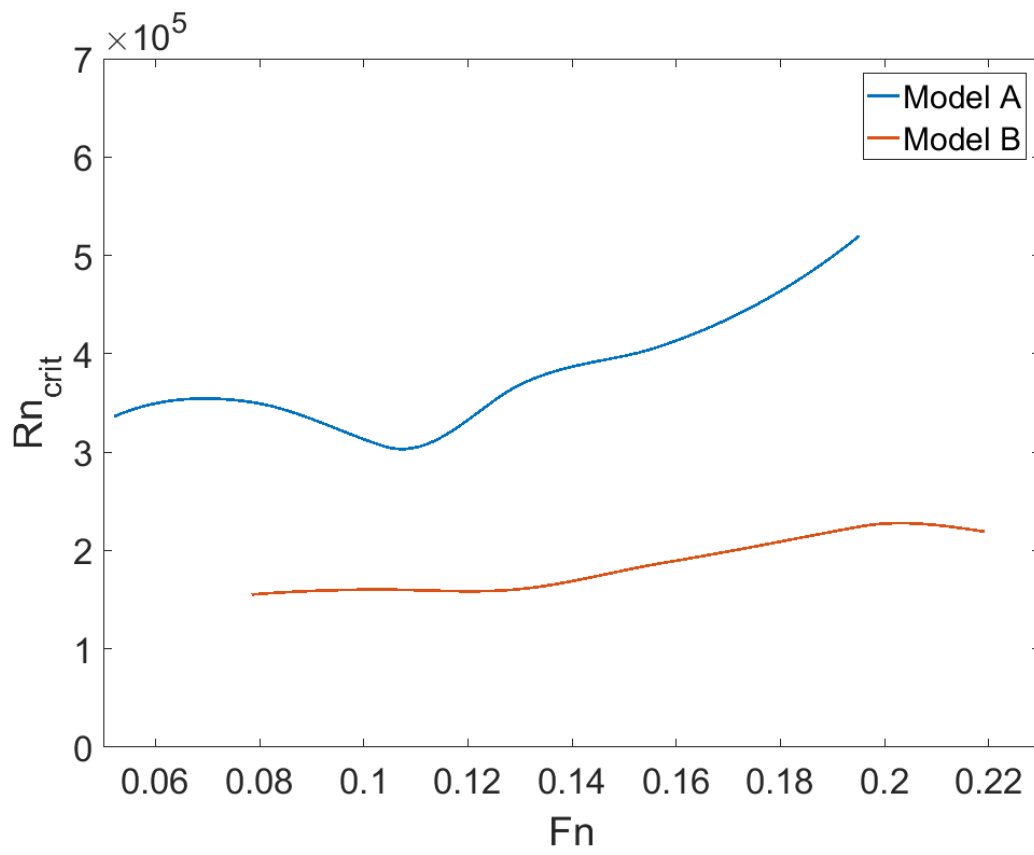


Figure 7.10: Experimentally determined critical length based Reynolds number, Rn_{crit} .

Chapter 8

Discussion

The comprehensive ship model testing and theoretical calculations performed in this report provides interesting results well worth a thorough discussion. This is the intention of the present chapter, where attempts are made to link the results presented so far to the known theory. In such a way the aim is to provide a scientific investigation to determine the various attributes connected to turbulence stimulation techniques in use today.

8.1 Turbulence stimulation techniques

When assessing the experimental results for model A at low speeds it is clear that the precision limit is substantially larger than the differences in measured resistance between the stimulation conditions. Even though this is the case the measured discrepancies are assumed to be reliable as they are largely consistent over the entire speed range. In addition these differences agree relatively well with the presented theoretical approach. For model B the precision limit is much smaller than the measured differences, hence the discrepancies in measured resistance between the stimulation techniques are absolutely significant over the entire speed range. Again, the theoretical approach manage to predict the differences in resistance between the conditions to a large extent.

As described in previous sections the utilized form factor, k_f , will decide the magnitude of the theoretically predicted resistance. In this report the utilized form factors were determined based on experimental results through Prohaska's method and low speed testing. Thus, one might question the validity of the current theoretical resistance predictions when they are compared to the very same experimental results. Also, by utilizing a fully turbulent friction line in the experimental determination significantly smaller form factor values would have been obtained. However the experimental estimates for k_f seem to agree well with a selection of available empiric formulas, implying that appropriate values were indeed chosen.

The measured resistance for conditions without any stimulation device are well below the

measured results when stimulation was applied. Based on this, it is evident that the application of turbulence stimulation does affect the measured total resistance to a large extent. For model A the C_T -curve corresponding to the Hama strip falls away to an almost horizontal line in the low speed region as clearly shown in figure 5.2. Similar trends are also evident for the Hama strip condition for model B, depicted in figure 7.4. Such a loss in resistance compared to both theoretical calculations and other stimulation conditions indicates that the Hama strips utilized in these experiments were not fully effective in generating turbulence at low speeds. This claim is supported by Larsson et al. (2010) who states that a C_T -curve of this shape should at once be suspected of being subjected to a partly laminar flow. For model A both the tripwire conditions and the sand strip produced results that were parallel to the assumed friction line when $Fn < 0.13$. Hence indications are made to that these stimulation techniques are in fact effective in generating turbulence immediately or shortly downstream of the stimulator, even at low speeds.

For model B even the measured results for the tripwire condition at the lowest speed indicates a non effective stimulation. One should keep in mind that much smaller Reynolds numbers are in play for model B when comparing the two models. Meaning that much smaller inertia forces are present compared to the viscous force contribution. Consequently, any turbulence generation is delayed. This difference is believed to cause a significant variation in stimulator efficiency between the two models. This is also made clear when determining the necessary roughness height, as a larger height was required in case of model B even though the stimulators were relatively placed further aft.

The differences between the various stimulation techniques are in general small for model A (in the range of 0.5 to 1.5 %). For model B similar results were obtained as the tripwire gave the largest resistance. Here however, the differences between the Hama strip and tripwire were much larger (in the range of 3 to 5.5 %). As these differences were substantially larger for the smaller model B, indications are made towards that more care should be taken in the choosing of a turbulence stimulation device on smaller ship models.

The method to determine the parasitic drag in this thesis is well supported by available theory. Especially by Shen et al. (2015) where a method to calculate the induced drag by a tripwire is derived. In this method the velocity at the roughness height, $u(k)$, is together with a constant drag coefficients, C_{trip} , the dominating parameters. In this thesis $u(k)$ was determined from simple boundary layer profile and local pressure approximations. From these approximations and the experimental results it is clear that the roughness height, k , is a crucial parameter in this calculation, as only slightly changing the roughness height will largely affect the induced drag.

Drag coefficients corresponding to each stimulation device were determined based on avail-

able literature and previous studies concerning both general fluid dynamic drag and induced drag by turbulence stimulation devices. Thus, the method does not provide the exact induced resistance. It is therefore intended as a rough determination method only. However, a relatively good agreement with the experimental results from both model A and B are evident when utilizing this approach. From figure 7.3 it is indicated that the predicted total resistance using this method is somewhat lower than the experimental results. Thus, in order to obtain an even more accurate determination of the parasitic drag the C_{trip} -values could be slightly adjusted. This is however outside the scope of this present report.

Due to a good agreement with theoretical results, all stimulation techniques are deemed to be effective in generating turbulence in the moderate to high speed regime. Thus, it may be fair to assume that the deviation in measured resistance between the conditions originate from the difference in induced drag connected to each device.

Based on this, the conclusion that the Hama strip is a highly efficient turbulence stimulator with only small amounts of induced drag is evident. The drag coefficient, C_{trip} , is approximately 2.5 times larger for the Hama strip than the tripwire. Hence, a connection between C_{trip} and efficiency in generating turbulence could be drawn. A plausible hypothesis is that an increased C_{trip} could be due to enlarged vortex shedding behind the device. Therefore, an explanation to the large C_{trip} for the Hama strip is that they are designed to generate more flow disturbances on the form of shredded vortices. The high efficiency in turbulence generation is also reflected by the low Rn_k given for the Hama strip. The making of the Hama strips however, proved to be largely time consuming and relatively complex compared to the other techniques tested.

The other two-dimensional turbulence stimulation technique tested in this work was the sand strip. For this technique all results indicates an efficient trip of the laminar flow. The reader should note that a relatively large roughness height was utilized for this condition compared to the determined required value. This was both due to the available sand grain selection at the time of testing and actions taken to simplify the mounting procedure. Thus, it is assumed that a smaller roughness height would still provide an efficient flow tripping as well as induce a smaller drag force. The large roughness height applied in the experiments is believed to directly cause the high measured resistance values for this condition.

Also the tripwires tested in the experimental part of this thesis proved to be efficient in generating turbulence. The exception seems to be for model B at the very lowest speeds. In general ship model experiments are not executed at such low Reynolds number as in this case, thus the tripwires are deemed efficient for all practical purposes. The mounting procedure is simple and was the least time consuming of the tested mechanisms.

Based on the experiments and theoretical analysis presented in this thesis a determination

of each turbulence stimulator's characteristics has been obtained. By comparing the roughness Reynolds number, Rn_k , for each turbulence stimulation mechanisms it is possible to obtain an indication of how efficient they are in generating turbulence. From table 4.3 it is evident that a large discrepancy between different stimulation devices exist when it comes to required roughness height. All tested mechanisms in this report were formed to have a Rn_k within these values. Since all mechanisms are deemed efficient in causing a turbulent transition at relevant ship model speeds, this approach may be regarded as a good approach to determine the required roughness height, at least from a ship model perspective.

So far in this report a variety of turbulence stimulator mechanisms have been presented theoretically and experimentally through different resistance analysis. Now, in order to determine the best or most preferred turbulence stimulation technique, an establishment of which parameters to base this assessment on is required. Examples here are the level of complexity in mounting each mechanism and uncertainty connected to i.e parasitic drag or the turbulence enhancement efficiency. Such criteria will be dependent on the objective of the current model test, and are thus subjected to change depending on each experiment carried out. As an example would the additional parasitic drag due to a tripwire be unacceptable when performing model tests on smaller high-speed vehicle models or hydrofoils. A contradiction would be the model test of a large oil tanker, where the model is in the order of 5-8 m and model speed is low. Then, correct flow modeling is of high importance as the frictional resistance is by far the largest resistance component. Thus, when considering the two model tests carried out in this present work, parameters that govern the preferred stimulation mechanisms may be summarized as follows:

- An efficient trip of the laminar flow causing a quick transition to turbulence downstream of the stimulator.
- Appropriate generation of parasitic drag, such that any loss in frictional resistance due to a laminar flow is, as much as possible, canceled out.
- A straight forward and untroubled mounting procedure.

When comparing the different stimulation techniques and their usage in practical model testing today a pattern is somewhat visible. For high speed models and on appendices, mechanisms that ensure a quick transition and cause minimum drag is utilized. Such devices include small grained sand strips and Hama strips. These methods however tend to increase in complexity and time spent on installation. Thus the much more simple procedure of the tripwire has been adopted as the standard method of turbulence stimulation, at least on conventional ship models.

As previously stated, the tripwires are deemed as an appropriate turbulence stimulation approach. In fact, by considering the established parameters for a preferable method, it would

be the most preferred turbulence stimulation method amongst the one discussed in this thesis. Reasons for this judgment are the ease of mounting, effective turbulence generation for all relevant speeds in ship model testing, and an appropriate amount of parasitic drag. However, one should note that some uncertainty is connected to the hypothesis that the parasitic drag of the trip wire cancels out the lost frictional resistance due to a laminar flow. This is further discussed in section 8.2.

An alternative to the trip wire could be to apply several fields of a sand paper type as seen in figure 3.6b. As established from this report, even devices with a small roughness height are capable of generating turbulence at relevant speeds for conventional ship model testing. Such devices cause a much smaller induced drag than mechanisms with a larger height such as the tripwire. Hence, by applying a stimulator with small roughness height shortly downstream of the ship model's FP, and then again at a location further aft where the flow could be subjected to relaminization, a fully turbulent flow might be ensured over the entire model hull with minimal parasitic drag. If we also assume the sand strip to be previously manufactured and applicable to all conventional models with a simple mounting procedure, this may seem like a better alternative than the wire.

As mentioned, the prevailing approach in this thesis is to consider ship models with relatively large submergence and low speed. However some interesting aspects connected to other models subjected to hydrodynamic testing are worth to discuss in order to fully illuminate each turbulence stimulation's potential. Appendages models, meaning a hydrofoil or a strut of some kind attached to the ship model can be noticeably affected by scale effects connected to laminar-turbulent flow. As a laminar boundary layer separation will increase the viscous pressure resistance compared to the turbulent full scale conditions, also if the appendages generates lift a laminar flow could cause spurious model results. For these reasons flow tripping devices are frequently applied on appendages (ITTC, 1990). To minimize the scale effects, turbulence should be generated immediately after the stimulation device without altering the drag in a too large extent. On the other hand, appendices are mostly located inside the turbulent boundary layer and wake in the aft body of the ship. Since the flow in both model and full scale is already turbulent there, the problem of turbulence stimulation on appendages might be less. However, a further study of the use of turbulence stimulation on appendages is outside the scope of this present report.

For testing of high-speed marine vehicles turbulence stimulation may be omitted if the length based Reynolds number exceeds $5 \cdot 10^6$ (ITTC, 2017a). However, if turbulence stimulation is required the risk of air suction must be considered. Due to this phenomenon tripwires are not recommended on high-speed models (ITTC, 2017a). It is worth to mention that when the model velocity exceed 3 m/s, even the distributed sand roughness can cause air suction (ITTC, 1990). Therefore, when this is the case application of square studs is recommended.

8.2 Location of turbulence stimulation

Regarding the placing of the stimulators, there seems to be a broad agreement to locate the stimulation devices at either 2.5 or 5 % of the ship model L_{PP} aft of FP. At SINTEF Ocean the standard operating procedure for larger ship models is to place the stimulators at section "19.5", corresponding to 2.5 % of L_{PP} provided that the ship model consists of 20 sections (which is often the case). This is a confirmation of that some deviation from the ITTC-guidelines of 5 % of L_{PP} does occur. The application of additional stimulators were not a subject of this study. Even though both models were fitted with bulbous bows, the bulbs were deemed too small to be subjected to additional turbulence stimulation. In the case of high-speed crafts ITTC (1990) recommends a set of test runs to determine the most appropriate location of the stimulators. Experience from SINTEF Ocean points to this as an event that virtually never happens due to both time and resource constraints. Turbulence stimulation on high-speed craft models was otherwise outside the scope of the work presented in this report.

The effects of different placing of a turbulence stimulator device was investigated by placing a Hama strip at three different locations (2.5, 5 and 10 % of L_{PP}) on model B. The resulting measurements established that the condition with the Hama strip furthest aft gave the largest resistance, for then to decrease as the stimulation device was moved closer to the stem. Hence, if transition at the stimulation device is assumed, this is a conflicting result when compared to theory. Therefore, it is fair to assume that transition to turbulence does not occur at the location of the Hama strip under these conditions. Further, the assumption that the Hama strip at 2.5 % does not serve as an effective tripping device seems credible to make, as the small measured resistance indicate large areas of laminar flow.

Reasons for a non-effective turbulence generation downstream of a turbulence stimulator could be various. Firstly, a sufficiently high length based Reynolds number, Rn_x , is required for the initially disturbance to evolve to turbulence. As Rn_x for model B with Hama strip at 2.5 % only was in the range of $2.4 \cdot 10^4$ to $1 \cdot 10^5$ this could seem like a credible explanation. Implying that any initial vortex shedding quickly die out downstream of the Hama strip causing a relaminization of the flow. Another aspect to consider is the effects of pressure gradients. As previously discussed, a negative pressure gradient will delay the onset of turbulence. This is particularly of interest when the turbulence stimulation is located in the shoulder area of the ship model, which was the case for the Hama strip at 2.5 %. Here the local flow velocity is increased causing a loss in hydrostatic pressure which again will suppress the turbulence generation.

The differences in induced parasitic drag is also an aspect to consider when investigating the placement of the turbulence stimulation. As discussed in section 6.1 the variations in local flow velocity at different stations along the hull will affect the induced drag notably. In the case of the Hama strip at 10 % of L_{PP} increased local velocity is not enough to explain the drastically increase in measured resistance alone if a laminar boundary layer profile is assumed. However, as mentioned, it is suspected that transition to turbulence occur upstream of the Hama strip in this case. Hence, a turbulent velocity profile should be utilized in the calculations. As illustrated in figure 7.7 the estimated resistance for this condition corresponds very well with the experimental results when this is the case. This is interpreted such that transition to turbulence does occur shortly upstream of the Hama strip placed at 10 % of L_{PP} . This is also agreeing well with the calculated natural extent of laminar flow based on the measured resistance for the condition without stimulation illustrated in figure 7.8.

In addition to ensuring an effective transition to turbulence, the placement of the stimulation device should consider the parasitic drag. This is clear as a good location ensures that the parasitic drag is canceled out by the reduction in resistance due to the region subjected to laminar flow upstream of the turbulence stimulator. According to ITTC (2011) this is a valid assumption when stimulation is applied at 5 % of L_{PP} . However little or no attempt to verify or investigate this hypothesis has been carried out. In this thesis an attempt of such investigations is made possible as the parasitic drag is quantified. Hence it may be compared to the loss in frictional resistance given from a fully turbulent compared to a partly laminar flow. From figures 6.10 and 6.11 it is clear that the dimensionless loss in frictional resistance due to a partly laminar flow, ΔC_R , is very much alike between model A and B. The dimensionless parasitic drag however is not, as indicated in figure 6.5. From this calculation it is evident that the parasitic drag for model B is much more significant than for the larger model A. Based on this, turbulence stimulators should be placed at different relative locations according to the model size.

In figure 8.1 the loss in frictional resistance is compared to the parasitic drag for the different stimulation techniques. Here transition is assumed at the stimulation device respectively at 2.5 and 5 % of L_{PP} for model A and B. From the figure 8.1a it is evident that the loss in resistance due to a laminar region is too large compared to the parasitic drag considering model A, especially in the low speed regime. At higher speeds the assumption that the parasitic drag equals the loss in resistance due to partly laminar flow seems to be a better approach if a trip wire or sand strip of decent size is applied. The Hama strip however generates a way too low drag force for this assumption to be valid. For model B a similar effect is indicated when the Hama strip is used. However, the trip wire produces a too large parasitic drag. During high speeds the trip wire seem to cause a parasitic drag twice the magnitude of the lost frictional resistance. Obviously this will cause an overestimation of the ship model resistance. Note that the values presented in figure 8.1 solely are based on the stimulation techniques which were actually tested in the towing tank. Thus, by for instance utilizing a thicker Hama strip

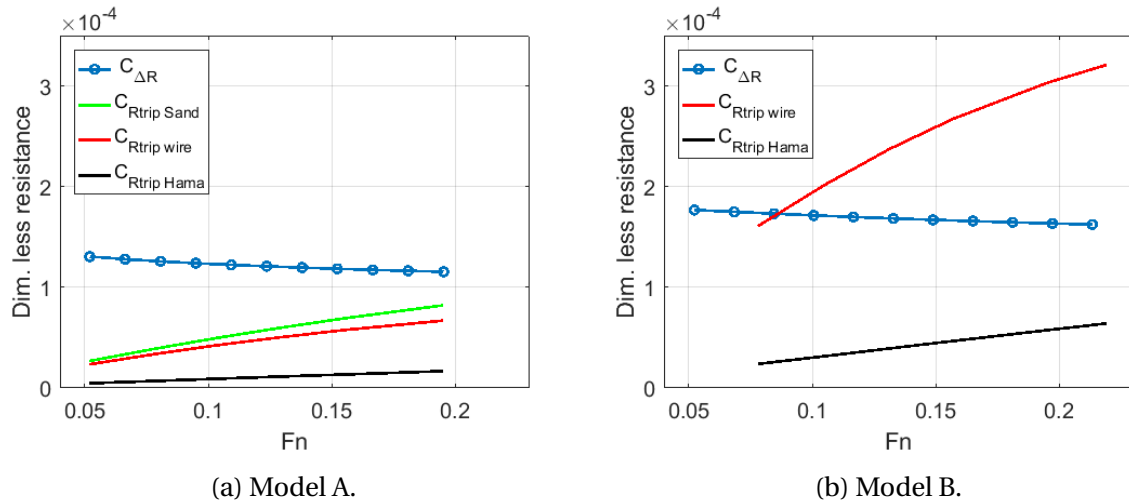


Figure 8.1: Dimensionless loss in frictional resistance due to a partly laminar flow , $C_{\Delta R}$, compared to dimensionless parasitic drag for different stimulators. Assumed transition to turbulence at location of stimulation device.

other, and probably more appropriate, values could be obtained.

In general, based on this theoretical approach, it is fair to assume that the application of turbulence stimulators closer to the stem than 5 % of L_{PP} on large ship models is a good procedure. In addition, it may be argued that turbulence stimulation techniques with a relatively large roughness height should be place further aft on smaller models. Also, smaller models are more prone to scale effects connected to induced drag by the stimulators. This is because the parasitic drag comprehends a larger part of the total ship model resistance than in the case of a large model.

8.3 Waiting time and other uncertainties

When assessing the results presented in this work it is important to be aware of the uncertainties connected to the measured ship model resistance. How certain parameters affect the laminar-turbulent transition should especially be considered, as this concerns the very essence of the current thesis. As previously described the main parameters of concern connected to a transition to turbulence in ship model testing are the surface roughness, pressure gradients and background turbulence. Since different test runs were performed with the same model, and same turbulence stimulators, the effects of surface roughness and pressure gradient will be equal. Thus they may be neglected when comparing similar test results. The background disturbances however could be believed to be a function of waiting time between runs, and could thus quite possibly change from one run to another. Not much research exists on the effects of variation in waiting times in ship model testing. Therefore series with a variation in waiting time were performed in the work with this thesis.

From table 5.3, it is clear that a variation in waiting times causes only small deviations in measured resistance. In fact, when considering the corresponding precision limit, which is relatively high at low speeds, these deviations may be neglected. Consequently it is fair to assume that the disturbances induced in the towing tank from a model traveling at low speed ($F_n < 0.1$) does not create any background turbulence affecting the transition to turbulence, even though the model is relatively large. For higher speeds the resistance increased with an order of 1 % by both decreasing and increasing the waiting time to respectively 5 and 60 minutes. Thus, no consistent results may be utilized to determine the effect of background turbulence in this case. A considerably reduction in standard deviation is however evident when the waiting time is increased to 60 minutes. Since the results are not consistent, indications are made to that other parameters than background turbulence affects the results when different waiting times are tested.

According to Gjevik et al. (2010) a standing wave may be generated in an enclosed basin or tank by the addition of linear wave components moving in opposite direction of each other. Such standing waves are often referred to as *Seiching* in available literature. As little damping effects are present in a towing tank, these waves will require a lot of time to die out. Due to the horizontally velocities induced by such a standing wave, they are very much a subject which will affect the measured resistance. No wave probes or any other measurements techniques were used to determine this wave elevation. However, according to Taylor et al. (2003) standing waves may build up enough energy to compromise otherwise steady state conditions if an insufficient waiting time is utilized. Based on this it seems fair that any scatter in measured resistance is affected by the build up of a standing wave moving back and forth in the towing tank with various periods.

This is further supported by examining the measured resistance for the dummy runs. The tendency amongst these runs was that somewhat higher values were measured compared to the mean value of repeated tests performed after the dummy run. This was particularly true for runs at higher speeds, where the dummy run values were in the order of 0.5 % larger than the corresponding mean values. As the dummy runs were performed in calm water, the result are not consistent with the theory of an increase in turbulence, and following frictional resistance, due to a higher background turbulence level in the towing tank.

Other uncertainties worth to consider are the large oscillations in measured resistance, especially during towing tests at low speed. One such time series is shown in figure 8.2. Clearly, the measured resistance is subjected to oscillations with a short period and a large amplitude compared to the mean value (in the order of 300 % larger). Even a negative resistance was logged which is obviously unphysical. These oscillations are believed to originate from any movements that the towing carriage, experience as it moves along the trackway. Since the resistance dynamometer is attached to the carriage these motions will affect the measure-

ments even though the ship model moves at constant speed. Although the amplitudes of the oscillations were large, a lot of data was recorded. For the low speed illustrated in figure 8.2 a total of 7 minutes was logged for each run, strengthening the reliability of the extracted mean value. In addition, runs were repeated several times to best construct a decisive precision limit. For the low speeds, this precision limit was substantially larger than for the higher speeds. This is believed to originate from the mentioned oscillations in measured resistance, as these were very much smaller for high speeds (in the order of 10 % of the mean value).

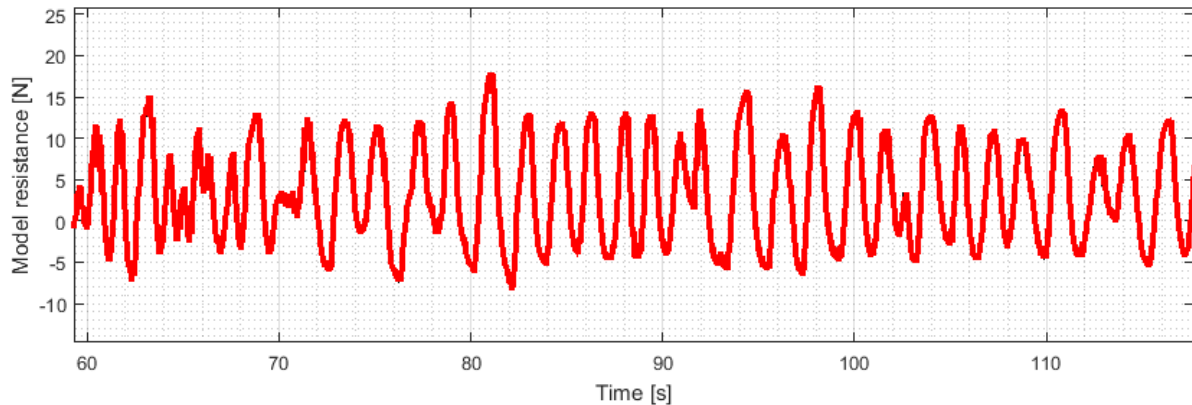


Figure 8.2: Cut out of a typical time series of measured resistance at $F_n=0.052$ for model A.

As the objective of this report is to compare measured resistance between different stimulation conditions on an otherwise similar model in a similar environment and set-up, any possible bias errors within the testing facility are deemed to not affect the results presented in this report. Thus the total uncertainty of the current model experiments are assumed determined by the precision limits calculated from the procedure in section 4.6.

8.4 Necessity of flow observation techniques

The common nominator for the majority of research performed on turbulence stimulation is the inclusion of any flow observation techniques in the model experiments. By studying the flow field one obtains valuable information of how the stimulation device actually affects the flow characteristics. The preferred observation technique should provide a firm determination of whether the flow is turbulent, laminar or transitional and, by all means be non-intrusive. A variety of such methods exists, and the optimal method may vary within test facilities dependent on available equipment and test procedures.

According to Molland et al. (2011) the most relevant flow determination methods in ship model testing are hot wire anemometry, laser Doppler velocimetry (LDV) and particle image velocimetry (PIV). Without such methods result may only be compared to a theoretical approach, which again are often based on empirical data from previous experiment. Hence by utilizing one of the mentioned techniques the integrity of a study involving turbulence

stimulation effectiveness would be largely increased.

Assuming access to a proper flow measurement technique. The introduction of the turbulence intensity, given by equation 2.12, as a parameter would provide a scientific description of the turbulent flow. This may then be used to assess the flow regions of particular interest, for instance the flow field immediately after the stimulation mechanism. Also, if experiments are performed with different stimulation mechanisms, this could be used to investigate any possible differences in the developing flow downstream of each stimulation device.

Chapter 9

Conclusion and Further Work

9.1 Conclusion

A comprehensive study, both theoretical and experimental, on the field of turbulence stimulation in ship model testing has been presented in this thesis. The necessity of turbulence stimulators is evident both by performing simple calculations and by analyzing experimental results. Today, a variety of stimulation mechanisms are in use. The most frequently used techniques in ship model testing are tripwires, studs and sand based stimulation devices. The Hama strip is mainly utilized on hydrofoils and ship model appendages. The mentioned stimulation techniques were all tested in this thesis, with the exception of studs.

By comparing the measured resistance for each stimulation condition to an assumed theoretical resistance, all stimulation techniques are deemed to be effective during relevant ship model speeds. On low speeds results indicate that the Hama strips utilized in this work are not fully effective in generating turbulence.

For all test results, a discrepancy in measured resistance between the stimulation methods is consistent over the entire speed range. Due to a good correlation with theoretical calculations, this discrepancy is believed to originate from differences in induced drag by each stimulation method. Further, the parameter governing the induced drag is the roughness height and drag coefficients corresponding to each stimulator type. By connecting the measured values to the theoretical approach it becomes clear that seemingly small changes in roughness height will affect both the ability to generate turbulence and the induced parasitic drag to a large extent.

Regarding placement of turbulence stimulation, some deviation from the recommended procedures seems to be suitable depending on model size. To ensure a turbulent transition at the stimulation and to generate appropriate induced drag, turbulence stimulation should be placed closer to the stem on larger ship models than on small models. The assumption that induced drag is canceled by the lost frictional resistance due to a laminar region up-

stream of the stimulator is somewhat speculative. Although it seems as a decent approach for tripping devices of a relatively large roughness height, such as a tripwire.

Due to an easy mounting procedure, effective turbulence generation and an appropriate amount of induced drag, the tripwire is recommended as the preferable stimulation technique. However, care must be taken when choosing the location of the stimulation. For a large ship model ($5\text{ m} < L < 8\text{ m}$) 2.5 % of L_{PP} aft of FP is a good location. For smaller models ($2\text{ m} < L < 5\text{ m}$) 5 % of L_{PP} , as according to ITTC-guidelines, seems like a suitable approach.

The main parameters affecting laminar-turbulent transition are pressure gradients, wall roughness and background turbulence. Various use of waiting time between test runs showed no indications toward a change in frictional resistance. Therefore the conclusion that laminar-turbulent transition in ship model testing may only be manipulated using different turbulence stimulation techniques is made.

9.2 Recommendations for further work

The experimental part of this study only covers ship models with a relatively large submergence and low speed. As this represents only a fraction of the ship types subjected to model testing, a study involving models of i.e high-speed crafts or semi displacement vessels would be of interest as turbulence stimulation also is applied in such cases. Also, models with a more slender bow section than the one utilized in this work would be interesting to examine from a turbulence stimulation point of view. For such models the pressure gradients are much smaller, quite possibly affecting the turbulence generation.

Another limitation of the present study is that no effects of the extent of the roughness elements in longitudinal direction are considered. A most relevant example would be the different effects in use of a narrow or a wide sand strip. This interesting topic is also much less referred to in available literature compared to the roughness height. Hence, this could serve as a highly relevant topic for any further studies. Also varying the roughness height of such stimulator types would help to confirm the presented method to determine induced drag.

In any further experimental studies regarding turbulence stimulation, it is highly recommended that some sort of flow observation technique is applied. This will provide certain establishments of each stimulator's efficiency in generating turbulence, as in contrast to this present study where only assumptions have been made in relation to available theory. To provide a scientific description of the flow at, or shortly downstream, of the stimulation device the turbulence intensity factor could be included. This provides however, that a sufficient flow observation technique is utilized.

References

- Conn, J. and Ferguson, A. (1967). Results obtained with a series of geometrically similar models. *Trans. RINA*, 110:255.
- Ersdal, S. (2004). *Lecture Note: Error Analysis of Experiments*. NTNU.
- Faltinsen, O. (2006). *Hydrodynamics of High-Speed Marine Vehicles*. Cambridge University Press.
- Feindt, E. G. (1957). *Untersuchungen über die Abhängigkeit des Umschlages laminar-turbulent von der Oberflächenrauigkeit und der Druckverteilung*. PhD thesis, Technische Hochschule Carolo-Wilhelmina zu Braunschweig.
- Gad-el Hak, M. (2000). *Flow Control: Passive, Active, and Reactive Flow Management*. Cambridge University Press.
- Gibbins, J. (1959). *On boundary-layer transition wires*. HM Stationery Office.
- Gillmer, T. C. and Johnson, B. (1982). *Introduction to naval architecture*. Airlife Publishing.
- Gjevik, B., Pedersen, G. K., and Trulsen, K. (2010). Lecture notes mek 4320 hydrodynamic wave theory.
- Grigson, C. (1999). A planar friction algorithm and its use in analysing hull resistance. *Trans RINA*.
- Hama, F. R. (1957). *An Efficient Tripping Device*. Journal of Aeronautical Sciences.
- Harrington, A. and Wells, J. D. (2011). Triswach small model testing. Technical report, NAVAL SURFACE WARFARE CENTER CARDEROCK DIV BETHESDA MD.
- Hoerner, S. F. (1965). *Fluid-dynamic drag: practical information on aerodynamic drag and hydrodynamic resistance*. Hoerner Fluid Dynamics.
- Hughes, G. and Allan, J. (1951). *Turbulence stimulation on ship models*. Society of Naval Architects and Marine Engineers.
- ITTC (1957). Skin friction and turbulence stimulation. *Proceedings of the 8th ITTC, Madrid, Spain*, 1.

- ITTC (1990). Report of the high-speed marine vehicles committee. *Proceedings of the 19th ITTC, Madrid, Spain*, 1:306–310.
- ITTC (2002). Recommended procedures and guidelines - resistance uncertainty analysis, example for resistance test, 7.5-02-02-02.
- ITTC (2011). Recommended procedures and guidelines - ship models, 7.5-01-01-01. pages 4–5.
- ITTC (2017a). Recommended procedures and guidelines - high speed marine vehicles resistance test, 7.5-02-05-01. pages 4–5.
- ITTC (2017b). Report of resistance committee. *Proceedings of the 28th ITTC, Wuxi, China*, 1:39–47.
- Kristiansen, T. (2017). *Lecture Notes MR8306 (lecture 6 and 7)*. NTNU.
- Larsson, L., Raven, H., and Paulling, J. (2010). *Ship Resistance and Flow*. Principles of naval architecture. Society of Naval Architects and Marine Engineers.
- Larsson, L., Stern, F., and Visonneau, M. (2013). *Numerical ship hydrodynamics: an assessment of the Gothenburg 2010 workshop*. Springer.
- Lewandowski, E. (1989). The effects of reynolds number, section shape, and turbulence stimulation on the lift of a series of model control surfaces. In *American Towing Tank Conference, 22nd*.
- Lewis, E. (1988). Principles of naval architecture: Volume ii-resistance, propulsion, and vibration, vol. 2, 2 edn, soc. *Naval Architects & Marine Engineers*.
- McCarthy, J., Power, J., and Huang, T. (1976). The roles of transition, laminar separation, and turbulence stimulation in the analysis of axisymmetric body drag. In *Proceedings, 11th Symposium on Naval Hydrodynamic*.
- Molland, A., Wellicome, J., and Couser, P. (1994). Resistance experiments on a systematic series of high speed displacement catamaran forms: variation of length-displacement ratio and breadth-draught ratio.
- Molland, A. E, Turnock, S. R., and Hudson, D. A. (2011). *Ship Resistance and Propulsion: Practical Estimation of Propulsive Power*. Cambridge University Press.
- Munson, B., Huebsch, W., Okiishi, T., and Rothmayer, A. (2013). *Fluid Mechanics*. Wiley.
- Murphy, A. J. and Hearn, G. E. (2007). A practical and robust method to experimentally determine the location of the region of transition from laminar to turbulent flow on a towed body. *The Transactions of the Royal Institution of Naval Architects Part A: International Journal of Maritime Engineering*, 149(A1):31–43.

- Murphy, J. C. (2010). A novel approach to turbulence stimulation for ship-model testing. Technical report, NAVAL ACADEMY ANNAPOLIS MD.
- Pattenden, R., Turnock, S., and Zhang, X. (2005). Measurements of the flow over a low-aspect-ratio cylinder mounted on a ground plane. *Experiments in Fluids*, 39(1):10–21.
- Reynolds, O. (1883). An experimental investigation of the circumstances which determine whether the motion of water shall be direct or sinuous, and of the law of resistance in parallel channels. *Proceedings of the Royal Society of London*, pages 84–99.
- Schlichting, H. (1968). *Boundary-layer theory*. McGraw-Hill.
- Schlichting, H. and Gersten, K. (2016). *Boundary-Layer Theory*. Springer Berlin Heidelberg.
- Shen, Y. T., Hughes, M. J., and Gorski, J. J. (2015). Resistance prediction on submerged axisymmetric bodies fitted with turbulent spot inducers. *Journal of Ship Research*, 59(2):85–98.
- Smith, A. M. O. and Clutter, D. W. (1959). The smallest height of roughness capable of affecting boundary-layer transition. *Journal of the Aerospace Sciences*, 26:229–245.
- Steen, S. (2014a). *Lecture Notes Experimental Methods in Marine Hydrodynamics*. NTNU.
- Steen, S. (2014b). *Lecture Notes Naval Hydrodynamics - Ship Resistance*. NTNU.
- Tagori, T. (1963). *A study of the turbulent stimulator device in the model experiment on ship*, volume 1.
- Tani, I. and Sato, H. (1956). Boundary-layer transition by roughness element. *Journal of the Physical Society of Japan*, 11(12):1284–1291.
- Taylor, J., Rea, M., and Rogers, D. (2003). The edinburgh curved tank. In *5th European Wave Energy Conference, Cork, Ireland*, pages 307–314.
- Tupper, E. C. (2013). *Introduction to naval architecture*. Butterworth-Heinemann.
- Van Manen, J. and Van Oossanen, P. (1988). Resistance. *Principles of naval architecture*, 2:1–126.
- White, F. (2006). *Viscous Fluid Flow*. McGraw-Hill international edition. McGraw-Hill Higher Education.

Appendix A

Complete Results for Each Run

A total presentation of the measured resistance corresponding to each performed run in the towing tank follows herein. Descriptions of the current stimulation condition are given in the table heading.

A.1 Model A

Test condition: No stimulation, model A
Waiting time: 5 min

Model scale[m/s]	Speed	Full scale[kts]	R_{Tm}	Remarks
	Fn			
0.60	0.08	6.20	6.768	
0.60	0.08	6.20	6.672	
0.60	0.08	6.20	6.675	
1.50	0.20	15.50	41.336	
1.50	0.20	15.50	41.459	
1.50	0.20	15.50	41.345	

Table A.1

Test condition:		No stimulation, model A		
Waiting time:		15 min		
Model scale[m/s]	Speed		R_{Tm}	Remarks
	Fn	Full scale[kts]		
1.50	0.20	15.50	41.146	Dummy run
0.40	0.05	4.13	3.011	
0.40	0.05	4.13	3.061	
0.40	0.05	4.13	3.081	
0.40	0.05	4.13	3.094	
0.40	0.05	4.13	3.088	
0.40	0.05	4.13	3.104	
0.40	0.05	4.13	3.088	
0.40	0.05	4.13	3.091	
0.40	0.05	4.13	3.047	
0.40	0.05	4.13	2.990	
0.40	0.05	4.13	3.067	
0.60	0.08	6.20	6.749	
0.60	0.08	6.20	6.699	
0.60	0.08	6.20	6.664	
0.80	0.10	8.27	11.804	
0.80	0.10	8.27	11.743	
0.80	0.10	8.27	11.757	
1.00	0.13	10.33	17.687	
1.00	0.13	10.33	17.718	
1.00	0.13	10.33	17.645	
1.20	0.16	12.40	25.807	
1.20	0.16	12.40	25.743	
1.20	0.16	12.40	25.750	
1.50	0.20	15.50	40.946	
1.50	0.20	15.50	40.936	
1.50	0.20	15.50	40.869	
1.50	0.20	15.50	40.916	
1.50	0.20	15.50	41.078	
1.50	0.20	15.50	40.997	
1.50	0.20	15.50	41.099	
1.50	0.20	15.50	41.004	
1.50	0.20	15.50	41.097	
1.50	0.20	15.50	41.150	

Table A.2

Test condition:		Tripwire 1, model A		
Waiting time:		15 min		
Model scale[m/s]	Speed		R_{Tm}	Remarks
	Fn	Full scale[kts]		
0.40	0.05	4.13	3.326	Dummy run
0.40	0.05	4.13	3.378	
0.40	0.05	4.13	3.366	
0.40	0.05	4.13	3.351	
0.40	0.05	4.13	3.359	
0.40	0.05	4.13	3.364	
0.40	0.05	4.13	3.374	
0.40	0.05	4.13	3.377	
0.40	0.05	4.13	3.379	
0.40	0.05	4.13	3.361	
0.40	0.05	4.13	3.346	
0.60	0.08	6.20	7.074	
0.60	0.08	6.20	7.082	
0.80	0.10	8.27	12.095	
0.80	0.10	8.27	12.070	
1.00	0.13	10.33	18.096	
1.00	0.13	10.33	18.097	
1.20	0.16	12.40	26.399	
1.20	0.16	12.40	26.361	
1.50	0.20	15.50	41.852	
1.50	0.20	15.50	42.095	
1.50	0.20	15.50	41.945	
1.50	0.20	15.50	41.950	
1.50	0.20	15.50	41.956	
1.50	0.20	15.50	42.008	
1.50	0.20	15.50	41.922	
1.50	0.20	15.50	41.882	
1.50	0.20	15.50	41.910	
1.50	0.20	15.50	41.943	

Table A.3

Test condition: Tripwire 1, model A
Waiting time: 5 min

Model scale[m/s]	Speed		R_{Tm}	Remarks
	Fn	Full scale[kts]		
0.60	0.08	6.20	7.055	
0.60	0.08	6.20	7.082	
0.60	0.08	6.20	7.043	
0.60	0.08	6.20	7.097	
1.50	0.20	15.50	42.391	
1.50	0.20	15.50	42.172	
1.50	0.20	15.50	42.368	

Table A.4

Test condition: Tripwire 1, model A
Waiting time: 60 min

Model scale[m/s]	Speed		R_{Tm}	Remarks
	Fn	Full scale[kts]		
0.60	0.08	6.20	7.078	
0.60	0.08	6.20	7.059	
0.60	0.08	6.20	7.046	
1.50	0.20	15.50	42.305	
1.50	0.20	15.50	42.225	
1.50	0.20	15.50	42.211	

Table A.5

Test condition:		Tripwire 2, model A		
Waiting time:		15 min		
	Speed			
Model scale[m/s]	Fn	Full scale[kts]	R_{Tm}	Remarks
1.50	0.20	15.50	42.30	Dummy run
1.50	0.20	15.50	42.12	First set of high speeds, calm water
1.50	0.20	15.50	42.11	
1.50	0.20	15.50	42.05	
1.50	0.20	15.50	42.16	
1.50	0.20	15.50	42.10	
1.50	0.20	15.50	42.04	
1.50	0.20	15.50	42.14	
1.50	0.20	15.50	42.13	
1.50	0.20	15.50	42.15	
1.50	0.20	15.50	42.16	
0.40	0.05	4.13	3.30	
0.40	0.05	4.13	3.35	
0.40	0.05	4.13	3.38	
0.40	0.05	4.13	3.40	
0.40	0.05	4.13	3.41	
0.40	0.05	4.13	3.42	
0.40	0.05	4.13	3.35	
0.40	0.05	4.13	3.35	
0.40	0.05	4.13	3.37	
0.40	0.05	4.13	3.38	
0.60	0.08	6.20	7.11	
0.60	0.08	6.20	7.04	
0.60	0.08	6.20	7.17	
0.60	0.08	6.20	7.15	
0.60	0.08	6.20	7.09	
0.80	0.10	8.27	12.19	
0.80	0.10	8.27	12.14	
0.80	0.10	8.27	12.02	
0.80	0.10	8.27	12.13	
1.00	0.13	10.33	18.26	
1.00	0.13	10.33	18.11	
1.00	0.13	10.33	18.29	
1.00	0.13	10.33	18.23	
1.20	0.16	12.40	26.49	
1.20	0.16	12.40	26.45	
1.20	0.16	12.40	26.50	
1.20	0.16	12.40	26.39	

Table A.6

Test condition: Tripwire 2, model A

Waiting time: 15 min

Model scale[m/s]	Speed		R_{Tm}	Remarks
	Fn	Full scale[kts]		
1.50	0.20	15.50	42.50	Second set of high speeds, after activity in tank
1.50	0.20	15.50	42.33	
1.50	0.20	15.50	42.29	
1.50	0.20	15.50	42.25	
1.50	0.20	15.50	42.22	
1.50	0.20	15.50	42.24	
1.50	0.20	15.50	42.21	
1.50	0.20	15.50	42.22	
1.50	0.20	15.50	42.22	
1.50	0.20	15.50	42.18	
1.50	0.20	15.50	42.21	

Table A.7: Tripwire 2 continue.

Test condition:		Hama strip, model A		
Waiting time:		15 min		
	Speed			
Model scale[m/s]	Fn	Full scale[kts]	R_{Tm}	Remarks
0.40	0.05	4.13	3.146	Dummy run
0.40	0.05	4.13	3.190	
0.40	0.05	4.13	3.037	
0.40	0.05	4.13	3.076	
0.40	0.05	4.13	3.094	
0.40	0.05	4.13	3.085	
0.40	0.05	4.13	3.114	
0.40	0.05	4.13	3.129	
0.40	0.05	4.13	3.131	
0.40	0.05	4.13	3.117	
0.40	0.05	4.13	3.126	
0.60	0.08	6.20	7.010	
0.60	0.08	6.20	7.030	
0.60	0.08	6.20	7.041	
0.60	0.08	6.20	7.018	
0.80	0.10	8.27	12.083	
0.80	0.10	8.27	12.071	
0.80	0.10	8.27	12.059	
0.80	0.10	8.27	12.028	
1.00	0.13	10.33	18.140	
1.00	0.13	10.33	18.085	
1.00	0.13	10.33	18.108	
1.00	0.13	10.33	18.080	
1.20	0.16	12.40	26.296	
1.20	0.16	12.40	26.236	
1.20	0.16	12.40	26.230	
1.20	0.16	12.40	26.194	
1.50	0.20	15.50	41.970	
1.50	0.20	15.50	41.861	
1.50	0.20	15.50	41.836	
1.50	0.20	15.50	41.789	
1.50	0.20	15.50	41.754	
1.50	0.20	15.50	41.780	
1.50	0.20	15.50	41.769	
1.50	0.20	15.50	41.746	
1.50	0.20	15.50	41.762	
1.50	0.20	15.50	41.755	

Table A.8

Test condition:		Sand strip, model A		
Waiting time:		15 min		
		Speed		
Model scale[m/s]	Fn	Full scale[kts]	R_{Tm}	Remarks
0.40	0.05	15.50	42.649	Dummy run
0.40	0.05	4.13	3.337	
0.40	0.05	4.13	3.376	
0.40	0.05	4.13	3.345	
0.40	0.05	4.13	3.393	
0.40	0.05	4.13	3.376	
0.40	0.05	4.13	3.412	
0.40	0.05	4.13	3.363	
0.40	0.05	4.13	3.350	
0.40	0.05	4.13	3.389	
0.40	0.05	4.13	3.345	
0.40	0.05	4.13	3.278	
0.40	0.05	4.13	3.268	
0.60	0.08	6.20	7.062	
0.60	0.08	6.20	7.121	
0.60	0.08	6.20	7.171	
0.60	0.08	6.20	7.159	
0.60	0.08	6.20	7.145	
0.80	0.10	8.27	12.185	
0.80	0.10	8.27	12.091	
0.80	0.10	8.27	12.197	
0.80	0.10	8.27	12.041	
0.80	0.10	8.27	12.268	
0.80	0.10	8.27	12.252	
1.00	0.13	10.33	18.315	
1.00	0.13	10.33	18.180	
1.00	0.13	10.33	18.321	
1.00	0.13	10.33	18.321	
1.00	0.13	10.33	18.196	
1.00	0.13	10.33	18.222	
1.20	0.16	12.40	26.492	
1.20	0.16	12.40	26.483	
1.20	0.16	12.40	26.514	

Table A.9

Model scale[m/s]	Fn	Full scale[kts]	RTm	Remarks
1.20	0.16	12.40	26.646	
1.20	0.16	12.40	26.604	
1.20	0.16	12.40	26.583	
1.20	0.16	12.40	26.586	
1.50	0.20	15.50	42.460	
1.50	0.20	15.50	42.837	
1.50	0.20	15.50	42.536	
1.50	0.20	15.50	42.521	
1.50	0.20	15.50	42.489	
1.50	0.20	15.50	42.482	
1.50	0.20	15.50	42.862	
1.50	0.20	15.50	42.900	
1.50	0.20	15.50	42.681	
1.50	0.20	15.50	42.401	
1.50	0.20	15.50	42.319	
1.50	0.20	15.50	42.393	
1.50	0.20	15.50	42.404	
1.50	0.20	15.50	42.395	
1.50	0.20	15.50	42.543	

Table A.10: Sand strip continue.

A.2 Model B

Test condition: No stimulation, model B

Waiting time: 8 min

Model scale[m/s]	Speed	Full scale[kts]	R_{Tm}	Remarks
	F_n			
0.39	0.08	7.73	0.635	Dummy run
0.39	0.08	7.73	0.608	
0.39	0.08	7.73	0.605	
0.39	0.08	7.73	0.605	
0.39	0.08	7.73	0.609	
0.39	0.08	7.73	0.610	
0.39	0.08	7.73	0.608	
0.39	0.08	7.73	0.610	
0.39	0.08	7.73	0.609	
0.39	0.08	7.73	0.612	
0.39	0.08	7.73	0.608	
0.52	0.10	10.30	1.087	
0.52	0.10	10.30	1.085	
0.65	0.13	12.87	1.680	
0.65	0.13	12.87	1.676	
0.78	0.16	15.45	2.381	
0.78	0.16	15.45	2.377	
0.97	0.19	19.30	4.001	
0.97	0.19	19.30	4.000	
1.09	0.22	21.77	6.035	
1.09	0.22	21.77	6.028	
1.09	0.22	21.77	6.027	
1.09	0.22	21.77	6.029	
1.09	0.22	21.77	6.019	
1.09	0.22	21.77	6.019	
1.09	0.22	21.77	6.022	
1.09	0.22	21.77	6.035	
1.09	0.22	21.77	6.033	
1.09	0.22	21.77	6.109	

Table A.11

Test condition: Hama strip 5% of L_{pp} , model B
Waiting time: 8 min

Model scale[m/s]	Speed	Full scale[kts]	R_{Tm}	Remarks
	F_n			
0.39	0.08	7.73	0.696	Dummy run
0.39	0.08	7.73	0.666	
0.39	0.08	7.73	0.665	
0.39	0.08	7.73	0.661	
0.39	0.08	7.73	0.659	
0.39	0.08	7.73	0.660	
0.39	0.08	7.73	0.659	
0.39	0.08	7.73	0.658	
0.39	0.08	7.73	0.654	
0.39	0.08	7.73	0.657	
0.39	0.08	7.73	0.658	
0.52	0.10	10.30	1.160	
0.52	0.10	10.30	1.162	
0.65	0.13	12.87	1.772	
0.65	0.13	12.87	1.773	
0.78	0.16	15.45	2.516	
0.78	0.16	15.45	2.516	
0.97	0.19	19.30	4.201	
0.97	0.19	19.30	4.190	
1.09	0.22	21.77	6.232	
1.09	0.22	21.77	6.229	
1.09	0.22	21.77	6.225	
1.09	0.22	21.77	6.225	
1.09	0.22	21.77	6.202	
1.09	0.22	21.77	6.201	
1.09	0.22	21.77	6.194	
1.09	0.22	21.77	6.190	
1.09	0.22	21.77	6.206	
1.09	0.22	21.77	6.219	

Table A.12

Test condition: Hama strip 2.5 % of L_{PP} , model B
Waiting time: 8 min

Model scale[m/s]	Speed		R_{Tm}	Remarks
	Fn	Full scale[kts]		
0.39	0.08	7.73	0.651	
0.52	0.10	10.30	1.134	
0.65	0.13	12.87	1.722	
0.78	0.16	15.45	2.474	
0.97	0.19	19.30	4.117	
1.09	0.22	21.77	6.150	

Table A.13

Test condition: Hama strip 10 % of L_{PP} , model B
Waiting time: 8 min

Model scale[m/s]	Speed		R_{Tm}	Remarks
	Fn	Full scale[kts]		
0.39	0.08	7.73	0.683	
0.52	0.10	10.30	1.188	
0.65	0.13	12.87	1.799	
0.78	0.16	15.45	2.549	
0.97	0.19	19.30	4.244	
1.09	0.22	21.77	6.241	

Table A.14

Test condition: Tripwire 5 % of L_{pp} , model B
Waiting time: 8 min

Model scale[m/s]	Speed	Full scale[kts]	R_{Tm}	Remarks
	F_n			
0.39	0.08	7.73	0.705	Dummy run
0.39	0.08	7.73	0.692	
0.39	0.08	7.73	0.696	
0.39	0.08	7.73	0.696	
0.39	0.08	7.73	0.693	
0.39	0.08	7.73	0.691	
0.39	0.08	7.73	0.687	
0.39	0.08	7.73	0.695	
0.39	0.08	7.73	0.714	
0.39	0.08	7.73	0.687	
0.39	0.08	7.73	0.690	
0.52	0.10	10.30	1.203	
0.52	0.10	10.30	1.205	
0.65	0.13	12.87	1.827	
0.65	0.13	12.87	1.826	
0.78	0.16	15.45	2.597	
0.78	0.16	15.45	2.594	
0.97	0.19	19.30	4.341	
0.97	0.19	19.30	4.331	
1.09	0.22	21.77	6.497	
1.09	0.22	21.77	6.468	
1.09	0.22	21.77	6.453	
1.09	0.22	21.77	6.454	
1.09	0.22	21.77	6.450	
1.09	0.22	21.77	6.446	
1.09	0.22	21.77	6.461	
1.09	0.22	21.77	6.455	
1.09	0.22	21.77	6.442	
1.09	0.22	21.77	6.452	

Table A.15

Appendix B

Complete Comparison of Experimental Results

In the following section a relative comparison between all tested stimulation techniques for each speed is given. The Difference and precision limits are given in percent.

B.1 Model A

	<i>w/o stim</i>	<i>TW 1</i>	<i>TW 2</i>	<i>Hama</i>	<i>sand</i>
<i>w/o stim</i>	-	-8.79	-9.12	-1.33	-8.63
<i>TW 1</i>	+9.64	-	-0.36	+8.17	+0.17
<i>TW 2</i>	+10.03	+0.36	-	8.57	0.53
<i>Hama</i>	+1.35	-7.55	-7.89	-	-7.40
<i>sand</i>	+9.45	-0.17	-0.53	7.99	-
<i>prec. lim</i>	± 1.42	± 0.8	± 1.25	± 1.01	± 1.27

Table B.1: Fn=0.052

	<i>w/o stim</i>	<i>TW 1</i>	<i>TW 2</i>	<i>Hama</i>	<i>sand</i>
<i>w/o stim</i>	-	-5.28	-5.72	-4.57	-6.00
<i>TW 1</i>	+5.57	-	-0.46	+0.75	-0.75
<i>TW 2</i>	+6.07	+0.47	-	+1.22	-0.29
<i>Hama</i>	+4.79	-0.74	-1.20	-	-1.49
<i>sand</i>	+6.37	+0.76	+0.29	+1.52	-
<i>prec. lim</i>	± 1.21	± 0.71	± 1.04	± 0.85	± 1.11

Table B.2: Fn=0.078

	<i>w/o stim</i>	<i>TW 1</i>	<i>TW 2</i>	<i>Hama</i>	<i>sand</i>
<i>w/o stim</i>	-	-2.60	-2.89	-2.42	-3.32
<i>TW 1</i>	+2.66	-	-0.30	+0.18	-0.74
<i>TW2</i>	+2.98	+0.30	-	+0.48	-0.44
<i>Hama</i>	+2.48	-0.18	-0.48	-	-0.92
<i>sand</i>	+3.43	+0.75	+0.44	+0.93	-
<i>prec. lim</i>	± 0.99	± 0.63	± 0.84	± 0.69	± 0.95

Table B.3: $F_n=0.104$

	<i>w/o stim</i>	<i>TW 1</i>	<i>TW 2</i>	<i>Hama</i>	<i>sand</i>
<i>w/o stim</i>	-	-2.28	-2.95	-2.31	-3.15
<i>TW 1</i>	+2.33	-	-0.68	-0.04	-0.89
<i>TW2</i>	+3.04	+0.69	-	+0.65	-0.20
<i>Hama</i>	+2.37	+0.04	-0.65	-	-0.85
<i>sand</i>	+3.25	+0.89	+0.20	+0.86	-
<i>prec. lim</i>	± 0.24	± 0.33	± 0.11	± 0.14	± 0.40

Table B.4: $F_n=0.13$

	<i>w/o stim</i>	<i>TW 1</i>	<i>TW 2</i>	<i>Hama</i>	<i>sand</i>
<i>w/o stim</i>	-	-2.30	-2.60	-1.80	-2.98
<i>TW 1</i>	+2.355	-	-0.31	+0.51	-0.69
<i>TW2</i>	+2.67	+0.31	-	+0.82	-0.38
<i>Hama</i>	+1.83	-0.51	-0.82	-	-1.20
<i>sand</i>	+3.07	+0.70	+0.39	+1.22	-
<i>prec. lim</i>	± 0.78	± 0.54	± 0.63	± 0.54	± 0.79

Table B.5: $F_n=0.156$

	<i>w/o stim</i>	<i>TW 1</i>	<i>TW 2</i>	<i>Hama</i>	<i>sand</i>
<i>w/o stim</i>	-	-2.27	-2.86	-1.95	-3.63
<i>TW 1</i>	+2.32	-	-0.60	+0.32	-1.39
<i>TW2</i>	+2.94	+0.61	-	+0.93	-0.79
<i>Hama</i>	+1.99	-0.32	-0.92	-	-1.71
<i>sand</i>	+3.76	+1.41	+0.79	+1.73	-
<i>prec. lim</i>	± 0.56	± 0.46	± 0.42	± 0.38	± 0.63

Table B.6: $F_n=0.195$

B.2 Model B

	<i>w/o stim</i>	<i>Hama 2.5 %</i>	<i>Hama 5 %</i>	<i>Hama 10 %</i>	<i>Tripwire 5 %</i>
<i>w/o stim</i>	-	-6.56	-7.80	-10.94	-12.38
<i>Hama 2.5 %</i>	+7.02	-	-1.33	-4.69	-6.23
<i>Hama 5 %</i>	+8.46	+1.35	-	-3.40	-4.96
<i>Hama 10 %</i>	+12.29	+4.92	+3.5234	-	-1.61
<i>Tripwire 5 %</i>	+14.13	+6.64	+5.22	+1.64	-
<i>prec. lim</i>	±0.61	-	±0.77	-	±0.80

Table B.7: Fn=0.078

	<i>w/o stim</i>	<i>Hama 2.5 %</i>	<i>Hama 5 %</i>	<i>Hama 10 %</i>	<i>Tripwire 5 %</i>
<i>w/o stim</i>	-	-4.21	-6.45	-8.58	-9.81
<i>Hama 2.5 %</i>	+4.39	-	-2.34	-4.57	-5.85
<i>Hama 5 %</i>	+6.89	+2.39	-	-2.28	-3.60
<i>Hama 10 %</i>	+9.39	+4.79	+2.34	-	-1.35
<i>Tripwire 5 %</i>	+10.88	+6.22	+3.7341	+1.37	-
<i>prec. lim</i>	±0.54	-	±0.70	-	±0.73

Table B.8: Fn=0.104

	<i>w/o stim</i>	<i>Hama 2.5 %</i>	<i>Hama 5 %</i>	<i>Hama 10 %</i>	<i>Tripwire 5 %</i>
<i>w/o stim</i>	-	-2.54	-5.29	-6.73	-8.13
<i>Hama 2.5 %</i>	+2.60	-	-2.83	-4.30	-5.74
<i>Hama 5 %</i>	+5.59	+2.91	-	-1.51	-2.99
<i>Hama 10 %</i>	+7.21	+4.49	+1.53	-	-1.51
<i>Tripwire 5 %</i>	+8.85	+6.09	+3.09	+1.53	-
<i>prec. lim</i>	±0.47	-	±0.63	-	±0.66

Table B.9: Fn=0.13

	<i>w/o stim</i>	<i>Hama 2.5 %</i>	<i>Hama 5 %</i>	<i>Hama 10 %</i>	<i>Tripwire 5 %</i>
<i>w/o stim</i>	-	-3.82	-5.43	-6.67	-8.35
<i>Hama 2.5 %</i>	+3.97	-	-1.67	-2.96	-4.70
<i>Hama 5 %</i>	+5.75	+1.70	-	-1.31	-3.08
<i>Hama 10 %</i>	+7.15	+3.06	+1.33	-	-1.79
<i>Tripwire 5 %</i>	+9.11	+4.94	+3.18	+1.82	-
<i>prec. lim</i>	± 0.40	-	± 0.56	-	± 0.59

Table B.10: $F_n=0.156$

	<i>w/o stim</i>	<i>Hama 2.5 %</i>	<i>Hama 5 %</i>	<i>Hama 10 %</i>	<i>Tripwire 5 %</i>
<i>w/o stim</i>	-	-2.85	-4.66	-5.75	-7.79
<i>Hama 2.5 %</i>	+2.93	-	-1.86	-2.98	-5.09
<i>Hama 5 %</i>	+4.89	+1.89	-	-1.14	-3.29
<i>Hama 10 %</i>	+6.10	+3.07	+1.15	-	-2.17
<i>Tripwire 5 %</i>	+8.45	+5.36	+3.40	+2.21	-
<i>prec. lim</i>	± 0.29	-	± 0.45	-	± 0.48

Table B.11: $F_n=0.195$

	<i>w/o stim</i>	<i>Hama 2.5 %</i>	<i>Hama 5 %</i>	<i>Hama 10 %</i>	<i>Tripwire 5 %</i>
<i>w/o stim</i>	-	-1.96	-2.90	-3.23	-6.41
<i>Hama 2.5 %</i>	1.99	-	-0.97	-1.29	-4.54
<i>Hama 5 %</i>	2.99	0.97	-	-0.33	-3.61
<i>Hama 10 %</i>	3.33	1.31	0.33	-	-3.29
<i>Tripwire 5 %</i>	6.85	4.76	3.75	3.40	-
<i>prec. lim</i>	± 0.23	-	± 0.39	-	± 0.41

Table B.12: $F_n=0.22$